STUDIES OF INTRACORTICAL MICROELECTRODE ARRAY PERFORMANCE AND FOREIGN BODY RESPONSE IN YOUNG AND AGED RATS

by

Nicholas Fredrick Nolta

A dissertation submitted to the faculty of
The University of Utah
in partial fulfillment of the requirements for the degree of

Doctor of Philosophy

Department of Bioengineering

The University of Utah

December 2016

The University of Utah Graduate School

STATEMENT OF THESIS APPROVAL

The thesis of **Nicholas Fredrick Nolta**

has been approved by the following supervisory committee members:

Patrick A. Tresco	, Chair	**12/1/2015** Date Approved
Alan Dale Dorval II	, Member	**12/1/2015** Date Approved
David W. Grainger	, Member	**11/17/2015** Date Approved
Robert W. Hitchcock	, Member	**12/1/2015** Date Approved
Florian Solzbacher	, Member	**12/4/2015** Date Approved

and by **Patrick A. Tresco** , Chair/Dean of

the Department/College/School of **Bioengineering**

and by David B. Kieda, Dean of The Graduate School.

ABSTRACT

Intracortical microelectrode arrays create a direct interface between the brain and external devices. This "brain-machine interface" has found clinical application by allowing patients with tetraplegia to control computer cursors and robotic limbs. Unfortunately, use of intracortical microelectrode array technology is currently limited by its inconsistent ability to record neural signals over time. It is widely believed that the foreign body response (FBR) contributes to recording inconsistency. Most characterizations of the FBR to intracortical microelectrodes have been in the rat using devices with simple architecture, while the only device currently used in humans, the Utah Electrode Array (UEA), is much larger and more complex. In this work, we characterized the FBR to the UEA and found that, unlike with simpler devices, implantation of a UEA results in extensive vascular injury and loss of cortical tissue. We also sought to determine which features of the FBR correlated with recording inconsistency and found that biomarkers of astrogliosis, blood-brain barrier leakage, and tissue loss were associated with decreased recording performance. Next, since a significant portion of potential brain-machine interface recipients are aged, we applied similar methods in an aged cohort of rats in order to understand the effect of aging on the FBR and recording performance. We found that, surprisingly, recording performance was superior in the aged cohort. Astrogliosis was again associated with decreased recording performance in the aged cohort. Finally, we continued our development and validation of a finite element model of

cytokine diffusion to assist in designing next-generation devices with a reduced FBR. Taken as a whole, this work provides meaningful insights into the mechanisms of inconsistent recording performance and discusses several promising avenues for overcoming them.

TABLE OF CONTENTS

LIST OF FIGURES

LIST OF TABLES

LIST OF ABBREVIATIONS

aCSF.....Artificial cerebrospinal fluid

BBB.....Blood-brain barrier

BCI..... Brain-computer interface

BMI.....Brain-machine interface

CCR2..... Chemokine (C-C motif) receptor 2

CD45.....Cluster of differentiation 45

CD68.....Cluster of differentiation 68

CSF .....Cerebrospinal fluid

CSPG.....Chondroitin sulfate proteoglycan

DAPI ..... 4',6-diamidino-2-phenylindole

DBS.....Deep brain stimulation

ECM..... Extracellular matrix

ECoG.....Electrocortigography

EGR-1 ..... Early growth response protein 1

FBGC ..... foreign body giant cell

FBR..... Foreign body response

GFAP ..... Glial fibrillary acidic protein

IBA-1 .....Ionized calcium-binding adapter molecule 1

IgG .....Immunoglobulin G

IL-1β ..... Interleukin 1β

IL-6 ..... Interleukin 6

IQR ..... Interquartile range

LPS ..... Lipopolysaccharide

MCP-1 ..... Monocyte chemotactic protein 1

MHC class II ..... Major histocompatibility complex class II

MMP-2 ..... Matrix metalloproteinase 2

MMP-9 ..... Matrix metalloproteinase 9

NADPH-d ..... Nicotinamide adenine dinucleotide hydrogen phosphate diaphorase

NeuN ..... Neuronal nuclei

NF160 ..... Neurofilament 160

NF200 ..... Neurofilament 200

NO ..... Nitric oxide

OPC ..... Oligo-proanthocyanidin

PBS ..... Phosphate-buffered saline

PDMS ..... Polydimethylsiloxane

PEG ..... Poly(ethylene glycol)

PGA ..... Poly(glycolic acid)

PMSC ..... Polydimethylsiloxane-modified N, O-carboxylic chitosan

p-NF-H ..... Phosphorylated axonal neurofilament subunit H

pNIPAm-co-AAc ..... poly(N-isopropylacrylamide)-co-acrylic acid

PVAc ..... Poly(vinyl acetate)

ROS ..... Reactive oxygen species

SCI ..... Spinal cord injury

SNR ..... Signal-to-noise ratio

TNF-α ..... Tumor necrosis factor α

UEA ..... Utah Electrode Array

ACKNOWLEDGEMENTS

I would like to thank my advisor, Dr. Patrick Tresco, for granting me the opportunity to work on this project, providing mentorship, and cultivating an exceptional lab group. Furthermore, I would like to thank the other members of the Tresco lab I have had the pleasure to work with: Elena Budko, Dr. Ben Christensen, Paul Crane, Scott Hudson, Dr. Robert Oakes, Michael Polei, Nikole Rhodes, Dr. John Skousen, Bharath Velagapudi, and Dr. Brent Winslow. I would like to thank my committee members: Dr. Alan Dorval, Dr. David Grainger, Dr. Robert Hitchcock, and Dr. Florian Solzbacher. I would also like to thank the Achievement Rewards for College Scientists foundation and Dr. Cecelia Foxley.

I would like to thank the friends, teachers, students, and staff I've met here in Utah – too many to name.

And of course, most of all, I'd like to thank my family.

CHAPTER 1

INTRODUCTION

1.1 Clinical Populations

Paralysis and limb loss can be extremely debilitating, completely changing a patient's ability to interact with the world. One in fifty Americans currently suffer from some form of paralysis, with 17% reporting "a little difficulty" in moving, 29% "some difficulty," 36% "a lot of difficulty," and 16% "completely unable to move" a part of their body [1]. The most common causes of paralysis are stroke, spinal cord injury (SCI), and multiple sclerosis [1]. The etiologies of paralysis are summarized in Fig. 1.1. Paralysis is typically incurable due to the limited regenerative capacity of human CNS tissue. For example, in a database of 13,000 SCI patients, 46% had complete (motor and sensory) paralysis upon admission and 42% still had complete paralysis at discharge from rehabilitation [2]. Less than 1% of SCI patients obtain complete neurologic recovery after rehabilitation [2].

Limb loss currently affects 1 in 190 Americans [3]. The prevalence of limb loss by type and etiology is summarized in Table 1.1. Our inability to regrow limbs and the difficulties inherent in limb transplantation make limb loss a similarly incurable condition. In the absence of a cure, patients with paralysis or limb loss often use assistive technologies to augment their abilities as much as possible. Examples of these technologies include wheelchairs, prosthetic limbs, and communication interfaces. These technologies, while

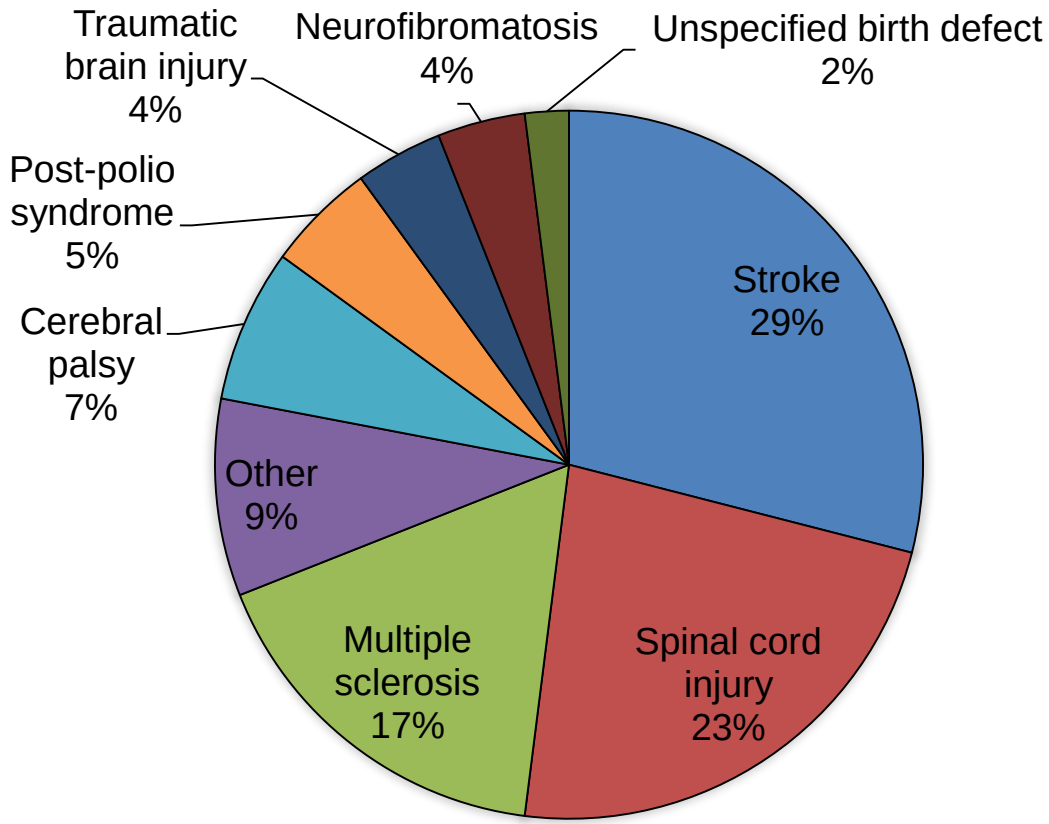

Fig. 1.1. Etiology of paralysis. Adapted from [1].

Table 1.1. Etiology of limb loss by type. Minor limb loss refers to loss of fingers or toes only. Estimated prevalence in the United States can be calculated by multiplying by 1,568,000. Derived from data in [3].

	All Types	**Major Lower**	**Minor Lower**	**Major Upper**	**Minor Upper**
All Etiologies	100.0%	39.7%	25.8%	2.6%	31.9%
Dysvascular Disease	54.0%	32.1%	19.3%	0.3%	2.2%
Trauma	44.9%	6.8%	6.4%	2.2%	29.6%
Cancer	1.1%	0.8%	0.1%	0.1%	0.1%

invaluable to patients, do not approach the exquisite capabilities of natural motor control. The field of brain-machine interfaces seeks to change that.

1.2 Brain-Machine Interfaces

Brain-machine interfaces (BMIs), also called brain-computer interfaces (BCIs), can give patients volitional control over prosthetic devices. As one example, BMIs can restore upper limb function in people with complete tetraplegia from SCI. To do so, an intracortical microelectrode array is placed in the patient's motor cortex in order to detect neuronal electrical signals. Then, the patient imagines moving their (paralyzed) arm. Neurons in the motor cortex of the patient's brain send signals using action potentials. In a healthy patient, these signals would propagate to neurons in the spinal cord, then muscles in the arm, and a movement would take place, but for a patient with SCI, the signals cannot travel down the spinal cord and no movement takes place. Instead, in this patient, the intracortical microelectrode array records neural activity, passes this information to a computer, and the computer interprets the signals and translates them into movement of a robotic arm. With practice, both the computer and the patient learn to communicate more efficiently with one another, ideally to the point that the patient can move the robotic arm as if it were their own.

BMIs of this sort have been successfully achieved in humans [4, 5] but have yet to enter widespread clinical use. Besides recording signals related to upper limb movement, BMIs have also been used in humans to collect speech information [6]. Investigators are also exploring the possibility of using signals from a BMI to control electrical stimulation of peripheral nerve or muscle tissue, causing specific muscles in the paralyzed arm or leg to

contract and avoiding the need for a robotic appendage [7].

BMIs can also function in the reverse direction, i.e., to send information directly into the brain by electrically stimulating neural tissue and inducing action potentials to occur. So far, this type of BMI has been used to provide a crude level of vision in humans [8]. BMIs could combine recording and stimulating functionality, allowing for a robotic arm with the ability to feel [9], or a memory prosthesis for patients with neurodegenerative diseases [10]. It is also important to note that the microelectrode arrays used to interface with the brain are very similar to devices used to interface with other parts of the body such as the cochlea [11] and the retina [12] to provide hearing/vision and peripheral nerves to record motor intent [13], induce somatosensation [14], and trigger skeletal [7] or sphincter muscle contraction [15]. Thus, hardware improvements in any of these applications have the potential to translate to the others.

The hardware used to interface with the brain varies according to the density of information needed to control the device. A binary yes/no signal roughly once per second is a sufficient data rate for patients to spell words letter by letter, and this low density of information can be obtained simply by placing electrodes on the scalp and recording large-scale neural oscillations [16]. Meanwhile, control of a multiple degree-of-freedom robotic arm requires hundreds of signals to be supplied continuously [17], which is obtained using microelectrode arrays implanted directly into cortical tissue. The tradeoff for obtaining a high density of neural information with a device implanted in cortical tissue is that the patient must undergo brain surgery and tolerate a foreign body in their brain, both of which pose risks to the patient. Electrocorticography (ECoG) or micro-electrocorticography devices, which rest on the surface of the brain, are seen as an intermediate between these

two paradigms in terms of information density and surgical risk [18].

The focus of this dissertation is on microelectrode arrays implanted into cortical brain tissue. These devices have the potential to extract the highest density of information and have the highest potential to restore complex abilities such as upper limb movement with high fidelity. At the same time, these devices also have the greatest potential to be influenced by biological events.

1.3 Intracortical Microelectrode Arrays

Intracortical microelectrode arrays generally fall into three design paradigms: microwires, planar silicon devices, and Utah Electrode Arrays (UEAs) (Fig. 1.2).

Microwires are the oldest and simplest design [19, 20] and are still used successfully in a wide variety of animals today. The design consists of wires with an electrically conductive core (e.g., tungsten) and an insulating coating (e.g., parylene-C). The tips of the wires are cut and sometimes sharpened. When inserted into brain tissue, electrical activity of neurons near the conductive tip can be recorded. A variety of materials and sizes have been used. Microwire electrodes can be assembled into arrays of microwires that are inserted all at once into brain tissue, or alternatively, into arrays that allow for individual positioning of microwires. Tucker Davis Technologies (Alachua, FL), MicroProbes (Gaithersburg, MD), FHC (Bowdoin, ME), and Plexon (Dallas, TX) sell microwire arrays, although some labs fabricate their own in-house [21-23].

Planar silicon or “Michigan” devices are created from silicon wafers using microfabrication techniques and can be designed to have recording sites not just at the tip, but anywhere along the length of the device [24, 25]. Planar silicon devices can also be

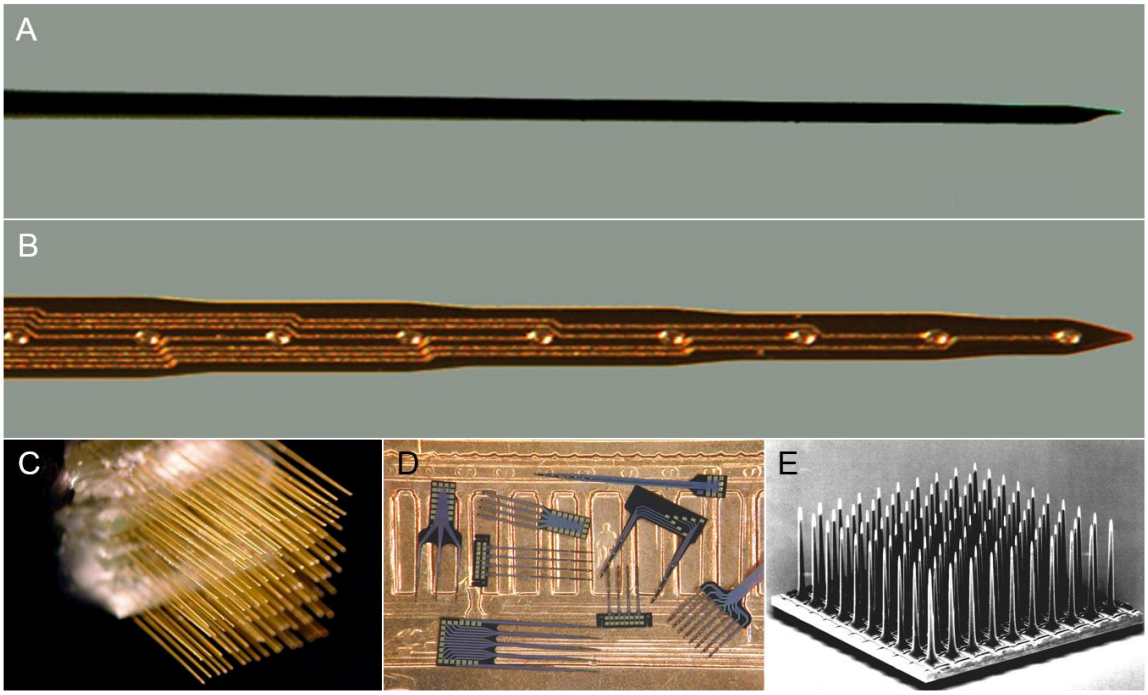

Fig. 1.2. Various designs of intracortical microelectrodes. (A) Single microwire electrode. (B) Single-shank planar silicon electrode. (C) Microwire array. (D) Multishank planar silicon electrodes, shown on top of a United States penny for scale. (E) Utah Electrode Array.

fabricated with multiple "shanks" with recording sites along the length of each shank, allowing the device to record from multiple locations in the brain at multiple depths. These can then in turn be stacked into a holder to record from a 3D volume of tissue. Planar silicon arrays are currently manufactured by NeuroNexus (Ann Arbor, MI) and FHC (Bowdoin, ME).

UEAs were developed at the University of Utah [26]. These devices are also fabricated from silicon wafers, but rather than creating the device on the surface of the wafer, a dicing saw is used to make a grid of deep cuts into the wafer, and then the square pillars that remain are chemically etched to form slender shafts. The tip of each shaft is able to record from nearby neurons, similar to a microwire array. The UEA is the only intracortical

microelectrode array that has been implanted chronically in humans [4, 5, 27]. Blackrock Microsystems (Salt Lake City, UT) currently manufactures devices of this design.

1.4 Recording Inconsistency

Intracortical microelectrode arrays will need to record neural signals from patients reliably for decades before they see widespread clinical use. A device that fails unexpectedly or that needs frequent replacement over time is clinically infeasible due to the risk and expense of brain surgery.

Examples of BMI performance multiple years after implantation of the microelectrode array exist for nonhuman primates [28-30] and humans [4, 27, 31]. Due to the effort and expense involved with training each subject, these studies have very small N (one, three, and two in [28-30], and one, two, and one in [4, 27, 31], respectively). Moreover, since the emphasis of such studies is on characterizing a working BMI, failures of any other subjects are not often discussed. Meanwhile, in studies where microelectrodes are used to simply record neural activity but not drive a BMI, it is feasible to use large cohorts of smaller animals and characterize device failure rates and longevity for the whole cohort. These large-N studies reveal that while microelectrodes can function for multiple years, the majority cease recording single unit action potentials much earlier, and those that do not fail typically experience unpredictable fluctuations and a gradual decrease in performance with time in mice [32], rats [33-36], guinea pigs [22], and cats [23, 37, 38].

Thus on the one hand, there are reports of successful BMI performance over multiple years in humans and nonhuman primates, and on the other, frequent failures and unpredictable performance in smaller animals. Two retrospective studies of work

performed in nonhuman primates help reconcile this discrepancy. Barrese et al. in 2013 compiled data from UEAs in 27 macaques over 17 years of experiments in the Donoghue lab [39]. This study reported failures (Fig. 1.3), fluctuations, and gradual decreases (Fig. 1.4) similar to studies in smaller animals. This study did not perform any histological analysis. A retrospective study by Schwarz et al. in 2014 compiled data from microwire arrays in eight rhesus monkeys over seven years of experiments [40]. This study did not provide data on reasons for terminating experiments with any of the subjects, did not say whether any animals were excluded due to early failures, and presented histology for only one animal. However, this study reported an overall higher degree of reliability and longevity than in most studies, albeit with similar fluctuations over time. These studies show that recording inconsistency is not unique to small animals – although it may be exacerbated in them – and that the high performance in BMI nonhuman primate studies

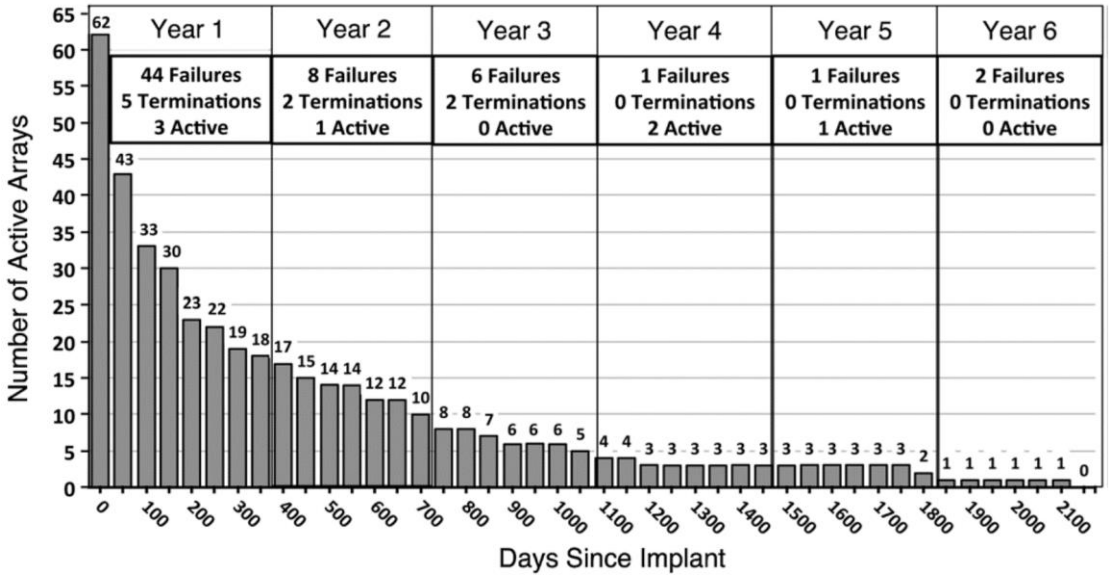

Fig. 1.3. Recording longevity of 62 UEAs implanted in 27 macaques, compiled retrospectively from 17 years of experiments. After one year, 17 of the initial 62 devices are still functional. A few devices were able to record for many years, however. Figure from [39].

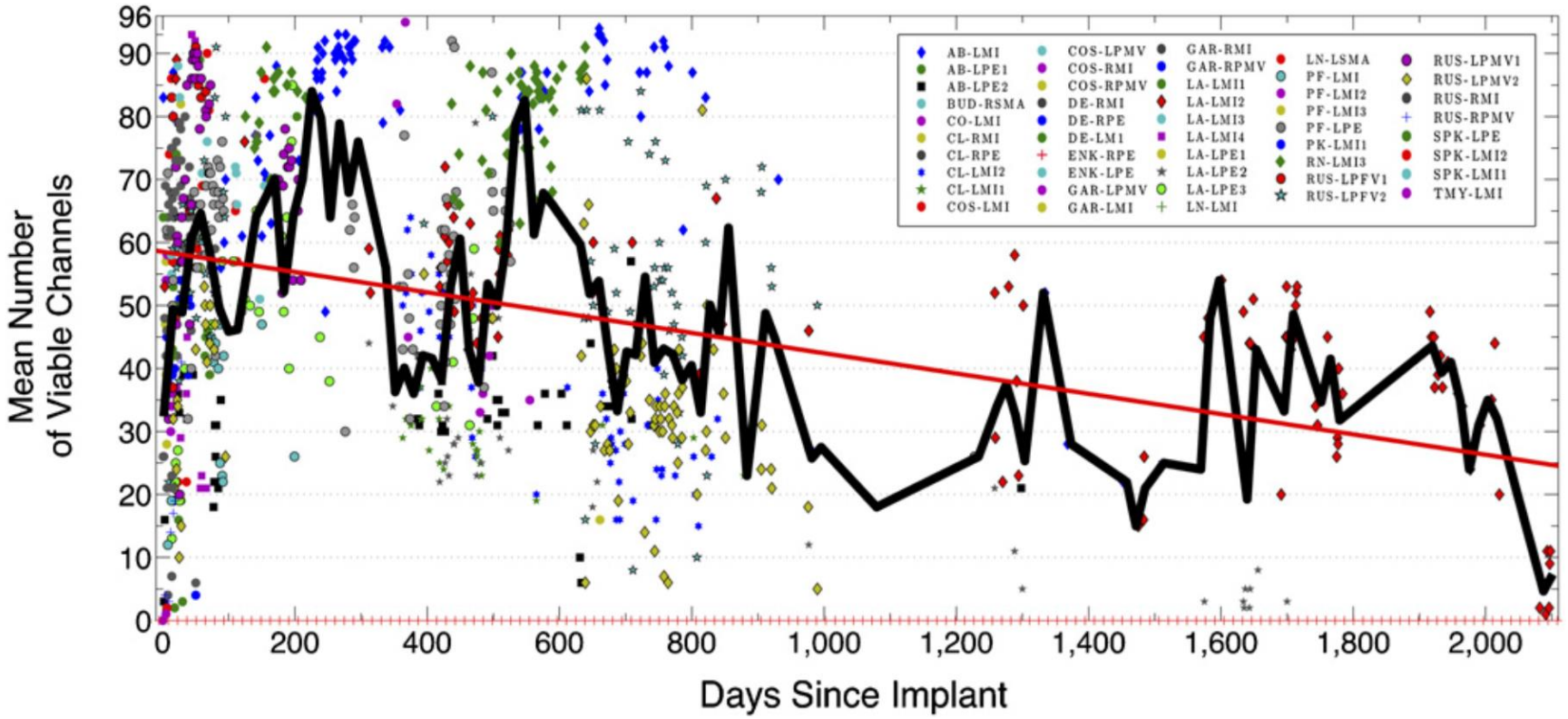

Fig. 1.4. Recording performance (number of electrodes able to record single unit action potentials) of 62 UEAs implanted in 27 macaques, compiled retrospectively from 17 years of experiments. Each of the shapes/colors of markers represent different arrays listed in the figure legend. The black line represents the average for all arrays in a 14-day bin. Bin boundaries are shown as red hatch marks on the horizontal axis. Red line represents a linear regression. Note the high degree of variability in performance between animals and over time, as well as the overall decline in performance. Figure from [39].

is likely partly explained by selection bias. Thus, recording inconsistency is considered a significant problem facing BMI development.

1.5 Mechanisms of Recording Inconsistency

A number of mechanisms have been proposed to explain recording inconsistency in intracortical microelectrode arrays. These mechanisms can be divided into two categories: device-related failure modes and biological failure modes.

Device-related failure modes include failures due to breakage or deterioration of the microelectrode itself. Detachment of the percutaneous connector from the skull is one common problem [22, 33, 39]. Breakdown of insulation materials, corrosion of electrode tip metal, and ingress of moisture into connector components have been reported [35, 36, 39]. The push toward wireless technology and advances in electrode materials and manufacturing techniques will likely reduce the rates of these failures.

Biological failure modes are a greater barrier to clinical usage since their mechanisms remain poorly understood. In order to record single unit action potentials, the recording site of a microelectrode must be within about 100 μm of a neuron's cell body when the neuron fires an action potential [41]. Therefore, if all neurons are killed within the first 100 μm, there will be no action potentials for the device to detect. Even if living neurons are present within 100 μm, if they become silenced by unfavorable extracellular conditions or lose connections to appropriate cortical circuits, the device will also fail to record useful action potentials. Another biological failure mode is if the device is pushed or pulled away from the cortical layers it is attempting to record from due to fibrotic tissue buildup under the array or settling of the array down into the brain, which has been reported in cats [37,

38] and nonhuman primates [39]. Although it is currently unknown which of these processes are most responsible for recording inconsistency, all of these processes are linked to the foreign body response (FBR).

1.6 The Foreign Body Response

A brief overview of the events of the FBR to medical devices in general will be provided here.

First, the implantation of a medical device necessarily involves tissue injury in order to position it within the target tissue [42]. This severs blood vessels, releasing blood into the extracellular space. The coagulation cascade and platelet aggregation stop bleeding and restore homeostasis [43]. Cells close to the injury may apoptose and/or necrose in response to the mechanical injury itself or to the altered extracellular milieu. Foreign pathogens may also be introduced by the injury.

Molecules from platelets, damaged blood vessels, apoptotic/necrotic cells, foreign pathogens, and the complement cascade [44] all trigger the multifaceted biological response known as inflammation. Mast cells, dendritic cells, and tissue-resident macrophages in the injured tissue are sensitive to these signals and become activated, releasing additional cytokines and signaling molecules [42, 45]. Molecules such as prostaglandins, histamines, and nitric oxide increase local blood flow and blood vessel permeability, causing the clinical hallmarks of inflammation: swelling, redness, heat, and pain [46]. Other cytokines attract neutrophils in the bloodstream to enter the tissue and phagocytize bacteria [47]. Neutrophils arrive within hours, and are characteristic of acute inflammation. After a few days, infiltrating lymphocytes and monocytes become more

predominant and the tissue transitions into chronic inflammation [47]. Once in tissue, monocytes mature into macrophages, which specialize in phagocytizing cellular debris and pathogens. Neutrophils and macrophages produce reactive oxygen species (ROS) that assist in killing and breaking down pathogens [48]. Neutrophils, lymphocytes, and macrophages not only respond to proinflammatory cytokines but produce their own proinflammatory cytokines, further escalating inflammation [42]. They are also capable of secreting anti-inflammatory cytokines, which are important for modulating the types and activation states of immune cells present and for preventing an excessive response. Anti-inflammatory cytokines assist in transitioning to the final stages of wound healing, where angiogenesis, proliferation of non-immune cells, and remodeling of the extracellular matrix (ECM) restore the tissue to its original state or to a stable scar [49, 50].

When an indwelling device is present, however, complement proteins, immunoglobulins, and other proteins interacting with the device's surface provide a continuous inflammatory stimulus [44]. Macrophages experience frustrated phagocytosis if the device is resistant to oxidative and enzymatic digestion and is too large to engulf. This causes them to enter activation states normally employed against multicellular parasites, and to fuse into large, multinucleated foreign body giant cells [51]. The nearby tissue remains in a persistently inflamed state, and often develops a fibrous capsule between the device/macrophages and the tissue [42]. Persistent inflammation and fibrous capsule formation can be problematic for the health of the patient and the functioning of the device in a wide variety of medical devices [42].

1.7 The FBR to Intracortical Microelectrodes

In the decades since the first report by Collias and Manuelidis in 1957 [52], dozens of studies have been published describing the implantation injury and FBR to a variety of designs of intracortical microelectrodes in many different animal models [52-69]. The typical distribution of FBR biomarkers are summarized in Fig. 1.5 and discussed below.

The implantation of the microelectrode into the brain severs blood vessels, causing bleeding and edema [63, 69, 70]. If a device with one or a few shanks is inserted and then immediately withdrawn, this initial injury or "stab wound" is small enough to be able to heal over the course of about four weeks, potentially with some residual astrocytic scarring, or astrogliosis, but little other signs of inflammation [53, 59, 71, 72]. In healthy tissue, astrocytes participate in the maintenance of homeostasis, regulation of vascular function, modulation of neuronal synapses, and information transmission via intracellular calcium waves [73-75]. In response to inflammation, astrocytes proliferate, thicken their processes, produce additional cytoskeletal filaments such as glial fibrillary acidic protein (GFAP), and form scar tissue that can persist after the initial inflammatory stimulus has subsided [76]. To date, the long-term result of a stab wound using a large, complex array like the UEA is unknown, and will be explored in Chapters 2-3.

In contrast to a stab wound, when the microelectrode is left indwelling in the brain, classic hallmarks of the FBR develop over the first few weeks of implantation and stabilize roughly eight weeks after implantation. Immediately adjacent to the device, a dense layer of activated macrophages forms [53-59]. Some of these cells appear to come from the brain's population of tissue-resident macrophages, microglia, but most are from blood-borne monocytes that have migrated into the area and matured into macrophages [77].

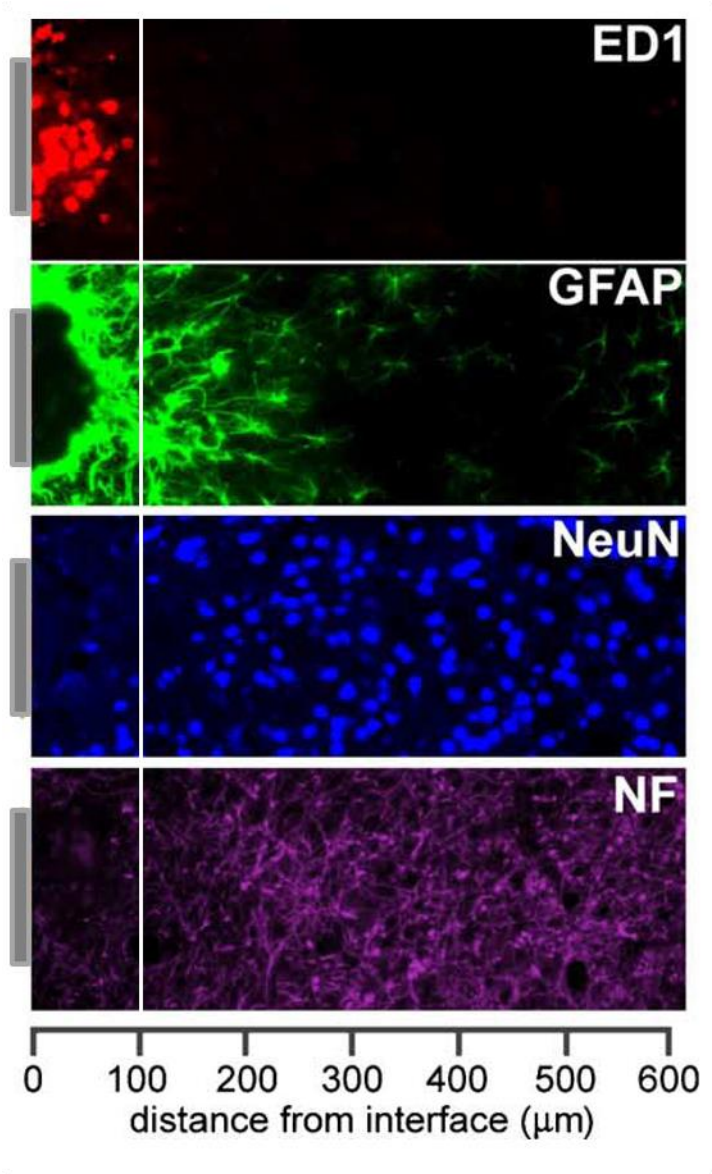

Fig. 1.5. Typical distribution of FBR biomarkers surrounding a single-shank planar silicon microelectrode. Images are representative horizontal sections of rat brain tissue four weeks after implantation. Activated macrophages (ED-1/CD68, red) are visible at the device-tissue interface. Surrounding the activated macrophage layer, hypertrophic astrocytes (GFAP, green) and reductions in neuronal nuclei (NeuN, blue) and neuronal processes (NF, magenta) are visible. The white line denotes the device's 100 μm recording range. Adapted from [53].

These cells are typically identified using antibodies against ionized calcium-binding adapter molecule 1 (IBA-1), which is a calcium handling protein that is expressed specifically in macrophages (including microglia). Their activated state is usually identified using antibodies against cluster of differentiation 68 (CD68) (also known as ED-1), which is a glycoprotein expressed at high levels in the lysosomes of macrophages that are actively phagocytizing material. Activated macrophages have also been found adhered to devices withdrawn from the brain [53-55]. In most of these reports, there are more activated macrophages in the brain tissue than on the withdrawn devices. Activated macrophages on explanted devices have been cultured *in vitro* and found to release the cytokines tumor necrosis factor alpha (TNF-α) and monocyte chemotactic protein 1 (MCP-1) (Fig. 1.6) [53].

Surrounding the activated macrophage layer is a region of astrogliosis and decreased neuronal nuclei and processes [52-62, 67, 78]. GFAP is the most common antibody target for identifying astrogliosis. Antibodies against various targets are used to identify neurons, including neuronal nuclei (NeuN) for neuronal cell nuclei, neurofilament 200 (NF200) for axons, and neurofilament 160 (NF160) for axons and dendrites. Axons in this region have also been reported to become demyelinated, as indicated by a lack of immunoreactivity for myelin markers in areas positive for axons [56].

Blood plasma proteins such as immunoglobulin G (IgG) are typically excluded from the brain parenchyma by the blood-brain barrier (BBB), but when the BBB is compromised near an inflammatory stimulus, these proteins can leak out into brain tissue. IgG, along with other plasma proteins such as fibrinogen, can trigger cell signaling cascades in neurons and astrocytes that can lead to morphological changes and apoptosis. These

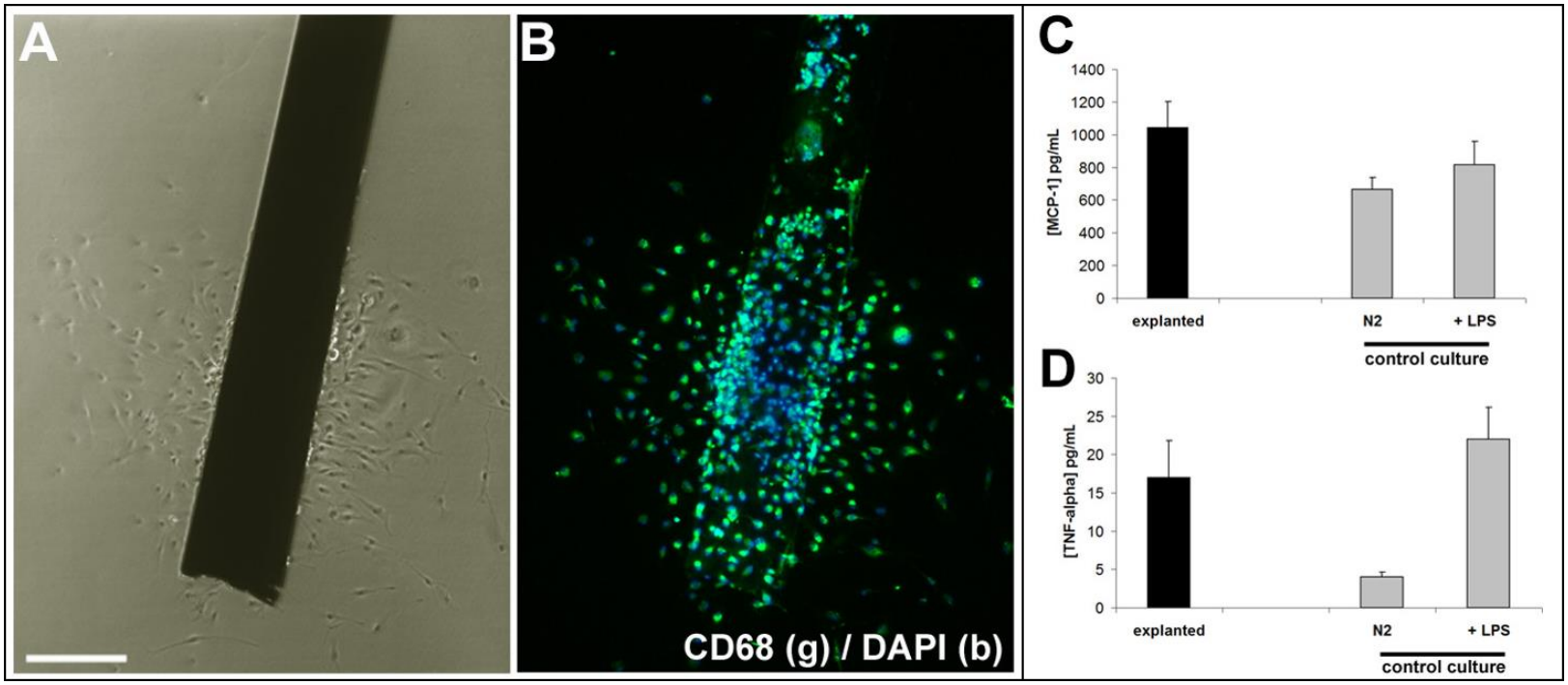

Fig. 1.6. Explanted planar silicon microelectrode cultured *in vitro* and labeled for activated macrophages (CD68) and cell nuclei (DAPI), shown under brightfield (A) and fluorescent (B) illumination. (C-D) Macrophages on explanted devices released MCP-1 and TNF-α at levels similar to positive control cultures of macrophages exposed to lipopolysaccharide (LPS). Adapted from [53].

plasma proteins, as well as changes in extracellular ionic concentrations that would be expected to coincide with their presence, may lead to neuronal degeneration and dysfunction [79].

Most of the existing literature on the FBR to intracortical microelectrode arrays has been conducted in the rat using simple devices with one or a few penetrating features. Meanwhile, the only device used clinically in humans is the much larger and more complex UEA. Chapters 2-3 make a unique contribution to this literature by providing the first in-depth characterization of the FBR to a large, complex, clinically relevant device such as the UEA in a rat model.

1.8 Relationships between the FBR and Recording Performance

Based on the literature described thus far, the FBR's causative role in recording inconsistency appears to be an attractive hypothesis. In recent years, investigators have begun the process of directly testing this hypothesis. If the FBR is responsible for recording inconsistency, it may be possible to directly correlate one or more features of the FBR with recording performance. These correlations may exist on an animal-to-animal basis (i.e., animals with a more severe FBR have reduced recording performance) or on an electrode-to-electrode basis (i.e., specific electrodes on an electrode array have a more severe FBR and reduced recording performance). Four studies, to our knowledge, have taken this approach of quantifying features of the FBR and correlating them with recording performance within a single cohort of animals.

The earliest study was by Freire et al. in 2011 from the Nicolelis lab [34]. In this study, 24 rats were implanted with microwire arrays, recorded from weekly, and sacrificed at

various time points from 1-24 weeks. Recording performance was highly variable across animals and time, but generally decreased with time. Immunohistochemical labeling of activated macrophages (CD68), apoptosis (caspase-3), calcium-dependent neural activity (early growth response protein 1 or EGR-1), neural activity in nitric oxide-producing neurons (nicotinamide adenine dinucleotide hydrogen phosphate diaphorase or NADPH-d), and metabolic activity (cytochrome oxidase) were quantified in a 141x141 μm square region around each electrode and correlated with recording performance (median action potential firing rates) from each week of recording. The authors concluded that all of these markers correlated well, but their data show strong correlations some weeks and weak correlations other weeks, and the patterns in timing are not consistent across animal groupings (Fig. 1.7). They also report that NADPH-d and cytochrome oxidase levels near electrodes were not statistically different from contralateral, unimplanted tissue, which would seem to undermine the idea that these markers could be used to understand biological mechanisms of recording inconsistency. Moreover, their quantification methods are atypical in the field and were inadequately described in the methods. Their paper provides an excellent example of recording inconsistency in rats, but does not provide useful data regarding the correlation of the FBR and recording performance.

Prasad et al. in the Sanchez lab in 2012 implanted microwire arrays in 25 rats for up to nine months [35]. The investigators immunohistochemically labeled macrophages (IBA-1), activated macrophages (CD68 and OX-6), and ferritin. Ferritin is an iron storage protein that is expressed in microglia when the BBB has been compromised and iron sequestration is needed. They also analyzed scanning electron microscopy images of electrode tips before and after implantation and measured electrode impedance at each

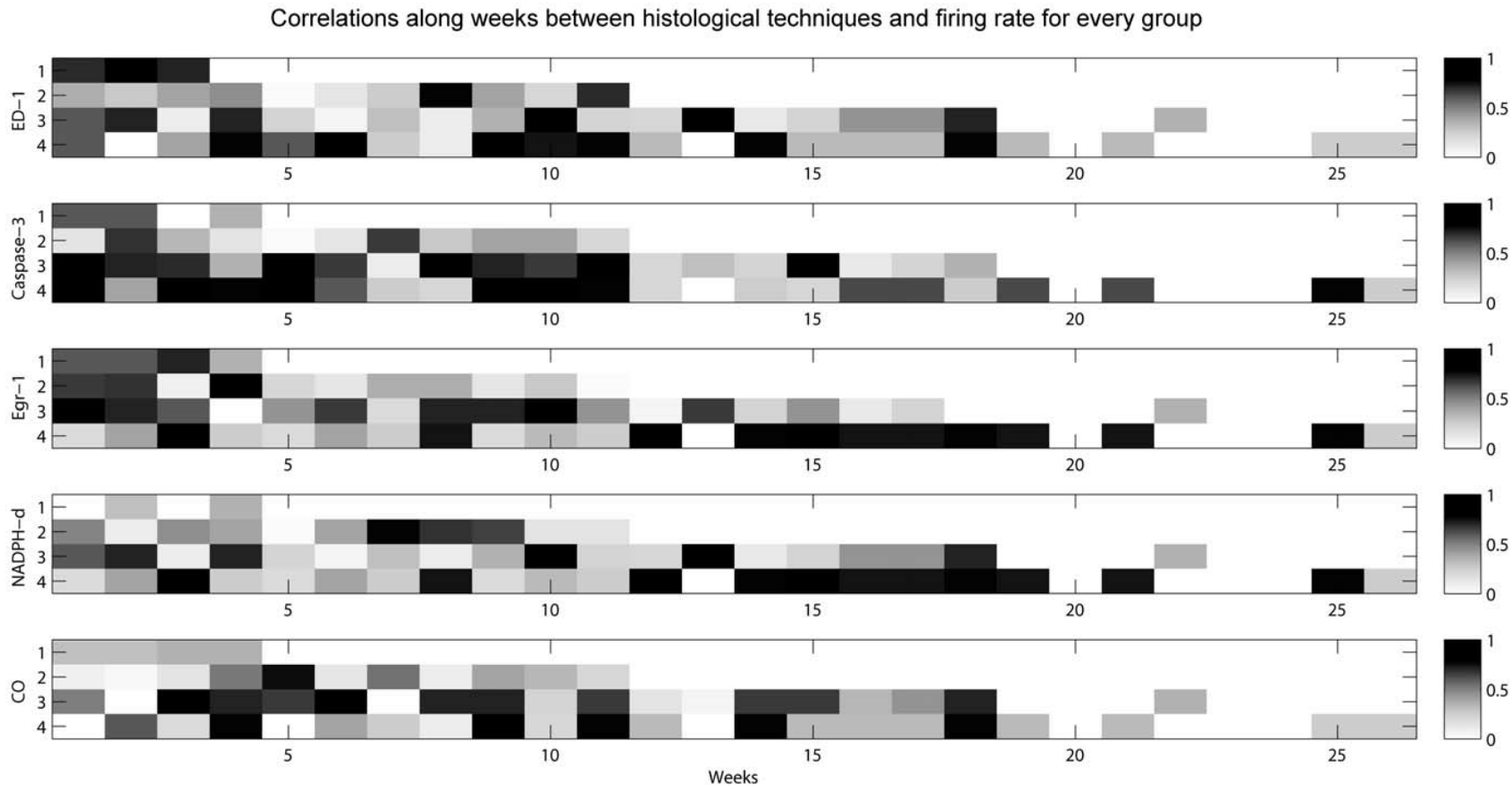

Fig. 1.7. Correlations of recording performance with five different biomarkers of the FBR. The horizontal axis is time in weeks. Darker squares represent higher nonparametric Spearman correlation coefficient values (which ranges from 0 to 1 based on the strength of correlation, regardless of whether the correlation is positive or negative). 1, 2, 3, and 4 refer to the different times of sacrifice. For example, for rats sacrificed at week 4, activated macrophages (ED-1) were highly correlated with performance in the first 3 weeks, and very poorly correlated in week 4. Reprinted from [34] under a Creative Commons Attribution license, © 2011 Freire M.A.M., Morya E., Faber J., Santos J.R., Guimarares J.S., Lemos N.A.M., Sameshima K., Preira A., Ribeiro S., and Nicolelis M.A.L.

recording session. In addition, they quantified blood serum and cerebrospinal fluid (CSF) levels of phosphorylated axonal neurofilament subunit H (pNF-H), which is a byproduct of axonal injury. The investigators did not present any statistical analysis of any of these metrics and instead relied on detailed descriptive qualitative analysis. They found that extremely high or low impedance values were usually related to degradation of electrode materials. They also found that high levels of pNF-H tended to correspond to reduced electrode performance. In their histological analysis, ferritin tended to correspond to reduced performance, but the various macrophage markers did not appear to have any relationship to recording performance. They also noted that greater amounts of bleeding at surgery led to reduced performance. Considering all of these factors together, the authors came to the conclusion that consistent recording performance depends on a combination of minimal bleeding during surgery, good electrode material integrity, and low levels of axonal injury over the duration of the experiment. Their conclusions are somewhat difficult to confirm, however, due to their presentation of histological quantification data in a table of 200 raw values and their presentation of combined analysis as a 3D scatterplot.

In 2013, Saxena et al. in the Bellamkonda lab implanted 56 rats with either planar silicon or microwire electrode arrays for three days or 16 weeks [80]. Most of the paper was focused on comparing the FBR and performance of these two different electrode designs. They found that microwire arrays were associated with reduced BBB dysfunction, increased matrix metalloproteinases 2 and 9 (MMP-2 and MMP-9), and increased performance relative to the planar silicon devices. However, since these are different devices, factors related to the device instead of the FBR could have been responsible for

the difference in recording performance. Therefore, within the microwire array cohort, they selected the animal with the highest performance and the animal with the lowest performance and found higher levels of IgG, reduced neuronal nuclei, and increased transcript levels for proinflammatory cytokines. Not discussed was the additional presence of a large lesion in the brain near half of the electrodes in the low-performing animal. While this report supports the hypothesis that the FBR and recording performance are related, comparing just two animals is not statistically convincing.

Prasad et al. in 2014 published a study similar in design to their 2012 study except with parylene-C insulated platinum-iridium microwires instead of polyimide insulated tungsten [36]. They reported that platinum-iridium was more resistant to corrosion than tungsten, though the insulation material still degraded. They did not measure serum or CSF pNF-H levels. They found similar relationships between impedance, recording performance, histological markers, and surgical bleeding as in their previous study; that is, high recording performance correlated with moderate electrode impedance, low levels of ferritin, and a low degree of bleeding at implantation. Their conclusions are more easily confirmed in this study, as shown in Fig. 1.8. There was no statistical analysis of correlation and the study was smaller (N = 12) than their previous study, but this study is perhaps the strongest existing evidence that the FBR is correlated with recording performance.

In Chapters 2-3 in this work, we employ an approach similar to these four papers, but avoid their shortcomings by working within a single cohort, using established quantitative immunohistochemical techniques [53-58], and performing rigorous statistical tests.

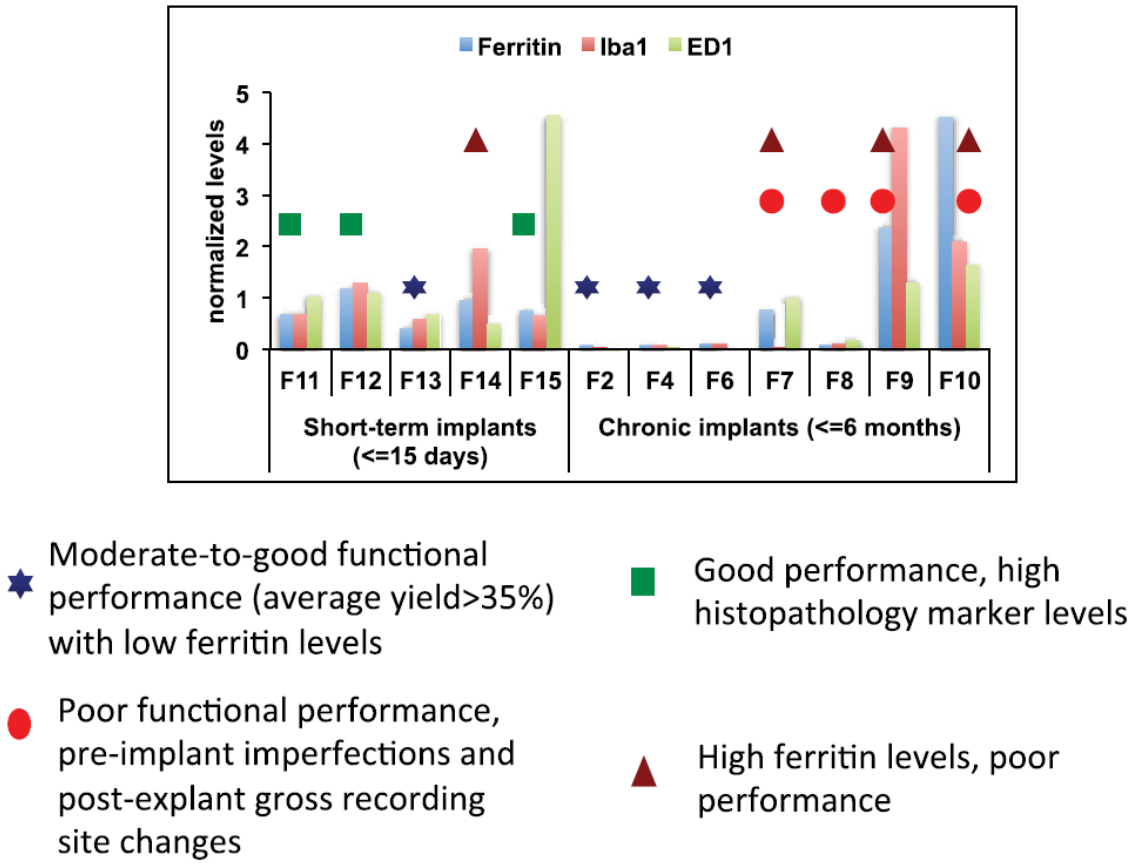

Fig. 1.8. Correlations of recording performance with three different biomarkers of the FBR. Individual animals are shown on the horizontal axis and grouped by implant duration. Normalized levels of the biomarkers are shown on the vertical axis. Symbols correspond to the authors' notes on performance and device materials degradation in relation to the biomarker levels. Reprinted from [36] under a Creative Commons Attribution license, © 2014 Prasad A., Xue Q.-S., Dieme R., Sankar V., Mayrand R.C., Nishida T., Streit W.J., and Sanchez J.C.

1.9 Aging and the FBR

Patients with paralysis and limb loss span a wide range of ages. The age distributions for people with paralysis and limb loss are shown in Figs. 1.9 and 1.10. Notably, 33.5% of individuals with paralysis are over 60 years old [1], and 42% of individuals with limb loss are over 65 [3]. Furthermore, young patients receiving a BMI are likely to eventually reach old age. A 20-year-old patient with high tetraplegia due to spinal cord injury who survives the first year after injury has a life expectancy of 57 years [81].

There is a remarkable lack of studies directly comparing the FBR to medical devices in young and aged animals [82]. However, numerous studies have examined the effects of aging on the immune system, the brain, and the brain's responses to injury and inflammation. These studies lead one to expect that the implantation injury and FBR would be increased when a microelectrode array is implanted into the aged brain.

Immunosenescence refers to the changes that occur in the immune system during normal aging. Numbers of naïve B and T lymphocytes are decreased and neutrophils and macrophages have a reduced capacity for phagocytosis and ROS production, decreasing the immune system's effectiveness at clearing pathogens [83, 84]. The influence of aging on cell signaling pathways is complex [83, 84], having the somewhat paradoxical effects of decreasing immune effectiveness but increasing overall levels of proinflammatory cytokines such as interleukin 1β (IL-1β) [85], interleukin 6 (IL-6) [86-89], and tumor necrosis factor alpha (TNF-α) [88, 90-93]. Decreased immune effectiveness and increased proinflammatory cytokines due to immunosenescence are believed to play a role in type 2 diabetes [90], atherosclerosis [93, 94], Alzheimer's [95], Parkinson's [88], osteoporosis [96], and delayed wound healing [97], in a multifaceted process termed "inflamm-aging"

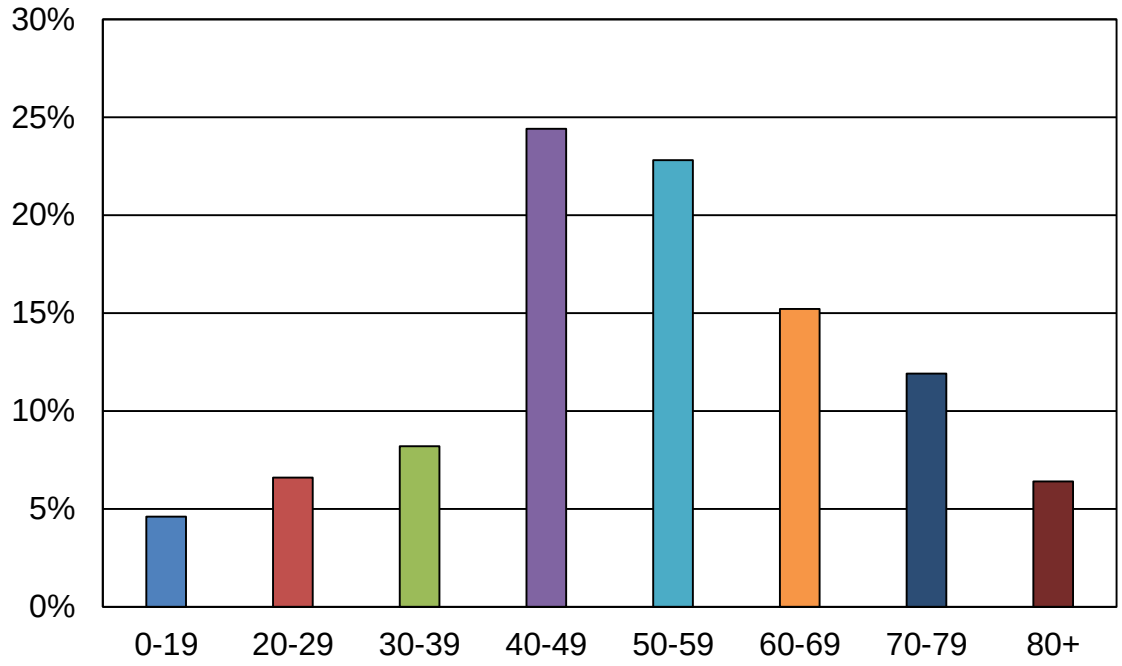

Fig. 1.9. Age distribution of people with paralysis. Adapted from [1].

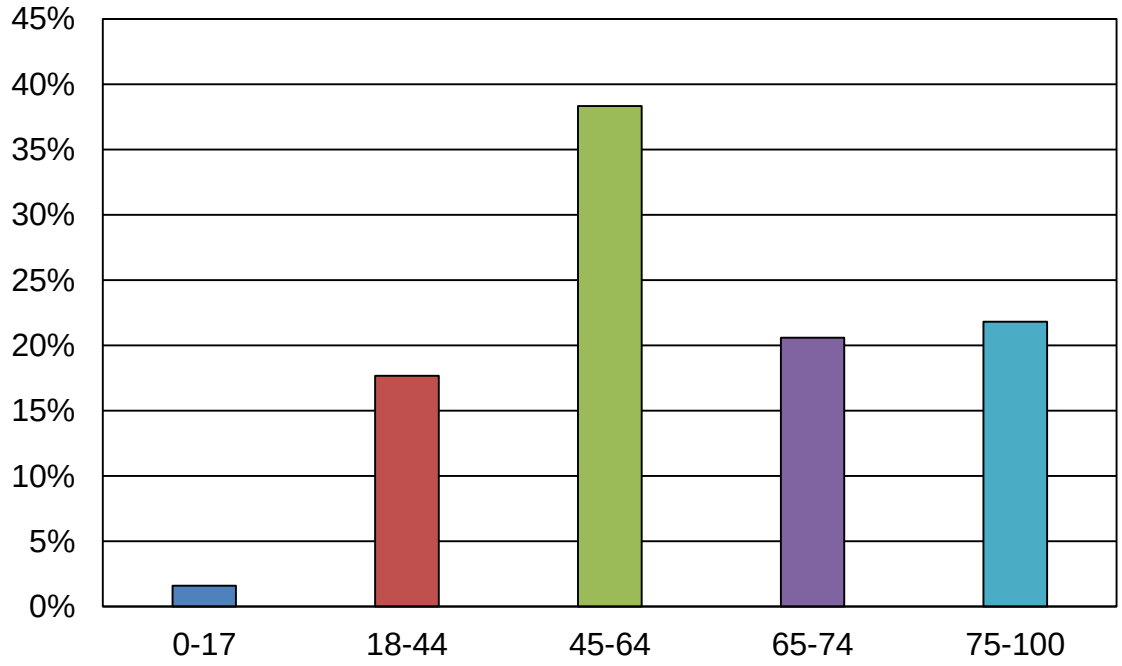

Fig. 1.10. Age distribution of people with limb loss. Derived from data in [3].

[98].

Aging also affects the brain. Microglia acquire a more reactive phenotype [99]. Their morphology becomes less ramified and more amoeboid [100-102]. They express increased markers of activation such as major histocompatibility complex (MHC) class II, cluster of differentiation 45 (CD45), and CD68 [101-103]. They also produce higher levels of proinflammatory cytokines such as IL-1β, IL-6, and TNF-α [100, 103, 104]. Astrocytes undergo changes as well, becoming more numerous and hypertrophic [105]. Mild neuronal cell death and reductions in dendrites and synapses occur naturally [106]. The risk of developing neurodegenerative diseases such as Alzheimer's [107] and Parkinson's [108] disease increases dramatically with aging.

Immunosenescence and the aging of the brain affect the brain's ability to respond to injuries. Aged patients have poorer clinical outcomes following ischemic stroke [109], traumatic brain injury [110], and aneurysmal subarachnoid hemorrhage [111]. Rodent models of brain injury show increased neural tissue loss following experimental brain injuries in aged rodents [112, 113].

Due to these factors, the injury caused by microelectrode array implantation may be greater in aged patients. Furthermore, the increases in proinflammatory cytokines, reactive microglial phenotypes, and neurodegeneration may exacerbate the neuroinflammatory sequelae associated with indwelling microelectrodes. However, no studies to our knowledge have examined the FBR to microelectrodes in aged animals. Fig. 1.11 shows the ages of rats used in 41 studies of the FBR to microelectrodes in the rat brain. The preference for young adult rats in these studies is likely to save costs.

In humans, it is known that recording from aged patients is possible. The ages of

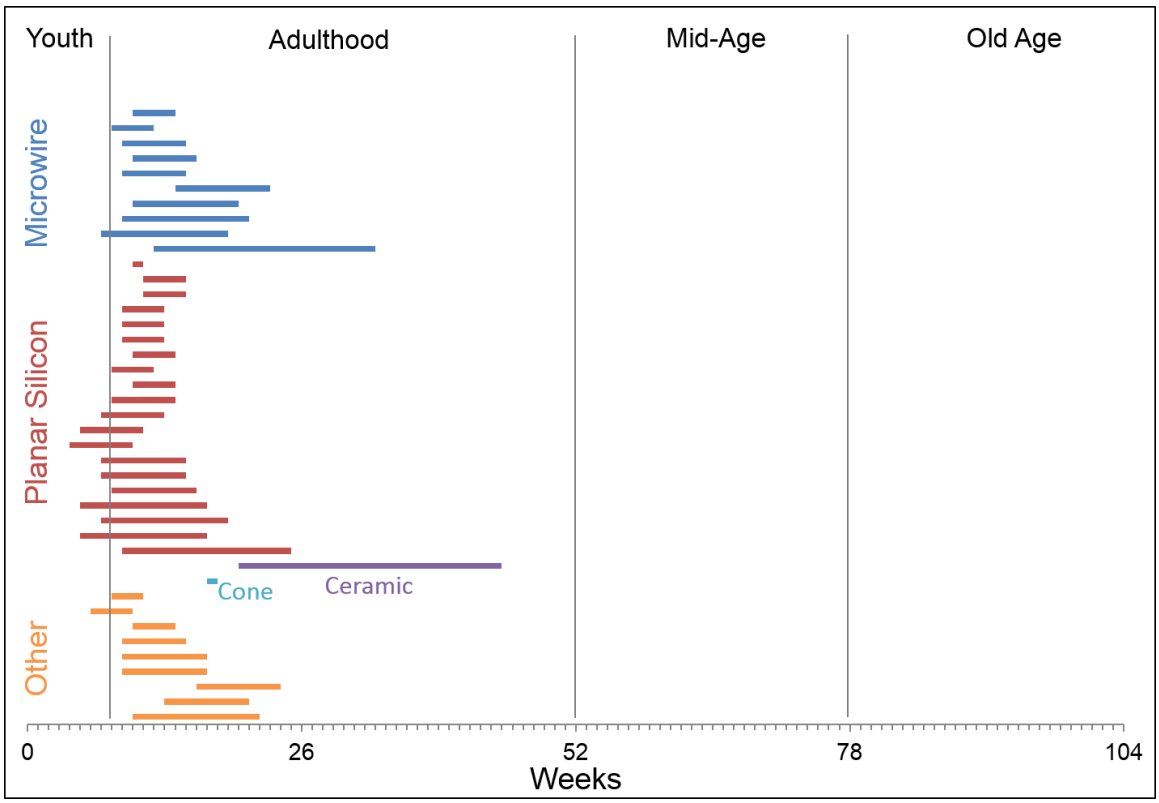

Fig. 1.11. Ages of rats used in 41 studies of the FBR to microelectrodes in the rat brain. The vast majority of studies used rats in early adulthood and no studies used rats of mid-age or old age.

subjects in published reports of BMIs in humans are 25 [27], 58 [4, 31], 66 [4], and 52 [5]. Since so few subjects have received BMIs so far, it is not known whether there are systematic differences in the recording performance of microelectrodes in aged versus young humans. The FBR to microelectrodes has not yet been evaluated in human patients.

The closest available literature, then, is arguably that on deep brain stimulation (DBS) electrodes. DBS electrodes are larger, single-shank devices implanted into deep brain areas as a treatment for drug-unresponsive Parkinson's disease. DBS electrodes are associated with increased rates of complications [114], somewhat decreased clinical benefit [115-117], and increased rates of cognitive and behavioral impairments [117] in aged patients.

We are not aware of any studies comparing the FBR to DBS electrodes in young and aged patients.

Based on existing literature regarding immunosenescence, the aging of the brain, clinical outcomes following brain injury, and clinical data on DBS electrodes, it is likely that the implantation injury and FBR to intracortical microelectrodes is exacerbated in aged animals. The literature discussed in the previous section furthermore suggests that increased injury and FBR would likely lead to reduced performance. Understanding whether this is the case – and if so, why – may lead to development of strategies that improve microelectrode performance in aged subjects. In Chapter 3, we present the first study of intracortical microelectrodes in aged animals.

1.10 Strategies to Reduce the FBR to Intracortical Microelectrodes

Numerous investigators began developing ways to reduce the FBR to intracortical microelectrodes even before the correlation studies reviewed in Chapter 1.8. A wide variety of strategies have been employed with varying degrees of success. Here, we review studies which implanted microelectrodes into cohorts of animals ($N \geq 3$) for at least two weeks and compared the FBR and/or recording performance versus controls. All of these studies were performed in rats unless otherwise noted. All histological comparisons were quantitative unless otherwise noted.

1.10.1 The Effect of Materials

The earliest studies focused on the choice of materials implanted in the brain. These studies found that silver [60, 71, 118-120], copper [60, 71, 119, 121], iron [60, 71], and

room temperature vulcanization silicone [60] were unsuitable due to their toxicity in brain tissue. Meanwhile gold, platinum, tantalum, tungsten, stainless steel, nichrome, iridium, silicon, and a wide range of insulating polymers all resulted in relatively similar FBRs [60, 71, 118-120, 122-124]. These studies were performed in a variety of small animals. It appeared most solid, chemically-inert, non-cytotoxic materials created a similar FBR, and that reducing the FBR below this level would likely require more sophisticated approaches.

1.10.2 The Effect of Coatings

Investigators have attached bioactive molecules to microelectrodes in order to reduce the FBR and improve neuronal proximity. He et al. in 2006 coated planar silicon microelectrodes with a nanoscale layer of the ECM protein laminin-1 [125]. They found an increase in activated macrophages one day after implantation and slightly decreased activated macrophages and astrogliosis four weeks after implantation. Neuronal cell density near the microelectrodes were similar. He et al. in 2007 attached the anti-inflammatory peptide α-melanocyte-stimulating hormone to planar silicon microelectrodes and reported decreased activated macrophages one and four weeks after implantation and decreased astrogliosis at four weeks [126]. Azemi et al. in 2011 coated planar silicon microelectrodes with the transmembrane protein L1, which mediates axonal growth and neuronal migration and survival [127]. They reported that L1-coated microelectrodes had increased numbers of neuronal cell bodies, increased axons, decreased astrogliosis, and decreased activated macrophages at all time points examined (one, four, and eight weeks). These studies implanted 3-4 animals per time point. A remaining question is whether the bioactivity of the various attached molecules was responsible for the improvements or

some other aspect of the coating, since the controls were uncoated devices.

Other investigators have coated microelectrodes with thin (< 1 μm) hydrogel coatings to reduce protein adsorption and cell adhesion. Lu et al. in 2009 coated 1 mm diameter polydimethylsiloxane rods with a poly(vinyl alcohol)/poly(acrylic acid) interpenetrating network polymer and found reduced astrogliosis six weeks after implantation [128]. They did not characterize the hydrogel's thickness, but based on their methods, it was likely thin. Rao et al. in 2012 coated polydimethylsiloxane rods with copolymer polyurethane and poly(ethylene glycol) (PEG) and reported reduced astrogliosis and increased numbers of neurons six weeks after implantation [129]. Gutowski et al. in 2014 applied an approximately 60 nm thick layer of copolymer poly(N-isopropylacrylamide) and acrylic acid (pNIPAm-co-AAc) crosslinked with PEG to planar silicon microelectrodes [130]. They reported reductions in astrogliosis and, unfortunately, reductions in neuronal cell bodies 24 weeks after implantation. Lee et al. in 2015 electrochemically deposited a 20-40 nm thick coating of poly(pyrrole-hyaluronic acid) to the recording sites of planar silicon microelectrodes and to the entire surface of uninsulated iridium microwires [131]. They found reduced astrogliosis three weeks after implantation around the microwires only. Thus, thin hydrogel coatings appear to have positive effects in some cases.

Thicker hydrogel coatings have also been employed. Lind et al. in 2010 compared microwire bundles coated in a thin layer of gelatin to microwire bundles embedded in a 300 μm diameter gelatin needle [132]. They found reduced activated macrophages around the gelatin needles one week after implantation, but no difference in activated macrophages or astrogliosis after six weeks. They also found that gelatin needles without microwire bundles produced less (or often no) astrogliosis compared to stab wounds with metal

needles of the same diameter, suggesting that thick gelatin coatings may assist in reducing the injury of implantation. Skousen et al. in 2014 coated planar silicon microelectrodes with a 400 μm thick layer of alginate and found reduced macrophages, activated macrophages, astrogliosis, and BBB leakage and increased neuronal cell bodies near the thickly-coated microelectrodes 16 weeks after implantation [58]. The investigators hypothesized that the hydrogel's permeability to proinflammatory cytokines was responsible for the improvements, a mechanism of action that will be discussed in greater detail in Chapter 1.11. Shen et al. in 2015 compared planar polydimethylsiloxane (PDMS) microelectrodes to thin parylene microelectrodes embedded in collagen and Matrigel, a commercially-available ECM product [133]. They reported reduced astrogliosis, reduced chondroitin sulfate proteoglycan (CSPG), and increased numbers of neurons near the ECM devices 16 weeks after implantation. Thick hydrogel coatings appear to be an effective approach for reducing the FBR, although they may require some redesign of the device.

1.10.3 The Effect of Systemically-Administered Drugs

Systemic pharmacological interventions have also been explored. Spataro et al. in 2005 administered the anti-inflammatory drug dexamethasone once or once per day for six days following implantation of a planar silicon microelectrode [66]. They reported qualitatively decreased astrogliosis versus controls for both drug regimes one and six weeks after implantation, but also observed qualitatively increased numbers of macrophages and increased laminin in blood vessels. Rennaker et al. in 2007 administered minocycline, an antibiotic with anti-inflammatory and neuroprotective properties, in the animals' drinking water two days prior and five days following implantation of microwire arrays [134]. They

found reduced astrogliosis one and four weeks after implantation as well as improved longevity of recording performance. Potter et al. in 2013 administered the antioxidant resveratrol the day before and during implantation of planar silicon microelectrodes [135]. They reported increased numbers of neurons, increased levels of the antioxidant enzyme catalase, decreased ROS, decreased BBB leakage, and decreased levels of toll-like receptor 4 (a marker of immune activation) two weeks after implantation, but not at four weeks. Meanwhile, they found decreased macrophages, decreased activated macrophages, decreased astrogliosis, and decreased cell nuclei at four weeks, but not at two weeks. Degenerating neurons (identified by Fluorojade-C) were decreased at both two and four weeks after implantation. Potter-Baker et al. in 2015 followed up on their previous work by administering daily injections of resveratrol and reported decreased ROS and decreased BBB leakage at two weeks, but not at 16 weeks after implantation [136]. They reported no difference in activated macrophages or numbers of neurons, but reported qualitatively decreased neurodegeneration at 16 weeks. Interestingly, daily saline injections decreased ROS but increased BBB leakage at two weeks.

Genetic knockout experiments have been conducted to identify targets for pharmacological intervention. Sawyer et al. in 2014 implanted planar silicon microelectrodes into MCP-1 knockout mice and reported increased numbers of neurons at two and eight weeks and decreased astrogliosis, BBB leakage, and macrophages at eight weeks [137]. They also found that daily injections of RS 102895, an antagonist of the MCP-1 receptor chemokine (C-C motif) receptor 2 (CCR2), increased numbers of neurons and decreased macrophages two weeks after implantation. Kozai et al. in 2014 implanted planar silicon microelectrodes into caspase 1 knockout mice [138]. Caspase 1 is required

for production of IL-1β and also becomes upregulated during neuronal cell death and degeneration. They found improved single unit recording performance in the knockout mice over a six-month experiment.

Systemically-administered drugs are clearly able to have an impact on the FBR and require no redesign of the microelectrode array. However, benefits will have to be weighed against side effects if these drugs are to be used in humans.

1.10.4 The Effect of Local Drug Delivery

Drug delivery close to the device-tissue interface has been pursued in order to increase local drug concentrations and avoid systemic side effects. Purcell et al. in 2009 injected the cell cycle inhibitor flavopiridol into the lateral ventricles at the time of implantation of planar silicon microelectrodes and found that impedance was reduced but single unit recording performance was not improved during the four-week experiment [139]. They found no significant differences in astrogliosis, neuronal density, and non-neuronal cell density. Misra et al. coated planar porous silicon microelectrodes with either dried saline or dried saline with Poloxamer 188, a PEG and poly(propylene glycol)-based triblock copolymer that seals ruptured cell membranes [140]. They reported reduced astrogliosis and activated macrophages two weeks after implantation, reduced astrogliosis four weeks after implantation, and no significant histological differences six weeks after implantation. Recording performance was unaffected. Hayn et al. in 2015 implanted rats with 400 μm diameter cannulae and injected either artificial cerebrospinal fluid (aCSF) or aCSF plus the neuroprotective drug memantine at the time of implantation [141]. They reported increased numbers of neurons, decreased astrogliosis, and no significant difference in macrophages

at two and six weeks after implantation. They also found that rats given memantine performed better on various behavioral tasks.

Investigators have also pursued controlled release strategies. Zhong et al. in 2007 coated planar silicon electrodes with a nitrocellulose-dexamethasone mixture and reported reduced astrogliosis and reduced neural process loss in coated devices one and four weeks after implantation compared to uncoated devices [78]. Activated macrophages and CSPG were both reduced one week after implantation but not at four weeks. Huang et al. in 2015 coated planar silicon electrodes with a 30 μm thick layer of polydimethylsiloxane-modified N, O-carboxylic chitosan (PMSC) and oligo-proanthocyanidin (OPC) [142]. PMSC is semi-hydrophilic, slowly degradable, and can be chemically incorporated with the antioxidant and anti-inflammatory drug OPC. The authors reported improved recording performance, decreased activated macrophages, decreased astrogliosis, and increased numbers of neurons associated with the coated devices over a four week indwelling period. In both these studies, since controls were uncoated, the effects may be due to the physical and chemical properties of the coatings rather than the drugs

Purcell et al. in 2009 seeded neural stem cells into alginate wells in planar silicon microelectrodes, hypothesizing that the cells' sustained release of neurotrophic factors would improve neuronal proximity to the device [143]. Cell-seeded devices had improved numbers of nearby neurons at one day and one week, but reduced numbers at six weeks and three months. The authors concluded that degradation of alginate and death of the neural stem cells led to the reversal in response.

1.10.5 The Effect of Device Architecture

Another approach under investigation is modification of microelectrode architecture. One simple modification is to reduce the size of the device. Stice et al. in 2007 compared the responses to 30 µm diameter microwires to 15 µm diameter microwires with a 10 µm thick degradable poly(glycolic acid) (PGA) coating [144]. They reported reduced astrogliosis associated with the 15 µm microwires four weeks after implantation. They also implanted 30 µm microwires with 10 µm thick PGA coatings and found their responses to be similar to the uncoated 30 µm microwires, suggesting that astrogliosis depended on the size of the non-degradable indwelling components, rather than the size of the device during insertion. Thelin et al. in 2011 implanted rats with steel microwires 50 or 200 µm in diameter and found reduced astrogliosis, reduced activated macrophages, and increased numbers of neurons near the smaller microwires 12 weeks after implantation [145].

Another simple modification is to increase the spacing between microelectrode shafts. This may reduce the FBR by preventing the FBR to each shaft from overlapping, and may also reduce implantation injury by sparing more blood vessels per area [146]. McConnell et al. in 2007 reported increased astrogliosis associated with four-shank planar silicon microelectrodes with 125 µm shank tip spacing compared to 200 µm spacing, four weeks after implantation [147]. The closer-spaced microelectrodes also happened to be smaller (30-100 µm wide tapered shank vs. 60-100 µm), so the effect of spacing outweighed the effect of device size. A later study by McConnell et al. in 2009 using the same devices reported increased activated macrophages, increased astrogliosis, increased hemosiderin-laden macrophages, reduced dendrites, and qualitatively reduced numbers of neurons near

the closer-spaced devices 16 weeks after implantation [72]. Lind et al. in 2012 attempted to establish an upper bound on the distance at which the FBRs of multiple devices interact [148]. They implanted rats with sets of five bundles of 32 13.5 μm diameter microwires embedded in 300 μm diameter gelatin needles (as in their 2010 study [132]) spaced 1 mm apart, and found that activated macrophages and astrogliosis were similar to single bundles, six weeks after implantation. Thus spacing appears to affect the FBR if the spacing is below some threshold distance, somewhere between 125 μm and 1 mm.

A more advanced modification has been to reduce device surface area using a lattice-style architecture. Seymour et al. in 2007 created devices that had a solid shank 48 μm thick and 70 μm wide with lattice features 5 μm thick and 4, 10, 30, or 100 μm wide extending off to one side [67]. They reported increased numbers of neurons and reduced numbers of nonneuronal cells around the outer edge of the lattice features compared to the shank, regardless of lattice thickness, four weeks after implantation. Skousen et al. in 2011 compared the FBR to solid planar silicon microelectrodes with lattice planar silicon microelectrodes and found decreased activated macrophages, decreased BBB leakage, and increased numbers of neurons near the lattice devices eight weeks after implantation [57]. Both of these studies compared devices with identical penetrating profiles, so the difference in FBR is most likely related to the reduction in surface area available for protein adsorption/activation and macrophage attachment rather than implantation injury.

1.10.6 The Effect of Mechanical Motion

In addition to the presence of a foreign material surface, mechanical motion of the implant relative to tissue can aggravate the FBR. Although this has long been observed in

highly mobile tissues such as muscle and subcutaneous compartments [149], recently investigators have explored whether the relatively small motions between a microelectrode and the brain can increase the FBR. Such motions, sometimes called micromotions, result from breathing and pulsatile blood flow [150]. In addition, if the microelectrode is tethered to the skull, head movements may move the microelectrode whenever the brain moves within the intracranial space. Biran et al. in 2007 reported that planar silicon microelectrodes tethered to the skull had increased activated macrophages, increased astrogliosis, reduced neuronal processes, and reduced numbers of neurons relative to microelectrodes free-floating in the brain four weeks after implantation [54]. The authors noted that other factors may be involved, such as the migration of meningeal fibroblasts down the microelectrode or the presence of bone screws, silicone, and acrylic. Thelin et al. in 2011 reported that microwires tethered to the skull were associated with increased activated macrophages, increased astrogliosis, and increased size of the implant cavity, but similar numbers of neurons 12 weeks after implantation [145]. Therefore, tethering appears to increase the FBR. Although tethering is typical for single unit recording studies, increasing the flexibility of the wire bundle between microelectrode and connector could reduce the effect of tethering. Wireless transmitters have also been developed [151], although their FBR has not yet been compared to tethered devices.

In order to separate the effects of tethering forces from other sources of motion, Lind et al. in 2013 implanted rats with 500 μm diameter parylene-coated needles made of either solid platinum or hollow carbon fiber [152]. Therefore, the only differences between the implants were increased inertial and gravity forces for the platinum implants due to their higher mass density (note that both implants were extremely stiff). They reported increased

astrogliosis in brain tissue six weeks after implantation, but no significant difference in activated macrophages or numbers of neurons. However, they did find increased activated macrophages adhered to explanted high-density implants. These results suggest that increased inertial/gravity forces alone are sufficient to increase the FBR, although the effect was not as great as tethering to the skull.

Reducing the stiffness of the device has also been proposed as a way to reduce motion by allowing the device to flex and move with brain tissue. Harris et al. in 2011 created 203 μm wide, 100 μm thick "mechanically adaptive" devices composed of poly(vinyl acetate) (PVAc) and cellulose whiskers that become soft upon implantation into brain tissue and compared their FBR to 50 μm diameter tungsten microwires coated with PVAc to a final diameter of 160 μm [153]. They reported increased numbers of neurons and decreased CSPG associated with the mechanically adaptive devices four weeks, but not eight weeks, after implantation. They also reported more diffuse astrogliosis for the mechanically adaptive devices eight weeks after implantation. Nguyen et al. in 2014 performed a similar experiment using 135 μm wide, 63 μm thick mechanically adaptive devices and 123 μm wide, 15 μm thick planar silicon devices coated with a 15 μm thick layer of PVAc [154]. They reported decreased astrogliosis and decreased BBB leakage surrounding the mechanically adaptive devices 2, 8, and 16 weeks after implantation. They found decreased labeling for macrophages and activated macrophages and increased numbers of neurons at 16 weeks only. Increased device flexibility appears to reduce the FBR, although the shapes and surface chemistries of experimental and control devices in these studies were not completely identical.

It is also important to note that the previously mentioned approaches of reducing device

size, adding thick hydrogel layers, and using lattice architecture may have the additional effects of increasing flexibility, providing a mechanical buffer, and increasing mechanical integration, respectively, so the success of these strategies may be partly explained by mechanical effects.

1.10.7 The Effect of Device Type

A handful of studies have compared completely different types of devices. These studies will only be discussed briefly since numerous variables in the designs of the devices could explain the differences in recording performance and FBR.

Ward et al. in 2009 implanted rats with microwire arrays, UEAs, and two types of planar silicon arrays [155]. Small cohorts and high variability prevented them from drawing comparative conclusions regarding recording performance and the FBR. Kozai et al. in 2012 compared extremely small PEG-coated "microthread" electrodes to planar silicon devices and found improved performance and qualitatively reduced markers of the FBR for the microthread electrodes [156]. Saxena et al. in 2013 reported improved recording performance and reduced markers of the FBR for microwire arrays compared to planar silicon devices [80]. Karumbaiah et al. in 2013 compared the FBR and recording performance among a variety of different planar silicon, microwire, and UEA designs, and again found favorable results for microwire arrays [157]. Vitale et al. in 2015 compared carbon nanotube fiber electrodes against platinum-iridium microwires and reported a reduced FBR associated with the carbon nanotube fiber electrodes, although their histological analysis is unusual [158].

1.11 Finite Element Modeling to Predict the FBR

The studies reviewed in the preceding sections show that it is possible to modulate the FBR to intracortical microelectrodes using a variety of different strategies. Almost all of these studies have been performed in rat, without recording single units, for eight weeks or less. Therefore the next step will be to select the most promising strategies and test them in larger animals, using functional devices, for durations of several months or more.

The trial-and-error approach of the studies in the preceding sections was necessary in order to identify workable strategies. However, as these strategies move into more expensive and time-consuming experimental paradigms, it becomes increasingly important to narrow down the design space to avoid unnecessary experiments.

In many fields of engineering, finite element modeling allows engineers to test and refine devices and structures *in silico* before full-scale testing. Recently, the Tresco lab has developed a finite element model of the FBR to intracortical microelectrodes. The model uses device geometry and the diffusive properties of brain tissue as inputs and provides predictions of the concentrations of proinflammatory cytokines in brain tissue surrounding a device as output. Higher predicted proinflammatory cytokine concentrations are expected to correspond to an increased FBR. While the model does not remotely approach the complexity of the FBR *in vivo*, it has been able to successfully predict the influence of device architecture and thick hydrogel coatings on the FBR in two studies by Skousen et al. [57, 58].

In Chapter 4, we continue validation of the model by comparing its predictions for the UEA to the *in vivo* results in Chapters 2-3. Furthermore, we expand our conceptual understanding of the model by examining predictions for different proinflammatory

cytokines with different diffusive characteristics. Finally, we demonstrate that the model can be used as an engineering tool to rationally design modifications to the UEA. We expect that with continuing validation and refinement, the model will speed the process of translating the strategies reviewed in the preceding sections into successful clinical devices.

CHAPTER 2

BBB LEAKAGE, ASTROGLIOSIS, AND TISSUE LOSS CORRELATE WITH SILICON MICROELECTRODE ARRAY RECORDING PERFORMANCE

Reprinted from Biomaterials, 53, Nolta N.F., Christensen M.B., Crane P.D., Skousen J.L., Tresco P.A., BBB leakage, astrogliosis, and tissue loss correlate with silicon microelectrode array recording performance, 753-62, © 2015, with permission from Elsevier.

2.1 Abstract

The clinical usefulness of brain machine interfaces that employ penetrating silicon microelectrode arrays is limited by inconsistent performance at chronic time points. While it is widely believed that elements of the foreign body response (FBR) contribute to inconsistent single unit recording performance, the relationships between the FBR and recording performance have not been well established. To address this shortfall, we implanted 4X4 Utah Electrode Arrays into the cortex of 28 young adult rats, acquired electrophysiological recordings weekly for up to 12 weeks, used quantitative immunohistochemical methods to examine the intensity and spatial distribution of neural and FBR biomarkers, and examined whether relationships existed between biomarker

distribution and recording performance. We observed that the FBR was characterized by persistent inflammation and consisted of typical biomarkers, including presumptive activated macrophages and activated microglia, astrogliosis, and plasma proteins indicative of blood-brain-barrier disruption, as well as general decreases in neuronal process distribution. However, unlike what has been described for recording electrodes that create only a single penetrating injury, substantial brain tissue loss generally in the shape of a pyramidal lesion cavity was observed at the implantation site. Such lesions were also observed in stab wounded animals indicating that the damage was caused by vascular disruption at the time of implantation. Using statistical approaches, we found that blood-brain barrier leakiness and astrogliosis were both associated with reduced recording performance, and that tissue loss was negatively correlated with recording performance. Taken together, our data suggest that a reduction of vascular damage at the time of implantation either by design changes or use of hemostatic coatings coupled to a reduction of chronic inflammatory sequela will likely improve the recording performance of high density intracortical silicon microelectrode arrays over long indwelling periods and lead to enhanced clinical use of this promising technology.

2.2 Introduction

Intracortical or penetrating silicon microelectrode arrays can record neural information from neurons in deeper cortical layers and send the signals to a computer in real time. This type of "brain-computer interface" or "brain-machine interface" has been a useful research approach and, more recently, has shown promise as a treatment for incurable neurological injuries and diseases. It has been shown that silicon microelectrode arrays implanted in

motor cortex can allow individuals with tetraplegia to control computer cursors [27] and multiple degree-of-freedom robotic arms [5] with conscious thought.

While such microelectrode recording arrays can function for several years in humans and other large animals [5, 23, 27, 28, 39], the majority exhibit inconsistent performance and fail to record single unit action potentials at much shorter time points. Studies systematically examining microelectrode array recording performance in multiple subjects have reported that the quality (signal-to-noise ratio) and quantity of single unit action potentials recorded by arrays fluctuate unpredictably and generally decrease over time in rats [33-36], guinea pigs [22], cats [23, 37, 38], nonhuman primates [39], and humans [159].

While the precise mechanisms are unclear, some of these reliability issues have been attributed to hardware-related problems including material degradation [35, 36, 39], percutaneous connector failure [22, 33, 39], and infection [39]. Some failures, however, occur without any ostensible hardware-related issues and are likely related to changes in the cortical tissue near the device related to the foreign body response (FBR) or may be exacerbated by inflammation elsewhere in the body. Our lack of knowledge about the biological mechanisms is a significant challenge to clinical implementation as FBR-related failures are poised to become the dominant failure mode after the engineering related problems are solved.

Since device performance requires the presence of functioning neurons within about 100 μm of the device's recording sites [41], one hypothesis of biologically-driven device inconsistency and failure is that the foreign body response (FBR) and associated inflammatory sequelae lead to neuronal death or electrophysiological silencing. Studies

have consistently reported the involvement of activated macrophages and microglia, secretion of pro-inflammatory cytokines, blood-brain barrier (BBB) leakiness, and reductions in neuron cell bodies, dendrites, and myelin near chronically implanted microelectrodes [52-62, 64, 65, 71, 72, 160]. Persistent inflammation, BBB leakiness, and/or neurodegeneration may cause neurons within the device's recording range to become silenced in the unfavorable extracellular environment, or they may lose their connectivity to other circuitry and stop reliably producing recordable action potentials. Another issue is gross movement of the implanted array due to fibrous encapsulation driven by the FBR [37-39].

Besides the FBR, another concern, particularly with large, high-density microelectrode arrays, is the initial damage to blood vessels that occurs during implantation [63, 70, 161], which has the potential to damage adjacent brain tissue similar to that seen after ischemic [146] or hemorrhagic [162] stroke. To better understand the impact of implantation injury, investigators have implanted devices and minutes later withdrawn them, then allowed the animals to recover (often called a "stab wound injury"). For single-shank planar silicon devices [53, 59], four-shank planar silicon devices [72], and single microwires [71], the injury of device insertion alone is not sufficient to cause significant brain tissue loss or persistent inflammation in brain tissue beyond a few weeks. For high-density microelectrode arrays with dozens of stiff, penetrating features separated by short distances, it has been shown that significant vascular injury occurs after implantation [63, 69, 70], but to our knowledge no studies have examined the long-term outcome after a stab wound injury created with a high-density silicon microelectrode array.

While the implantation injury and FBR to microwire and planar silicon devices with

one or a few microwires or shanks are well described in the rat brain, the FBR to high-density microelectrode arrays with regularly spaced penetrating features is less well understood. This is important since these are the types of devices used in nonhuman primate studies and preclinical trials in humans. Therefore, to better understand the implantation injury and FBR of a more clinically relevant microelectrode recording array, we used a combined histological and electrophysiological approach to study stab wound injuries and the FBR to 4X4 Utah Electrode Arrays (UEAs) chronically implanted in young adult rat cortex, and examined whether the histological features of the FBR corresponded with changes in single unit recording performance.

2.3 Materials and Methods

2.3.1 Microelectrodes

UEAs were purchased from Blackrock Microsystems, Salt Lake City, UT. The arrays had a 4X4 rectangular grid of 1 mm long microelectrodes spaced 400 µm apart (Fig. 2.1 A) and were similar in overall design to those used in nonhuman primate [39, 163] and

Fig. 2.1. (A) UEA before implantation. Scale bar = 1 mm. (B) Electrophysiological recording session with an awake and behaving rat implanted with a UEA. (C) Representative waveforms from a recording session in which single unit action potentials were isolated on 5 of the 16 microelectrodes.

clinical studies [5, 27]. The wiring diagram relating connector pins to the locations of microelectrodes on the array was supplied from the manufacturer. For long-term implantation experiments, the UEA, connector, and associated wiring were fitted into a custom-fabricated polyurethane headstage, sterilized with ethylene oxide, and allowed to outgas for at least 12 h prior to surgery. For stab wound injury experiments, UEAs with identical design but no associated wiring were glued to a stainless steel wire mounted perpendicular to the backside of the array (so that the array could be held in a stereotactic frame) and similarly sterilized and outgassed.

2.3.2 Animal Surgery

All procedures involving animals were approved by the University of Utah Animal Care and Use Committee. Adult male Sprague-Dawley rats weighing approximately 300-350 g (N=28) were anesthetized by isoflurane and their heads shaved. The animals were positioned in a stereotactic frame and the scalp was disinfected with 70% isopropyl alcohol and betadyne. A midline incision was made along the length of the skull and the exposed scalp was dried using cotton applicators. A 3-4 mm diameter craniotomy was created over primary motor cortex using an air driven drill bit with sterile saline rinses to prevent excessive heating. Holes for screw placement were created using a stereotactically mounted air driven dental drill. The dura was pierced and reflected with a 25 gauge needle, and the UEA inserted into brain tissue by lightly pushing on the backside of the array with hand held forceps. The reference wire was tucked beneath the edge of the craniotomy over the exposed surface of the brain and the ground wire was tunneled a short distance beneath the scalp posterior to the incision site. The headstage assembly (including the mounted

UEA, ground/reference wires, and electrical connector) was then fixed to the skull using stainless steel screws and photocurable acrylic adhesive. The incision was then sutured shut around the connector. Elizabethan collars (Kent Scientific, Torrington, CT) were used to prevent rats from manipulating the implant site after surgery. Three additional rats were used to study the effect of implantation induced damage in the absence of the foreign body response. For these stab wound injury experiments, each rat underwent a similar surgery, except that the array was implanted stereotactically and withdrawn two minutes later and no headstage assembly was employed.

2.3.3 Electrophysiological Recordings

Rats were allowed to recover for one week, after which neural recordings were obtained from freely moving animals (Fig. 2.1 B) for a period of five minutes at weekly intervals using a Cerebus data acquisition system (Blackrock Microsystems, Salt Lake City, UT) and analyzed offline using Plexon Offline Sorter (Plexon, Dallas, TX) (Fig. 2.1 C). Single units were isolated in principal component space using a manually assisted sorting algorithm. Signal-to-noise ratio (SNR) was determined by dividing the peak-to-peak amplitude of the average waveform of an isolated unit by the RMS noise floor on that microelectrode.

2.3.4 Failure Analysis

In order to track the cause and time course of device failure, animals were examined at each recording session for signs of mechanical failure (headstage/connector failure or broken lead wires) or for a loss of all or nearly all recordable single unit activity. If there

were no observable hardware-related issues, failure was attributed to the FBR. Animals with devices that failed were sacrificed within six hours in most cases. Animals with devices that did not fail were sacrificed at week 12. All animals were included in further histological investigations.

2.3.5 Euthanasia and Tissue Preparation

At sacrifice, rats were anesthetized and perfused transcardially with phosphate buffered saline (PBS) followed by 4% paraformaldehyde in PBS. Their brains were removed from the skull and the arrays dissected free. Brains and arrays were postfixed for 24 h in 4% paraformaldehyde and equilibrated in a 30% sucrose solution before 30 µm horizontal brain sections were obtained using a cryostat.

2.3.6 Immunohistochemistry and Microscopy

Free-floating brain sections were blocked overnight in PBS with 4% v/v goat serum (Invitrogen, Carlsbad, CA), 0.5% v/v Triton-X 100, and 0.1% sodium azide then incubated overnight with the following primary antibodies in blocking solution: CD68 (ED-1, AbD Serotec, Raleigh, NC, .25 µg/ml) to identify activated macrophages and microglia, IBA-1 (Wako Chemicals USA, Inc., Richmond, VA, .5 µg/ml), IgG (biotinylated goat anti-rat IgG, Southern Biotec, .5 µg/ml) to assess BBB leakage, GFAP (DAKO North America Inc., Carpinteria, CA, 2.9 µg/ml) to examine astrocyte cytoskeleton location and hypertrophy, NF200 (Sigma, St. Louis, MO, 8 µg/ml) to examine the spatial distribution of axons, and biotinylated tomato lectin (Burlingame, CA, 4 µg/ml) to label blood vessels. Sections were then rinsed three times with PBS for 1 h each before being incubated

overnight in fluorescently labeled secondary antibodies plus 10 µM DAPI to label cell nuclei, then finally rinsed again three times with PBS for 1 h each. All incubations were performed at room temperature on a rocker. The same protocol was used on explanted arrays to identify adherent cell types. Sections were mounted on slides and coverslipped in Fluoromount-G (Southern Biotec) then imaged with a confocal microscope. For retrieved arrays, images were taken using a confocal microscope 5x air objective or a 40x water objective with the array submersed in a petri dish. Due to anti-mouse secondary antibody cross-reactivity with high concentrations of endogenous rat IgG in tissue sections, the IBA-1 image was used to eliminate IBA-1-negative areas from some CD68 images, since all activated macrophages should also be IBA-1+. All histological images are maximum intensity projections.

2.3.7 Determination of Void Volume

To calculate the volume of damaged neural tissue, 2D cavity areas in histological sections were manually described in Photoshop (Adobe Systems Inc., San Jose, CA) (Fig. 2.5 B-C). The prismoidal formula:

$$V = \frac{L}{3}\left(A + \sqrt{AB} + B\right)$$

was used to estimate the cavity volume *V* lying between two sequential sections separated by distance *L* and having 2D void areas *A* and *B*, then summed over all sections. In addition, the extent of tissue shrinkage from histological processing was confirmed to be < 2% (linear shrinkage) by measuring distances between microelectrode tracts in sections, which were known to be spaced 400 µm apart.

For visualization purposes, one animal's cavity was rendered in SolidWorks (Dassault

Systèmes SolidWorks Corporation, Waltham, MA) by tracing and manually registering histological sections then using the loft tool to form a solid.

2.3.8 Statistics

SNR values and average number of units per microelectrode for a subset of animals which had isolated units over multiple recording sessions were compared between the first and last successful recording sessions using a paired t-test. SNR and immunohistochemical marker intensity values between edge and center microelectrodes at the last session were compared using Student's t-test. Outliers in the data were identified using an interquartile test, with outliers lying above or below 1.5*IQR (interquartile range) ± Q3 or Q1, respectively. The proportions of microelectrodes with isolated single units for microelectrodes located in brain tissue versus microelectrodes associated with tissue loss areas were compared using a z-test for two population proportions. P values below 0.05 were considered significant.

2.4 Results

2.4.1. Failure Analysis

Most devices failed within the first five weeks, the majority due to hardware-related issues (Fig. 2.2). Of these, loosening or failure of the headstage was the predominant failure mechanism (ten animals). Breakage of the wire bundle was also a major hardware-related failure mode (five animals), but was mitigated by limiting animal grooming through the use of Elizabethan collars. After the first two weeks, the FBR accounted for a significant portion of failures (eleven animals). Two devices recorded single units to the

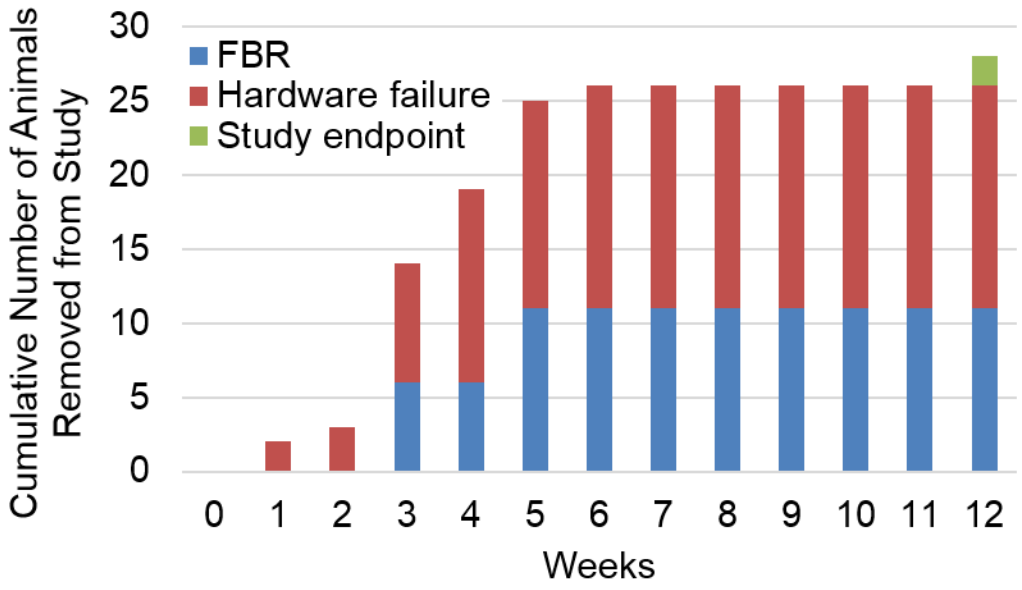

Fig. 2.2. Summary of recording failure modes over the course of the study. Devices failed due to such hardware-related issues as headstage loosening and breakage of lead wires or due to reasons related to the foreign body response. Two animals exhibited single unit recording over the study 12 week indwelling period. All animals were examined histologically.

12 week study endpoint.

At dissection, six of the eleven devices that failed due to the FBR were either tilted to one side or observed in a more superficial location relative to their original implantation position. In these cases it appeared as though fibrotic tissue from the FBR and tissue remodeling associated with the lesion cavity worked in concert to cause the change in array position. The arrays from these 6 animals were otherwise functioning properly at the time of sacrifice. Their headstages were still firmly anchored to the skull and there was no observable damage to any of the wires or connections as indicated by physical inspection or suggested by electrophysiological data.

2.4.2 Electrophysiology

Recording performance was variable over time in individuals and generally decreased over the 12 week period. Isolated single units were obtained from a total of 16 animals in this study. Of those, 10 animals had isolated single units in more than one recording session and are summarized in Fig. 2.3. The average number of units per microelectrode decreased from .37 to .19 between the first and last successful recording sessions ($p = 0.0002$). Additionally, the average SNR of units decreased from 11.3 to 9.4 between the first and last recording sessions ($p = 0.01$).

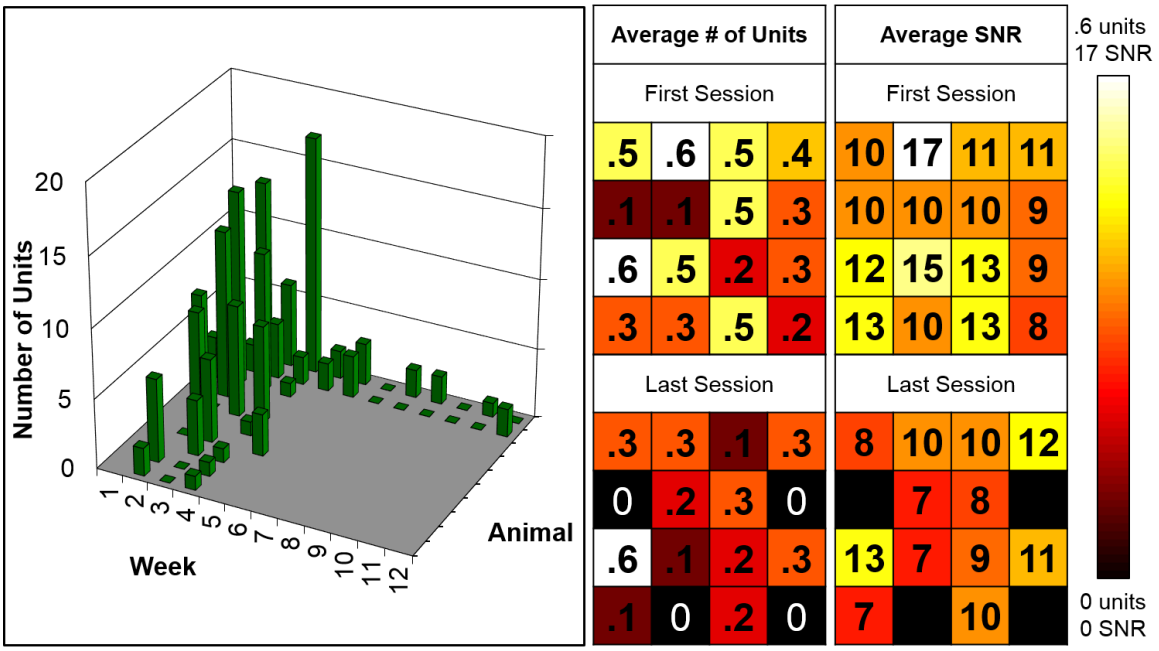

Fig. 2.3. Summary of recording performance for animals which had isolated units on at least two recording sessions. (Left) Number of single units isolated at each recording session for each animal over time. (Right) First session and last session averages for each microelectrode position as viewed from the top of the 4X4 UEA. Both the average number of units and the average SNR decreased significantly from the first to the last recording sessions ($p = 0.002$ and 0.01, respectively).

2.4.3 Explanted Arrays

Microelectrode arrays from the animals with implant durations six weeks or less were, in all but one case, easily removed from the brain after intracardiac perfusion without tearing or removing brain tissue. Retrieved arrays were uniformly covered with CD68 immunoreactivty, indicative of activated macrophages and activated microglia (Fig. 2.4 A). The majority of cell nuclei on the explanted array co-localized with CD68 immunoreactivity, suggesting that activated macrophages and activated microglia were the predominant cell types. A small number of unidentified CD68- DAPI+ cells were also present. Most CD68+ cells were amoeboid in shape, but several were found to have fused into foreign body giant cells (FBGCs) (Fig. 2.4 B). These FBGCs typically had 10-15 nuclei and a flattened, spreading cytoplasm with IBA-1+ immunoreactivy at cell margins [164]. The arrays for the two 12-week animals had significantly greater amounts of CD68+ fibrotic tissue encapsulation on the underside of the array.

2.4.4 Histological Description of the FBR

The tissue response in both implanted animals and stab wounded animals included significant areas of cortical tissue loss and inflammation similar to lesions observed after ischemic [146] and hemorrhagic [162] stroke produced experimentally in rat cortex. The lesions appeared as cavities on the brain surface and often contained darker tissue in the otherwise cleared, perfused brain tissue (Fig. 2.5 A). The size and shape of the cavity was variable between animals but tended to have a jagged, pyramidal shape, with the pyramid's base at the brain surface and the tip pointing down into cortex. Fig. 2.5 D-G shows a 3D reconstruction of a representative cavity 500 to 1500 μm below the brain surface for

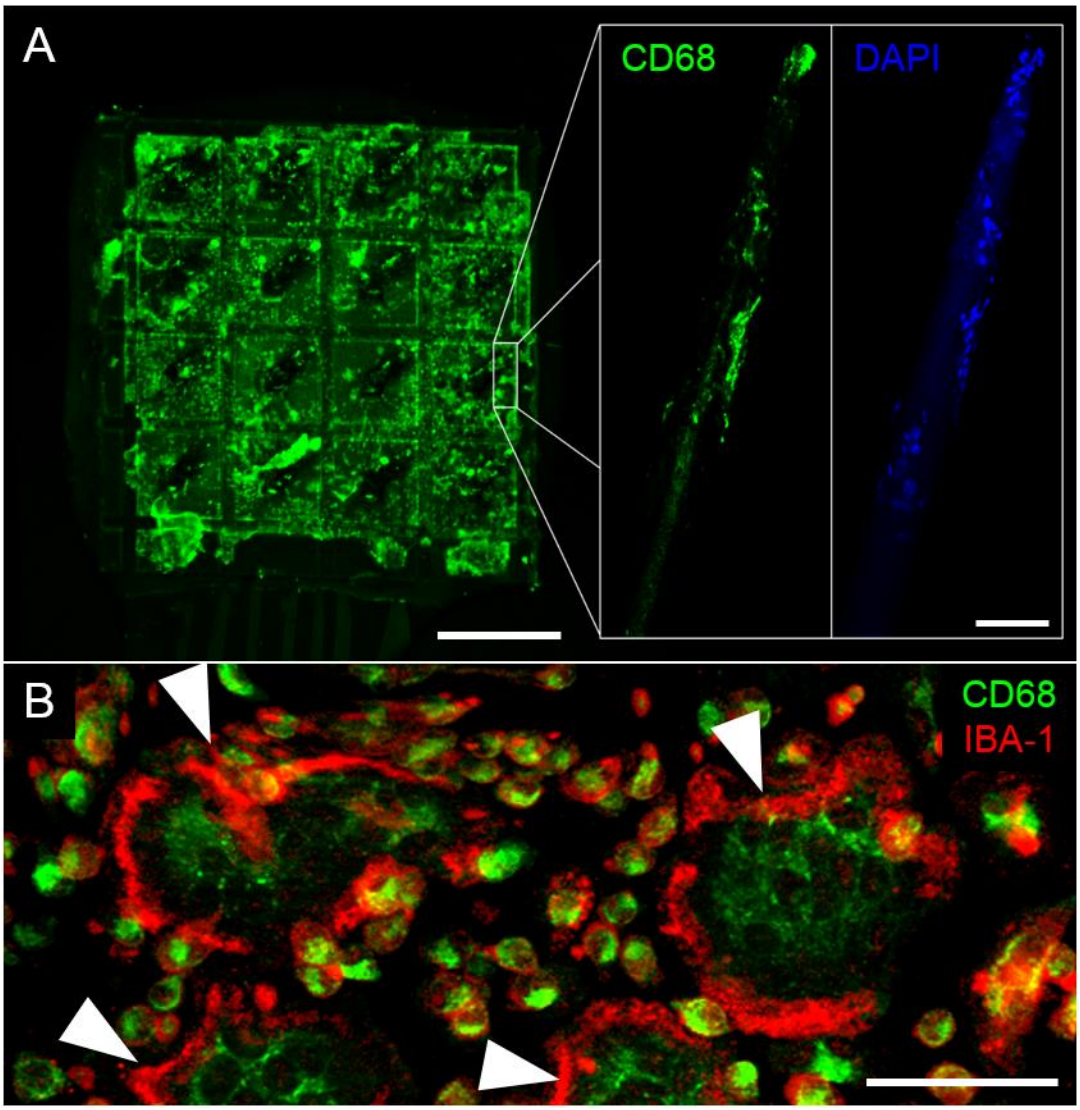

Fig. 2.4. (A) Representative maximum-intensity projection of CD68 immunoreactivity (green) on the surface of a retrieved UEA. The data indicates that activated macrophages were uniformly distributed across all tissue-contacting surfaces of the array. Scale bar = 500 µm. Inset shows close-up of a microelectrode shaft. Most cell nuclei (DAPI, blue) co-localized with CD68, suggesting that activated macrophages were the predominant adherent cell type. Inset scale bar = 50 µm. (B) Some CD68+ cells appeared to have fused into multinucleated foreign body giant cells (arrowheads). These cells had 10-15 nuclei and a flattened, spreading cytoplasm with IBA-1+ immunoreactivy at cell margins [164]. The other CD68+ cells tended to have smaller, amoeboid morphologies with CD68 and IBA-1 labeling throughout the cell. Scale bar = 50 µm.

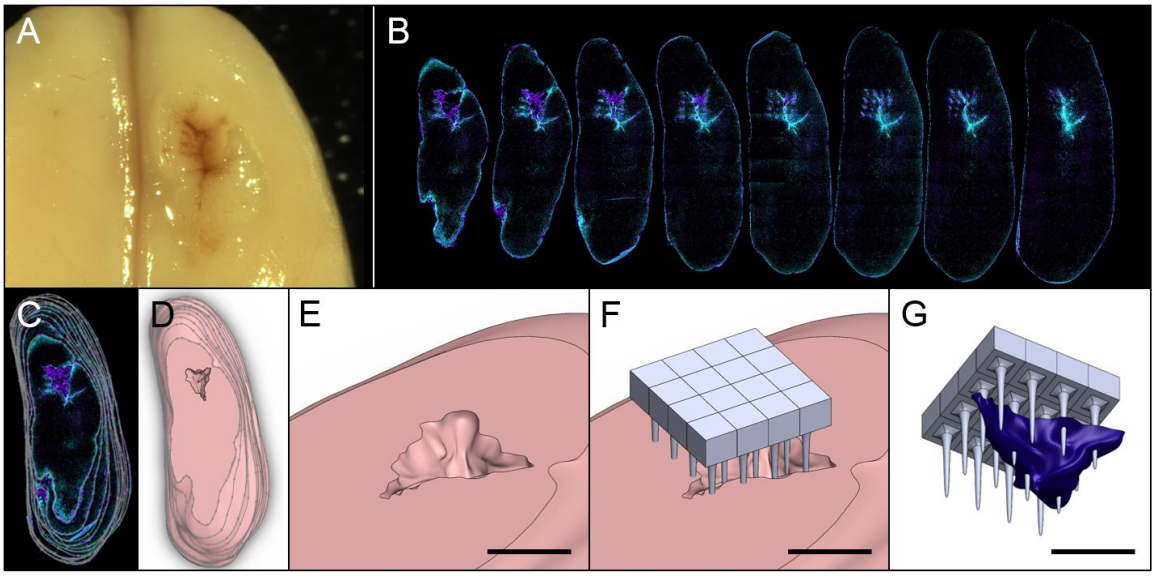

Fig. 2.5. Measurement of surface brain tissue loss volume. (A) Photograph of cortex after perfusion and device removal, showing a cavity and colored tissue. (B) Horizontal serial sections through the depth of the implantation site shown in A imaged at constant magnification. (C) Section images stacked together in SolidWorks with outlines. (D) Stacked images filled in to create a solid 3D model of the brain. (E) Close-up of cavity area. (F) Scale model of UEA aligned in position. Note that only tissue sections from halfway down the electrode shafts to a depth of 1 mm below the tips were rendered. (G) View of cavity volume (purple shaded area). Scale bars in E-G = 1 mm.

the same animal shown in Fig. 2.6.

The size of the cavity was variable from animal to animal. For reference, the brain volume encompassed between all the 16 microelectrodes was 1.2 x 1.2 x 1 mm, or 1.44 mm^3. 19% of animals had a lesion cavity with a volume less than 0.72 mm^3 (half of the brain volume between the microelectrodes), 31% had a cavity between half and the full volume, and 50% had a cavity volume larger than the array volume. No clear trend was observed in lesion volume versus time. It is worth noting that in all but one case, the rats did not exhibit noticeable functional or behavioral changes, despite this significant loss of cortical tissue.

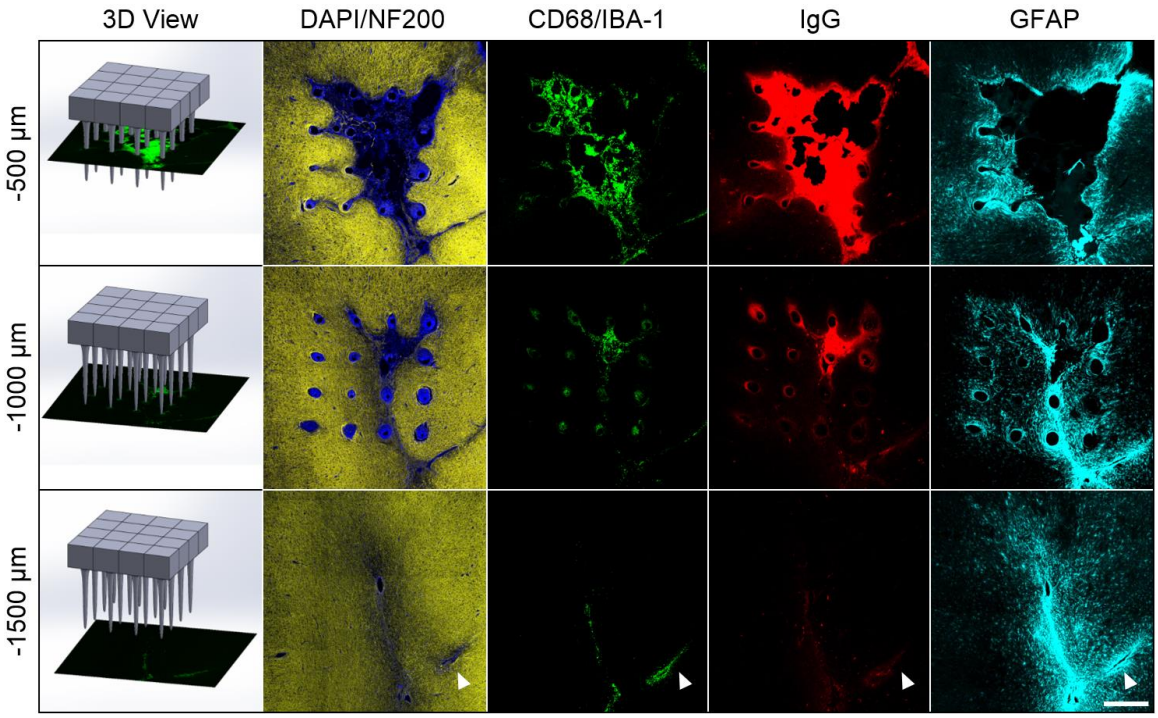

Fig. 2.6. Representative horizontal sections from an animal sacrificed at 4 wks showing cell nuclei (DAPI, blue), axons (NF200, yellow), activated macrophages (CD68/IBA-1 colocalization, green), BBB leakage (IgG, red), and astrocyte cytoskeleton (GFAP, cyan). Sections from three different depths are shown; 3D view illustrates approximate position of sections relative to UEA. Lacy, hypercellular, CD68+, IBA-1+, IgG+, NF200- areas of damaged neural tissue covered a large portion of the UEA footprint in superficial cortex (-500 µm), while microelectrodes not near tissue loss areas had a FBR typical of single shank electrodes. In deeper cortex, the tissue loss area was smaller. Arrowheads indicate a region of increased CD68, IgG, and GFAP immunoreactivity and decreased NF200 immunoreactivity associated with a large blood vessel. Scale bar = 500 µm.

In with fragile, lacy, hypercellular tissue that was positive for CD68 (activated macrophages and activated microglia), what appeared to be blood constituents (perhaps from ongoing angiogenesis and uncleared vasculature), and IgG, but was not positive for neuronal antigens (Fig. 2.6). Surrounding the cavity was a region of astrocytes with upregulated GFAP, CD68+ cells, IgG immunoreactivity indicating BBB leakiness, and decreased levels of NF200 immunoreactivity. The lesion cavity was anisotropic with depth: generally, 500 µm below the brain surface, or halfway down the lengths of the

microelectrodes, the cavity was at least as wide as the footprint created by the square base section of the array; nearer the tips the cavity narrowed to occupy a smaller fraction of the array footprint; 500 μm below the microelectrode tips the cavity was rarely visible but there were frequently regions of upregulated GFAP immunoreactivity, increased IgG immunoreactivity, and decreased NF200 immunoreactivity surrounding larger blood vessels that resided below the array microelectrode tips (Fig. 2.6, arrowheads).

Away from the cavity, the FBR to individual microelectrodes had a biomarker distribution similar to what has been previously described for implants with a single penetrating microelectrode shaft [52-62, 64, 65, 71, 72]. This included a layer of CD68+ activated macrophages and activated microglia at the biotic-abiotic interface, surrounded by a layer of increased GFAP immunoreactivity and a diffuse zone of IgG immunoreactivity, indicating leakage of the BBB near each microelectrode tract. Axons could not be found in the CD68+ area immediately surrounding the microelectrode, but were present just outside that zone. In some cases, axons showed a thicker, neuroregenerative phenotype that appeared to wrap around the microelectrode similar to that reported for microwire electrodes [52, 56, 61].

2.4.5 Stab Wound Injuries

In stab wound injury experiments, the arrays were extracted two minutes after insertion using a stereotactic manipulator without difficulty. Upon removal, the arrays were covered on their underside with blood but had no adherent brain tissue (Fig. 2.7 A). The surface of the brain at the stab wound injury site showed signs of hemorrhage but no surface damage other than the 16 small puncture wounds created by the microelectrode shafts of the array.

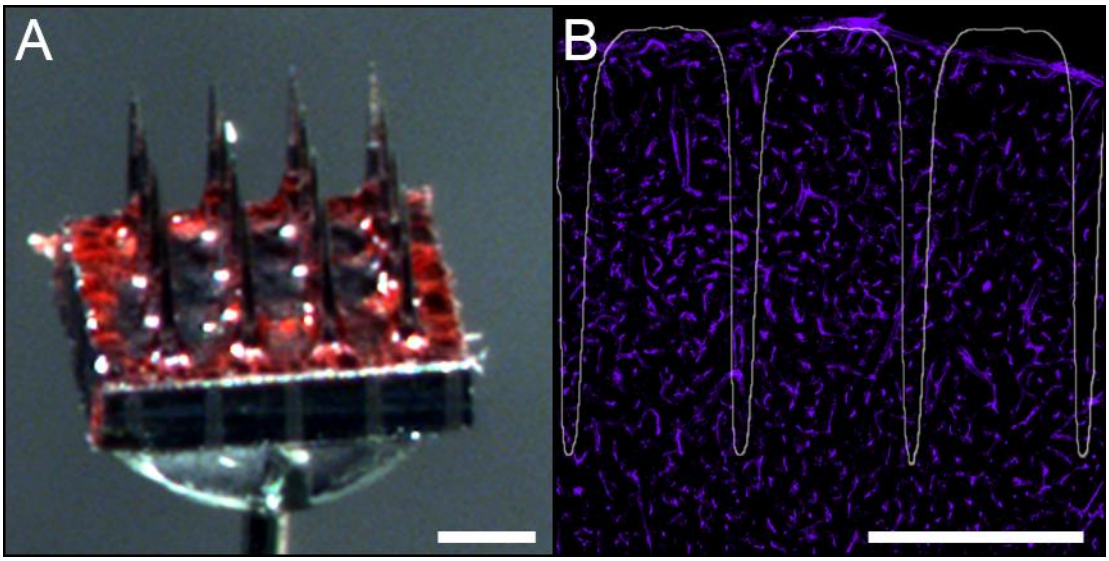

Fig. 2.7. (A) UEA withdrawn two minutes after implantation into brain tissue, showing the presence of blood but no cortical tissue attached to the UEA. (B) Representative 30 µm coronal section of rat motor cortex showing blood vessel distribution (tomato lectin, purple) and a scale outline of a 4X4 UEA is superimposed to show that each microelectrode shaft can transect multiple blood vessels of various sizes. Scale bars = 500 µm.

However, after sacrifice four weeks later, stab wounded animals were found to have lesion cavities similar in size and shape to those observed in implanted animals. Stab wounded animals showed reduced immunoreactivity for CD68 and a more compact border of GFAP upregulation at the margins of the cavity compared to implanted animals (Fig. 2.8).

Analysis of vasculature contralateral to the implant site allowed us to estimate that a significant number of blood vessels are transected during implantation of a 4X4 UEA. Fig. 2.7 B shows a coronal view of blood vessels labeled with tomato lectin in rat cortex with an outline of a UEA, revealing how the dense vascularization of cortex makes vascular damage inevitable given the UEA's architecture. Many descending arterioles and hundreds of capillary beds are disrupted following the implantation of a 4X4 UEA into rat cortex.

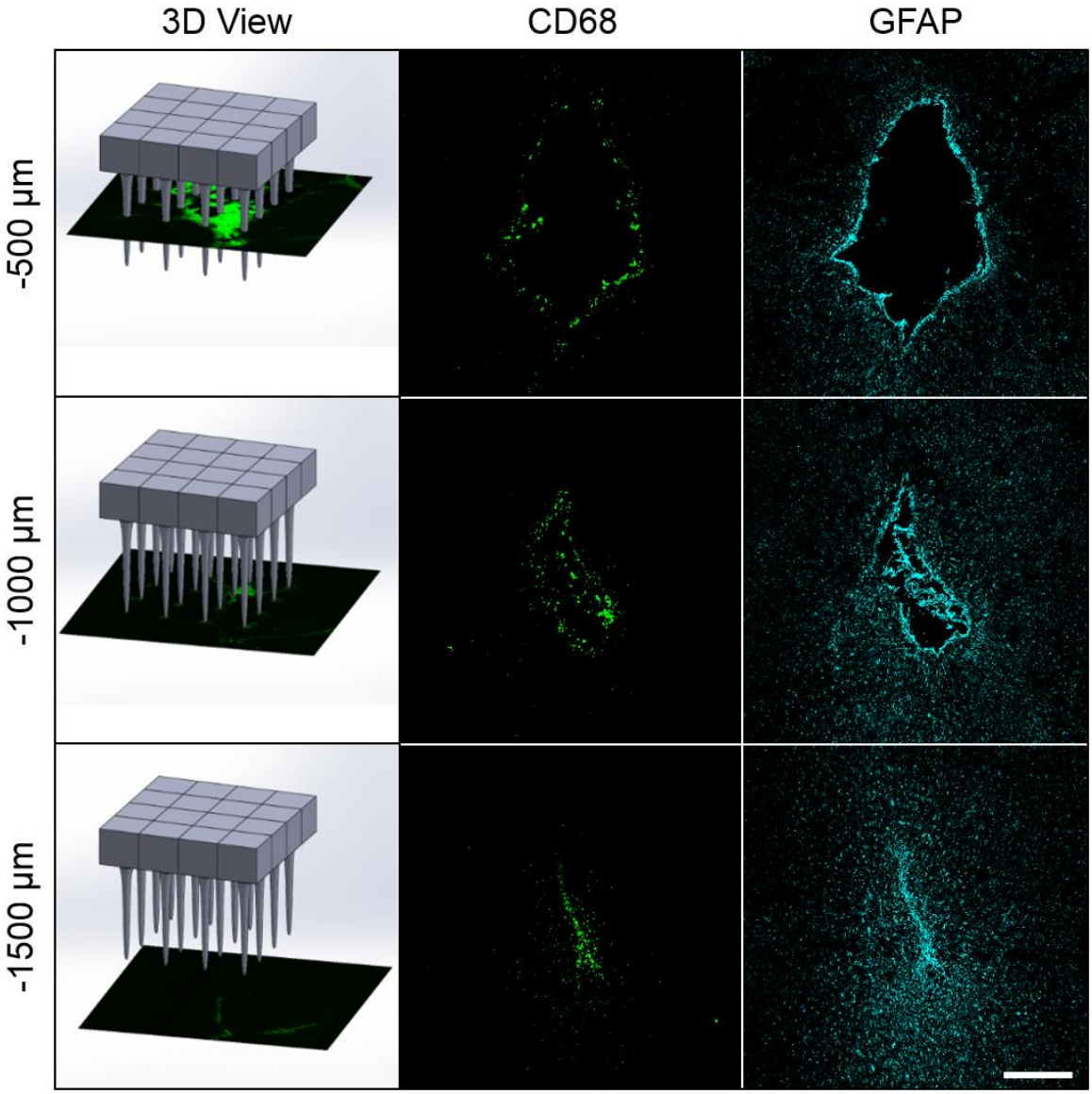

Fig. 2.8. Representative horizontal sections from an animal four weeks after surgery in which the UEA was implanted and removed two minutes later (stab wound injury) showing activated macrophages and microglia (CD68, green) as well as astrocyte cytoskeletonal upregulation (GFAP, cyan). Sections from three different depths are shown; 3D view illustrates approximate position of sections relative to UEA. Significant brain tissue loss was visible in superficial sections. The degree of tissue loss was similar for stab wounds and implants, however CD68 immunoreactivity was reduced around stab wound cavities after 4 weeks. Scale bar = 500 µm.

2.4.6 Relationships between Recording Performance and Histology

At final recording sessions, the average SNR for microelectrodes on the edge of the array was 10.1, while the average for microelectrodes in the center was 7.9, a statistically significant difference ($p = 0.05$) (Fig. 2.9). Quantification of immunofluorescent biomarker-associated signal intensity within a 100 µm radius of microelectrode tips revealed that center microelectrodes had significantly higher levels of GFAP and IgG immunoreactivity, indicating that astrogliosis and BBB leakiness were associated with reduced recording quality (Fig. 2.9).

Based on histological images, each microelectrode recording tip was categorized as being in brain tissue or in a lesion cavity (Fig. 2.10 A). Microelectrodes in brain tissue were significantly more likely to record single units, both at the last recording session ($p = 0.01$) and over the device lifetime ($p = 0.001$) (Fig. 2.10 B).

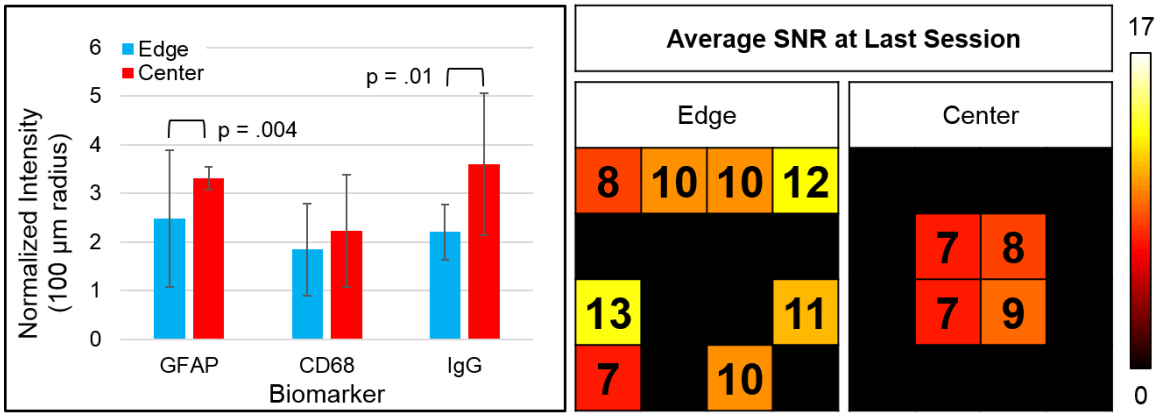

Fig. 2.9. Quantification of FBR biomarkers within 100 µm of the 12 edge microelectrodes vs. the 4 center microelectrodes revealed significantly greater levels of GFAP and IgG, suggesting that astrogliosis and BBB leakiness were greater near center microelectrodes ($p = .004$ and .01, respectively). Comparison of recording performance for edge microelectrodes vs. center microelectrodes at the last session revealed a significant deficit in SNR for center microelectrodes ($p = .05$).

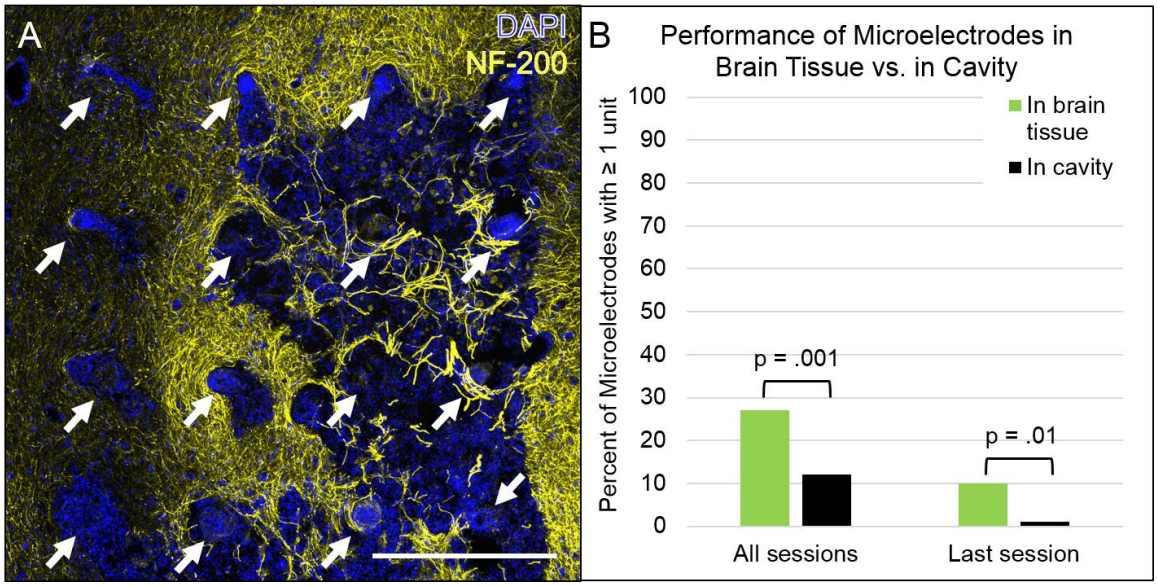

Fig. 2.10. (A) Evaluation of the effect of tissue integrity on single unit recording performance. First, microelectrode tracts were identified (arrows). Microelectrodes were then classified as being in brain tissue or in a cavity. Scale bar = 500 µm. (B) Across all animals, microelectrodes located in intact brain tissue were significantly more likely to record single units, both at the last session ($p = .01$) and over all sessions ($p = .001$).

Attempts to relate recording performance and the spatial distribution of other FBR biomarkers, as well as t-tests comparing average immunofluorescent signals for microelectrodes with single units vs. microelectrodes without single units and linear regression analysis of SNR values vs. immunofluorescent biomarker signals, yielded no statistically significant relationships.

2.5 Discussion

In this study, we found that the FBR to a 4X4 UEA in rat cortex differs from that of simpler devices that create a single penetrating injury. Specifically, implantation results in a lesion consisting of a substantial loss of cortical tissue and shows a response characterized by persistent inflammation throughout the indwelling period. We suspect that the wound

healing response likely involves continual tissue remodeling of the implantation site and beyond that may underlie the temporal changes in recording performance that have been described by others [22, 23, 33-39, 159] related to movement of the device and changes in the surrounding brain tissue. We found that vascular injury at implantation is sufficient to create these lesions, and using a statistical approach, we also found that biomarkers of astrogliosis, BBB leakiness, and lesions were all associated with reduced recording performance.

Available evidence suggests that vascular injury is the mechanism responsible for the loss of cortical tissue observed in this study. Since surface cavities were observed after four weeks in stab wounded animals, the mechanism of cavity formation is related to the initial injury of implantation and not solely caused by FBR-related inflammatory sequela. The reduced amount of CD68 immunoreactivity in stab wounded animals at the cavity margin was likely due to the lack of an indwelling device providing a persistent inflammatory stimulus. It is known that silicon microelectrode arrays sever, stretch, and burst blood vessels during implantation [70, 161], which was confirmed by our observations of bleeding at the brain surface after implantation and deposits of blood in histological sections. Moreover, experimental models of ischemic [146] and hemorrhagic [162] stroke in the rat both report losses of brain tissue similar to what we observed here.

Varying amounts of vascular injury is therefore the most likely explanation for the differences in the FBR to complex devices like the UEA that consist of many regularly spaced microelectrode shafts and what has been observed with other devices that create a single penetrating injury. There are a number of reasons why vascular damage would be more extensive for a high-density microelectrode array than for a microelectrode with a

single penetrating feature. Most obviously, a larger number of closely spaced, rigid penetrating features means that the probability of hitting, stretching and damaging descending arterioles is increased. Also, a large number of penetrating features spaced at fixed intervals makes it difficult to avoid surface vessels, unlike with smaller devices that can be more strategically placed [165]. Furthermore, issues with tissue compression and shearing are greater for large, complex arrays and can cause vascular damage distal to the array [70]. Finally, disruption of multiple blood vessels may exacerbate the extent of neural tissue damage. For example, Shih et al. found that occluding multiple cortical descending arterioles in proximity to one another produced a cavity similar to what we have observed, while occluding a single descending arteriole did not result in a large cavity, but rather a small region of neural cell death approximately 0.2 mm^3 in volume [146]. In summary, high-density silicon microelectrode arrays likely cause more extensive vascular damage than microelectrodes with a single penetrating feature, which provides an explanation for the loss of brain tissue we observed in this study but had not previously observed with simpler devices we have studied using a similar approach [53-58].

Other investigators have implanted high-density microelectrode arrays in rats, and some, but not all, report areas of brain tissue loss. Williams et al. reported "large acellular lesions" associated with some microelectrode tracts one week after implantation of a 20-channel microwire array in rat cortex [166]. Saxena et al. implanted 16-channel microwire arrays for 16 weeks and presented histology from a rat with poor recording performance alongside a rat with superior performance, and though their analysis focused on quantification of immunofluorescent signals, a cavity representing lost neural tissue associated with about half of the microelectrodes is visible in the image of the poorly-

performing device [80]. Finally, Ward et al. implanted a variety of microelectrode arrays into rats. While their histological images are difficult to interpret and only an N = 1 for each device is presented, there are areas of tissue loss in several of the figures [155].

Other studies do not report significant loss of brain tissue [34-36, 134, 167, 168]. Brain tissue loss may be underreported since most of the histological analysis has focused on the recording or tip regions of microelectrodes. However, there may also be differences in device design or surgical approach that reduce the amount of vascular damage and thus affect lesion volume. If this is indeed the case, it will be necessary to do controlled studies to identify optimal strategies, since neither rat strain, device type, electrode count, electrode spacing, dural removal, dural sealant, or insertion speed seem to provide a clear correlation with neural tissue loss when comparing such studies.

Meanwhile, in larger animals, there are reports of device settling, where high density silicon arrays are found sunken inside a depression on the cortical surface [37-39, 68, 169, 170]. This type of surface cavity has been observed at time points as short as seven days [169] and as long as multiple years [39], with a depth similar to what we observed in this study, although with a shape more closely matching the rectangular microelectrode array's base. Until more detailed histological evaluation of the area near the depression is carried out, ideally including stab wound injury experiments, it will be unclear whether such neural tissue loss is related to the initial vascular damage and /or subsequent tissue remodeling associated with the chronic foreign body response. We also suspect that another failure mode, gross device movement, may be related to remodeling of adjacent brain tissue following the initial vascular damage. Whether such movement may explain the inconsistent recording performance observed using such devices is unknown. The results

from this study would support the notion that both are involved, since fibrosis and tissue loss were associated with devices that had failed to record single units and were found displaced from the initial implantation site. The method of anchoring the device to the skull may also be important. Our approach in this study was similar to that used in large animal studies in that the microelectrode array was allowed to float on the cortex supported only by its wire bundle.

We also found that certain features of the FBR were associated with degradation of recording performance. The finding that the reduced SNR for center microelectrodes corresponded to higher levels of GFAP and BBB leakiness (as evidenced by IgG immunoreactivity) supports similar conclusions by Prasad et al., who reported that elevated immunoreactivity for ferritin, an iron storage protein that is increased by hemorrhage and/or a leaky BBB, correlated with reduced electrode performance, although this relationship was not analyzed statistically [35, 36]. A leaky BBB would create an unfavorable ionic environment for neuronal signaling, as well as contribute to neuroinflammatory cascades that lead to neurodegeneration and demyelination. BBB leakiness may prevent the closest neurons from surviving and/or firing properly, reducing SNR by allowing only more distant neurons with lower SNR to be detectable. Increased GFAP immunoreactivity may contribute by changing the distance between sensed neurons and the recording surface. Centrally located microelectrodes likely have increased BBB leakiness and GFAP immunoreactivity because they are surrounded on all sides by the vascular injury and FBRs of the other microelectrodes that provide a compounding source of proinflammatory cytokines and plasma proteins, while edge microelectrodes have healthy brain tissue on at least one side that may facilitate proinflammatory cytokine and

plasma protein clearance.

Meanwhile, the location of a microelectrode in brain tissue rather than in a lesion area also was related to recording performance. Lesion areas were mostly devoid of neurons and had a high amount of BBB leakiness and inflammation near their borders. Microelectrodes that were displaced from their original implantation site out of brain tissue would appear in a cavity area in such an analysis, so this also suggests that array movement, when it does occur, can be problematic for recording. The lack of other significant correlations may have been due to the low statistical power of our study group size. It is also worth noting that the high incidence of hardware-related failures were likely related to the thin, growing skulls of rats at this age.

Efforts by ourselves and other investigators have already shown some success in reducing the FBR, reducing BBB leakiness, and improving neuronal survival near chronically indwelling microelectrodes in studies in rats using single-shank silicon microelectrodes. However, this study also suggests that if such strategies are to be extended to high-density microelectrode arrays with many closely-spaced penetrating features, the problem of vascular damage and tissue loss must also be addressed. A number of techniques may reduce vascular damage. For example, decreasing the spatial density of microelectrodes is a straightforward approach. Lind et al. reported that multiple microwire bundles spaced 1 mm apart did not interact and were histologically similar to single microwire bundles [148], Liu et al. reported improved recording performance for sparse arrays (spacing 620 μm) versus dense arrays (spacing 380 μm) in cats in the first 125 days [23], and McConnell et al. reported reduced GFAP immunoreactivity surrounding four-shank planar silicon probes with 200 μm versus 125 μm spacing in rats at four weeks [147].

Another idea would be to implant single microelectrodes one at a time (perhaps with robotic assistance) exclusively in locations in between surface vessels, which would reduce vascular damage [165]. Approaching the cortex from below, rather than through the pia, has been accomplished in nonhuman primates [28] and could reduce vascular damage by transecting the smaller end branches of vasculature while leaving the larger pial vessels and penetrating arterioles/venules intact. It is also plausible that using softer and smaller microelectrodes may reduce vascular damage. Lastly, administering neuroprotective drugs [146], limiting bleeding by using hemostatic agents, and using immunomodulatory therapy may help limit the secondary cell damage to neural tissue caused by inflammatory sequelae. Our observation that away from the lesion cavity the FBR to edge microelectrodes appeared similar to that of a silicon microelectrode with a single penetrating feature is encouraging. If the problem of vascular damage can be addressed, recent strides in reducing the FBR to single penetrating microelectrodes may be applicable to high-density silicon microelectrode arrays and eventually translate into improved device performance in clinical settings.

2.6 Conclusions

We found that the FBR to a 4X4 UEA in rats is not the same as the FBR to devices that create a single penetrating injury, in that the UEA causes a more significant lesion to brain tissue that manifests itself in a cavity devoid of neuronal elements. Our results indicate that vascular damage is responsible for this difference in response. In addition we found that BBB leakiness, astrogliosis, and tissue loss were associated with reductions in recording performance. Moving forward, next generation high-density single unit

recording microelectrode arrays should be designed to reduce vascular damage caused by implantation as well as to reduce inflammatory sequela associated with the FBR over the indwelling period.

CHAPTER 3

ADVANCED AGE IS NOT A BARRIER TO CHRONIC INTRACORTICAL SINGLE UNIT RECORDING IN RATS

Manuscript submitted to the Journal of Neural Engineering on 23 Nov 2015. Authors: Nolta N.F., Christensen M.B., Tresco P.A.

3.1 Abstract

Available evidence suggests the brain and the immune system undergo changes with age that increase a person's susceptibility to injury, inflammation, and neurodegeneration. Since a large proportion of potential brain-machine interface (BMI) patients are aged individuals, we studied the foreign body response (FBR) and recording performance in 18-month-old rats implanted with a 4x4 Utah Electrode Array (UEA). We found that single unit recording performance was more robust over the 12-week indwelling period compared to a similar study using the same device and a similar surgical approach in young adult rats. Like the earlier study, the amount of neural tissue loss and astrogliosis was inversely correlated with recording performance. A comprehensive forensic analysis suggested that the improvement in recording was related to increased skull thickness in the older cohort

and decreased grooming behavior, which together reduced forces on the headstage and extended recording lifetime. The results indicate that advanced age is not a limiting factor for use of BMIs and further reinforces the notion that reducing implantation injury, the FBR, and headstage-related forces are important design goals for next-generation single unit recording arrays.

3.2 Introduction

Paralysis, which can result from a number of central nervous system diseases or injuries, currently affects 1 in 50 Americans [1]. Sixteen percent of these patients are completely unable to move a part of their body [1]. Meanwhile, limb loss affects 1 in 190 Americans [3]. In both of these patient populations, the loss of specific motor functions imposes a significant lifelong burden on the patient's comfort, productivity, and independence.

BMIs are in development to restore motor functions for individuals with paralysis or limb loss. Already, BMIs have provided patients with tetraplegia volitional control over computer cursors [27, 31] and robotic arms [4, 5]. Unfortunately, the performance and reliability of these systems are not robust enough for widespread clinical adoption. Available evidence suggests that reducing the FBR to the implanted microelectrode arrays may improve performance and reliability [35, 36, 171, 172].

The population of people with paralysis and limb loss includes a significant number of aged individuals. Fifty-six percent of individuals with paralysis are over the age of 50, and 33.5% are over 60 [1]. Eighty percent of individuals with limb loss are over 45, and 42% are over 65 [3]. Therefore, brain-machine interfaces should be evaluated in aged as well

as young subjects. Moreover, most young patients will eventually reach at least middle age. Even in the extreme case of high tetraplegia due to spinal cord injury, a 20-year-old patient who survives the first year after injury has a life expectancy of 57 years [81].

During aging, the immune system undergoes senescence. Aged individuals have reduced numbers of naïve B and T cells, decreased stimulated phagocytosis and reactive oxygen species (ROS) production by neutrophils and macrophages, and dysregulation of cell signaling pathways [83, 84]. These changes result in delayed wound healing [97] and increased levels of proinflammatory cytokines [83, 84]. The brain also changes with age. Microglia, the brain's tissue-resident macrophages, acquire a more reactive phenotype [99]. Microglia become larger and less ramified, express increased markers of activation such as major histocompatibility complex (MHC) class II and clusters of differentiation 68 and 45 (CD68 and CD45), and produce higher levels of proinflammatory cytokines such as tumor necrosis factor alpha (TNF-α) and interleukins 1-β and 6 (IL1-β and IL-6) [100-104]. Astrocytes become more numerous and hypertrophic [105]. Mild neuronal loss and reductions in dendrites and synapses occur naturally [106]. In addition, the aged brain becomes more susceptible to developing neurodegenerative diseases that involve more radical loss of brain tissue such as Alzheimer's disease [107] and Parkinson's disease [108]. The processes of immune senescence, inflammation, and neurodegeneration are thought to be linked to one another and are the subject of continued research.

Due to these changes, aged patients may present a uniquely challenging environment for the successful integration and functioning of an intracortical microelectrode array. First, the injury of implantation may be greater in aged patients. Aged patients have poorer clinical outcomes following brain injuries such as ischemic stroke [109], traumatic brain

injury [110], and aneurysmal subarachnoid hemorrhage [111], and aged rodent models show increased loss of neural tissue following experimental injuries [112, 113]. The implantation of a microelectrode also causes injury. With small, simple devices, the injury of implantation alone is not sufficient to cause permanent loss of neural tissue. This has been established by implanting a microelectrode, immediately withdrawing it, and histologically evaluating the implant site weeks later [53, 59, 71, 72]. Larger, more complex devices of the type used for BMIs create a more significant injury [70] that results in permanent loss of neural tissue [171]. Since microelectrodes can only record neural signals within about 100 μm of their recording sites [41], extensive tissue loss can reduce recording performance. If implantation injury is exacerbated in aged individuals, reducing implantation injury will need to be a high priority for next-generation intracortical microelectrode arrays.

Another concern is that aged patients may develop a more severe FBR to intracortical microelectrodes. Within two weeks, microelectrodes in brain tissue become covered with a layer of activated macrophages that secrete proinflammatory cytokines [53]. Astrocytes in the vicinity of these activated macrophages become hypertrophic and form a glial scar [52-61, 72, 171]. Plasma proteins such as immunoglobulin G (IgG), which are normally excluded by the blood-brain barrier (BBB), leak into brain extracellular space and activate macrophages and complement [55-59, 72, 171]. Demyelination [52, 55, 61] and degeneration of neuronal processes [52-54, 61, 72] accompany these reactions. This has led to the hypothesis that the FBR leads to recording inconsistency and failure by causing neurons within the recording range to become silenced or disconnected from cortical circuitry.

Support for this hypothesis is mounting. One study reported that increased levels of neurodegenerative protein products in blood samples were associated with reduced recording performance at chronic time points in rats [35]. Another study found that when rats were given an anti-inflammatory drug, recording performance was improved [134]. Another study reported that knockout mice missing an enzyme necessary for IL-1β production largely preserved their initial recording performance, in contrast to wild type mice whose performance declined throughout a 26-week experiment [138]. These and other studies [36, 171, 172] suggest that reducing the severity of the FBR may improve recording performance. In aged patients, since the immune system generates more inflammation and neural tissue is more sensitive to degeneration, reducing the FBR may be even more important for recording quality.

Perhaps the most relevant data available are those comparing clinical outcomes from deep brain stimulation (DBS) devices implanted in young and aged patients. Aged patients receiving DBS electrodes have increased rates of complications [114], somewhat decreased clinical benefit [115-117], and increased rates of cognitive and behavioural impairments [117]. Despite these concerns, no studies to our knowledge have examined intracortical microelectrode arrays in aged animals. Fig. 3.1 shows an analysis of 41 studies that have examined the FBR to intracortical microelectrodes in rats. The data indicate that there has been a strong preference for studying rats in the early part of adulthood. The ages of patients in human BMI studies are 25 [27], 52 [5], 58 [4, 31], and 66 [4], so it is known that recording is at least possible in some aged humans. In order to gain a better understanding of the effect of age on the FBR and recording performance, we implanted 4x4 UEAs into aged rats for 12 weeks, analyzed recording performance and the FBR, and

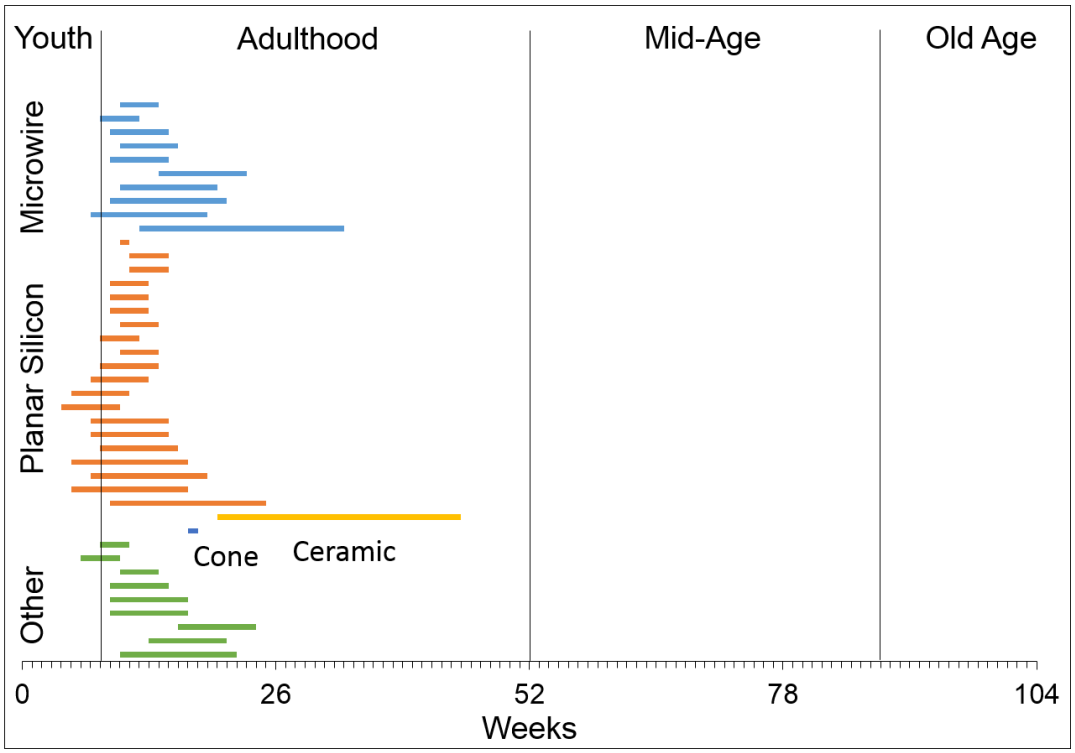

Fig. 3.1: Ages of rats used in 41 studies of the FBR to microelectrodes in the rat brain. The majority of studies used rats in early adulthood, and no studies used rats of mid-age or old age.

then compared these results against a previous study in young rats.

3.3 Materials and Methods

3.3.1 Microelectrodes

UEAs were purchased from Blackrock Microsystems, Salt Lake City, UT. The arrays had a 4x4 rectangular grid of 1 mm long microelectrodes spaced 400 µm apart (Fig. 3.2 A) and were similar in overall design to the 10x10 microelectrode recording arrays used in nonhuman primates [39, 163] and in clinical studies [5, 27]. The wiring diagram relating connector pins to the locations of each microelectrode on the array was supplied by the manufacturer so that discrete forensic evaluation of the FBR and single unit recording

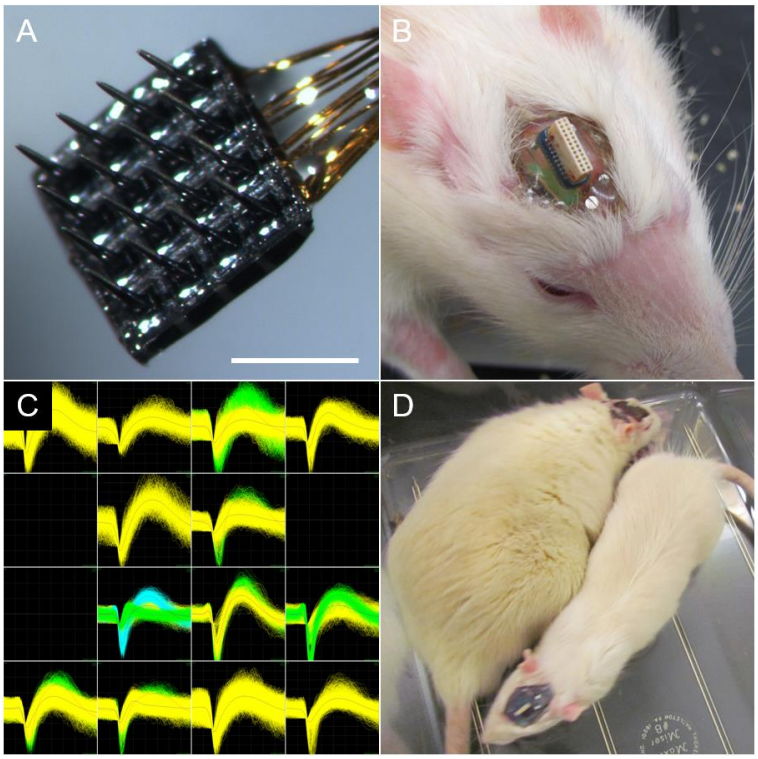

Fig. 3.2. Materials and methods. (A) 4x4 UEA before implantation. Scale bar = 1 mm. (B) Aged rat headstage four weeks after implantation. Some screws are visible through the clear acrylic headstage. (C) Waveforms from a recording session three weeks after implantation with 21 units on 13 channels. (D) 18-month-old, 800 g rat alongside a 15-week-old, 400 g rat.

could be performed. UEAs were sterilized with ethylene oxide and allowed to outgas for at least 12 h prior to surgery.

3.3.2 Animal Surgery

All procedures involving animals were approved by the University of Utah Animal Care and Use Committee. Male Sprague Dawley retired breeder rats approximately eight months of age were fed *ad libitum* and housed in pairs until they became too large to share a single cage. Rats were aged to at least 72 weeks before implantation.

Eight rats were anesthetized with isoflurane and their heads were shaved. The rats were

positioned in a stereotactic frame and the scalp was disinfected with 70% isopropyl alcohol and betadyne. A midline incision was made along the length of the skull and the exposed scalp was dried using cotton applicators. Four stainless steel screws (Fine Science Tools, Foster City, CA) were screwed into the skull after drilling pilot holes with a pneumatic dental drill. A rectangular craniotomy approximately 3x5 mm was created over the right primary motor cortex using a pneumatic dental drill with sterile saline rinses to prevent excessive heating. The dura was pierced and reflected with a 25 gauge needle. The UEA's associated connector was held in a stereotaxic manipulator, so that the UEA hung horizontally supported by the stiffness of the wire bundle, and was positioned over the craniotomy. The UEA was then inserted into brain tissue by lightly pushing on the backside of the array with forceps. The reference wire was also inserted into the brain using forceps. The craniotomy was then covered with Kwik-Cast silicone (World Precision Instruments, Sarasota, FL). After the silicone set, the UEA's connector was positioned over the center of the skull and fixed in place between four screws set at angles into the cranial ridge using photocurable acrylic adhesive (1187-M, Dymax, Torrington, CT). The ground wire was tunneled a short distance under the skin behind the head. Fig. 3.2 B shows a close-up of the UEA connector and acrylic headstage in a rat four weeks after implantation.

3.3.3 Electrophysiological Recordings

Rats were allowed to recover for one week, after which time neural recordings were obtained from freely moving animals for a period of five minutes twice per week using a Cerebus data acquisition system (Blackrock Microsystems, Salt Lake City, UT) and

analyzed offline using Plexon Offline Sorter (Plexon, Dallas, TX) (Fig. 3.2 C). Single units were isolated in principal component space using a manually assisted sorting algorithm. Signal-to-noise ratio (SNR) was determined by dividing the peak-to-peak amplitude of the average waveform of an isolated unit by the RMS noise floor on that microelectrode. The recording performance for a particular week was determined using the better of the two sessions for each individual microelectrode on the array.

3.3.4 Failure Analysis

In order to track the cause and time course of device failure, animals were examined at each recording session for signs of headstage/connector failure, broken lead wires, or for a loss of recordable neural activity. If there were no observable hardware-related issues and the UEA was still functional at the time of recording, then failure was attributed to the FBR. Animals with devices that did not fail were sacrificed 12 weeks after implantation.

3.3.5 Euthanasia and Tissue Preparation

At sacrifice, rats were anesthetized and perfused transcardially with phosphate buffered saline pH 7.4 (PBS) followed by 4% paraformaldehyde in PBS. Their brains were removed from the skull and the arrays dissected free. Brains and arrays were postfixed for 24 h in 4% paraformaldehyde in PBS and equilibrated in a 30% sucrose solution before 30 µm horizontal brain sections were obtained using a cryostat.

3.3.6 Immunohistochemistry and Microscopy

Free-floating brain sections were incubated overnight in PBS with 4% v/v goat serum (Invitrogen, Carlsbad, CA), 0.5% v/v Triton-X 100, and 0.1% sodium azide then incubated overnight with the following primary antibodies in blocking solution: CD68 (ED-1, AbD Serotec, Raleigh, NC, .25 µg/ml) to identify activated macrophages and microglia, IBA-1 (Wako Chemicals USA, Inc., Richmond, VA, .5 µg/ml) to label all macrophages and microglia, IgG (biotinylated goat anti-rat IgG, Southern Biotec, .5 µg/ml) to assess BBB leakage, GFAP (DAKO North America Inc., Carpinteria, CA, 2.9 µg/ml) to examine astrocyte cytoskeleton location and hypertrophy, NeuN (EMD Millipore, Billerica, MA, 1 µg/ml) to identify neuronal nuclei, and NF160 (Sigma-Aldrich, St. Louis, MO, 5 µg/ml) to visualize axons/dendrites. Sections were then rinsed three times with PBS for 1 h each before being incubated overnight with appropriate fluorescently labeled secondary antibodies plus 10 µM DAPI to label cell nuclei, then finally rinsed again three times with PBS for 1 h each. All incubations were performed at room temperature on a rocker. The same protocol was used on explanted arrays to identify adherent cell types. Sections were mounted on slides and coverslipped in Fluoromount-G (Southern Biotec) then imaged with a confocal microscope. For retrieved arrays, images were taken using a confocal microscope 5x air objective or a 40x water objective with the array submersed in PBS in a petri dish. Due to anti-mouse secondary antibody cross-reactivity with high concentrations of endogenous rat IgG in tissue sections, the IBA-1 image was used to eliminate IBA-1-negative areas from some CD68 images (since all activated macrophages should also be IBA-1+) and the IgG image was subtracted from the neuronal nuclei image to reduce the brightness of cross-reactive labeling. These image adjustments were not performed on

images for quantification. All histological images are maximum intensity projections.

3.3.7 Measurement of Lesion Cavity Volume

To calculate the volume of damaged neural tissue, 2D cavity areas in histological sections were manually described in Photoshop (Adobe Systems Inc., San Jose, CA). The prismoidal formula:

$$V = \frac{L}{3}\left(A + \sqrt{AB} + B\right)$$

was used to estimate the cavity volume *V* lying between two sequential sections separated by distance *L* and having 2D void areas *A* and *B*, then summed over all sections.

3.3.8 Image Quantification

The adhesion of tissue to some but not all microelectrode shafts made traditional image quantification methods, where immunofluorescence is generally quantified beginning at the edge of the microelectrode track, impossible. Instead, here immunofluorescence was quantified from the outer edge of the dense CD68+ layer if it was visible. If it was not visible, the dense CD68+ layer was presumed to have adhered to the explanted microelectrode, and immunofluorescence was quantified from the edge of the track hole as usual. Thus, measured immunofluorescence values represented the average immunofluorescence intensity of brain tissue outside the dense CD68+ layer in both cases and inside a circular 100 μm radius centered on the track for all microelectrode tracks, normalized to the average immunofluorescence in three 636x636 μm areas in a similar region of cortex in the contralateral hemisphere in each section as a control.

3.3.9 Statistics

Outliers in the data were identified using an interquartile test, with outliers considered as those lying above or below 1.5*IQR (interquartile range) ± Q3 or Q1, respectively. To better understand the relationship between recording performance and the FBR, we compared individual microelectrodes within a 4x4 array that recorded a single unit versus microelectrodes that did not over a variety of metrics using z-tests for two population proportions or Student's t-tests. P values below 0.05 were considered significant.

3.4 Results

3.4.1 Aged Rat Model

Rats were aged in our animal facility to at least 18 months before implantation, reaching an average weight of 935 ± 135 g. At this age the rats were obese, mostly sedentary, poorly groomed, and required softer bedding to control foot sores. Fig. 3.2 D shows an implanted 73-week-old rat next to a 15-week-old adult rat, an age typical for microelectrode array FBR studies [35, 36, 53-59, 67, 72, 78, 80, 134, 136, 147, 152, 153, 155, 156, 171].

3.4.2 Failure Analysis

Failure modes are summarized in Fig. 3.3. One animal died of unrelated complications of old age four weeks after implantation. Another animal experienced a complete loss of recordings after five weeks. Upon dissection, this animal was found to have a large white blood cell and macrophage-filled lesion cavity in the implant area. Another animal's headstage became detached after seven weeks. The remaining five implanted animals continued to record single units through the 12-week study endpoint.

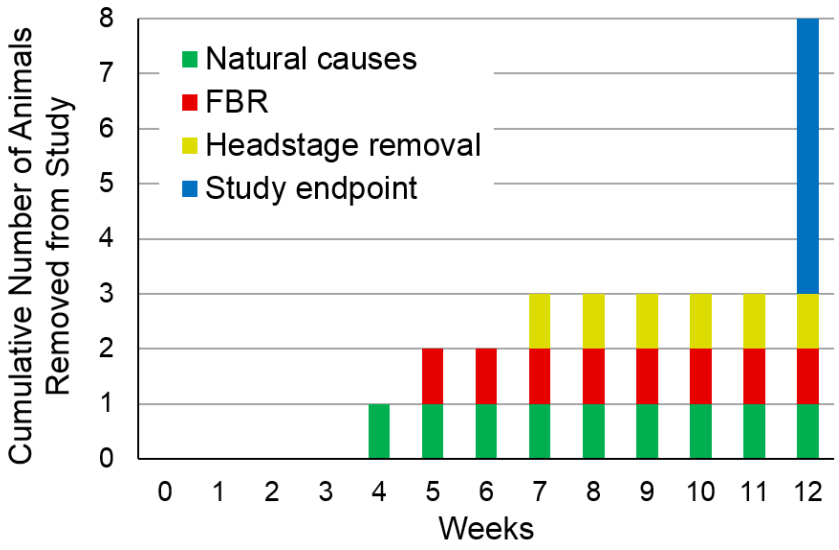

Fig. 3.3. Summary of failure modes. One animal died of old age and one was removed due to headstage removal. Another animal had a complete loss of recording ability at five weeks despite a functional UEA and was found to have had a large white blood cell-filled lesion at its implant site. The remaining five animals continued to record to the 12-week study endpoint.

3.4.3 Electrophysiology

In two of the eight animals, single unit action potentials could not be isolated during any of their recording sessions, even though their devices appeared to be recording electrical activity and there were no indications of any problems with the implantation or surgical recovery. One of these animals died of old age four weeks after implantation and the other lost its headstage at seven weeks.

In the other six animals, single unit action potentials were isolated on most recording sessions. Recording performance varied across animals and across time, but was generally highest at weeks 3-4 and decreased thereafter (Fig. 3.4). Peak performance, or the best recording session for each rat, was 12.7 ± 5.9 units. Both the average number of units and the SNR were negatively correlated with time ($p < 0.001$).

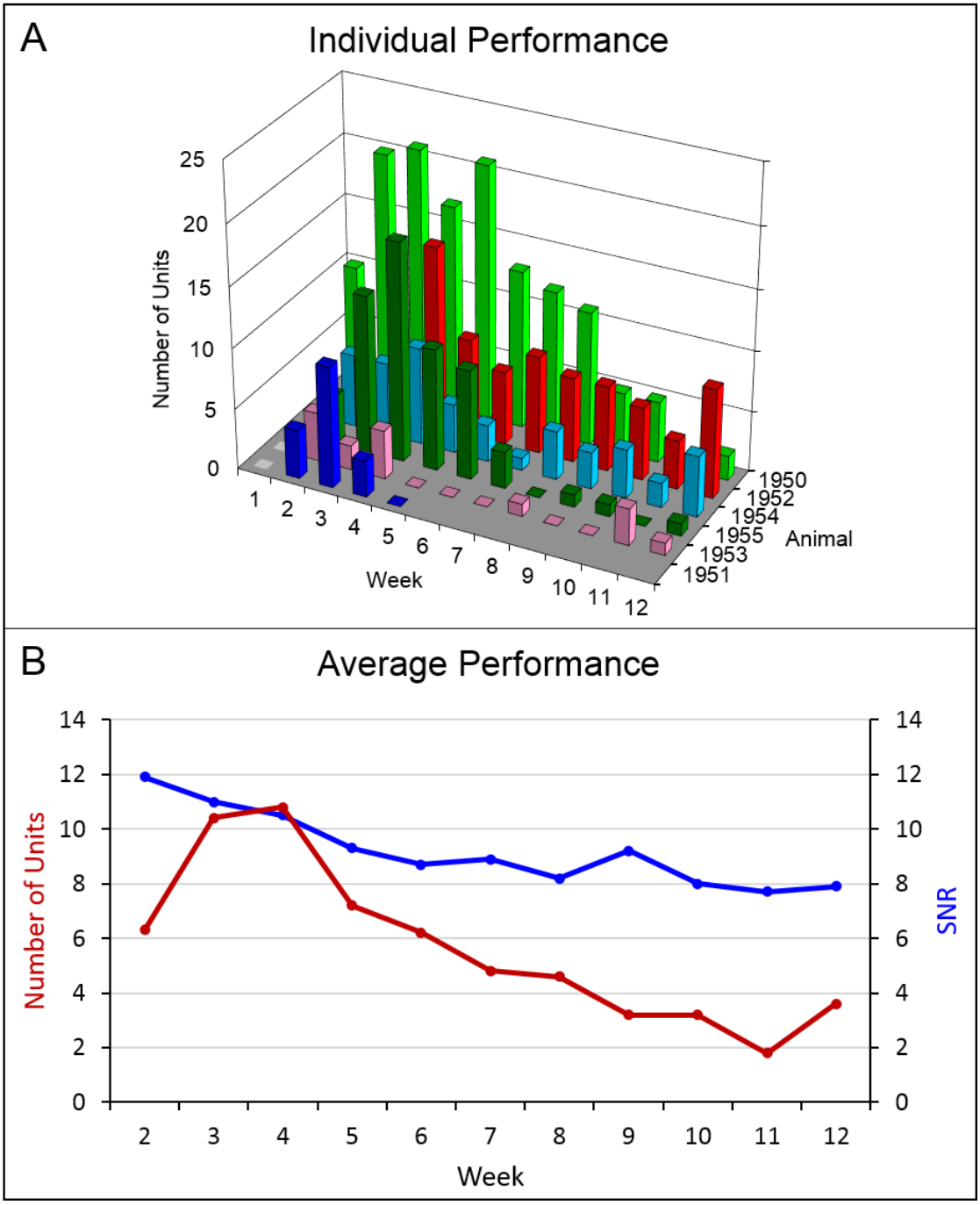

Fig. 3.4: Summary of recording performance over time for the six animals that recorded units. (A) Individual performance. (B) The average number of single units recorded was highest at weeks 3-4 and decreased thereafter. SNR slowly decreased over the indwelling period. Both of these negative correlations with time were significant at $p < 0.001$.

3.4.4 Explanted Arrays

All of the explanted arrays were encapsulated in fibrotic tissue that was much thicker than the outer meningeal layers and was attached to the skull, making the dissection very difficult. The amount of attached tissue ranged from just covering the base of the array (as shown in Fig. 3.5 A, N=4) to enveloping much of the array (N=4). An immunohistochemical analysis of explanted arrays revealed that a large number of CD68+ activated macrophages/microglia were present in the adherent tissue, especially near the base of the array (Fig. 3.5 B).

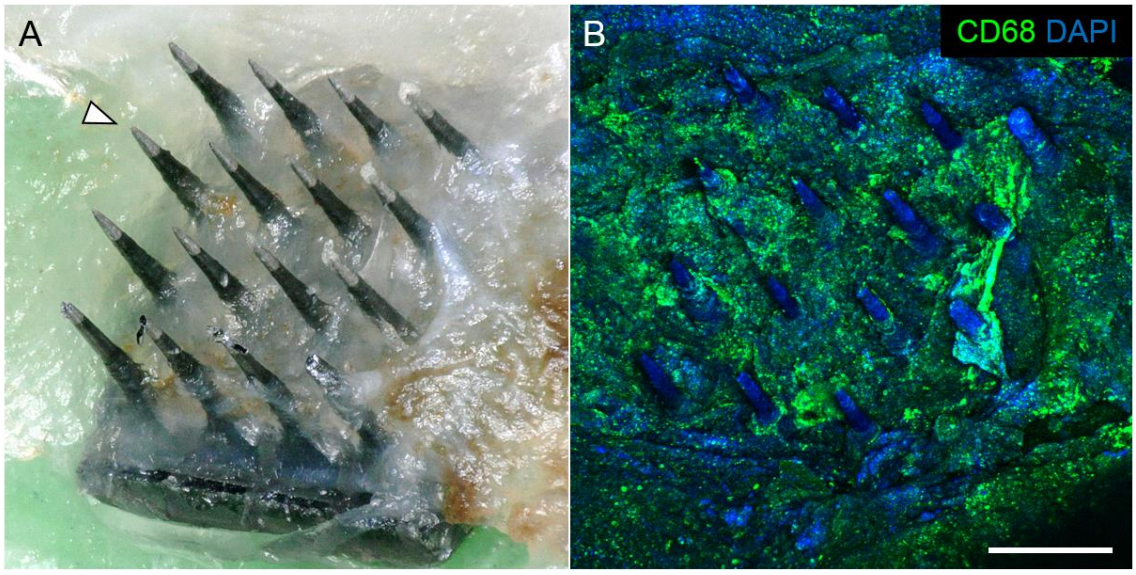

Fig. 3.5. Explanted arrays. (A) Representative photograph of a UEA explanted after 12 weeks. The base was fully encapsulated, the shafts were partly encapsulated, and the tips were mostly free of tissue. Arrowhead indicates the electrode identified in Fig. 3.6. (B) Large numbers of activated macrophages (CD68) and cell nuclei (DAPI) are associated with the tissue on the retrieved UEA, especially at the base. Scale bar = 500 µm.

3.4.5 Description of the FBR

After removing the brain from the skull, a lesion in the surface of the brain was visible where the UEA was previously seated. The lesion cavities were variable in size and shape, but tended to be pyramidal, becoming narrower with depth into the cortex. Perfused neural tissue at the margins of the lesion cavity also had a slightly darker color. In four rats, the lesion appeared to encompass the entire array. These were the same rats with explanted arrays that were completely encapsulated. In the other rats, the lesions were narrower and appeared to extend in some cases to the microelectrode tips. These smaller lesion cavities were filled with fluid and lacy connective tissue with CD68+ activated macrophages present. Fig. 3.6 A shows a reconstruction from histological sections of one such cavity in the same rat as shown in Fig. 3.5. Lesion cavities were not always under the array and in some cases extended into adjacent brain regions. The average lesion volume was 1.3 ± 0.6 mm^3.

In horizontal sections, the lesion cavity appeared as a gap in the tissue (Fig 3.6 B-D). The border of the cavity had high immunoreactivity for IgG, decreased immunoreactivity for neuronal nuclei and neurofilament, and increased immunoreactivty for GFAP. The cavities were partially filled with lacy, CD68+ tissue. Microelectrode tracks were visible in cases where the array was not completely encapsulated. Each microelectrode track fit one of two general descriptions: either they appeared as an empty hole in the section, or they appeared as a smaller empty hole surrounded by a dense ring of CD68+ immunoreactivity (Fig. 3.7). The microelectrode tracks with little or no CD68+ immunoreactivity in tissue sections tended to correspond to microelectrodes that had more tissue attached to the explanted microelectrodes.

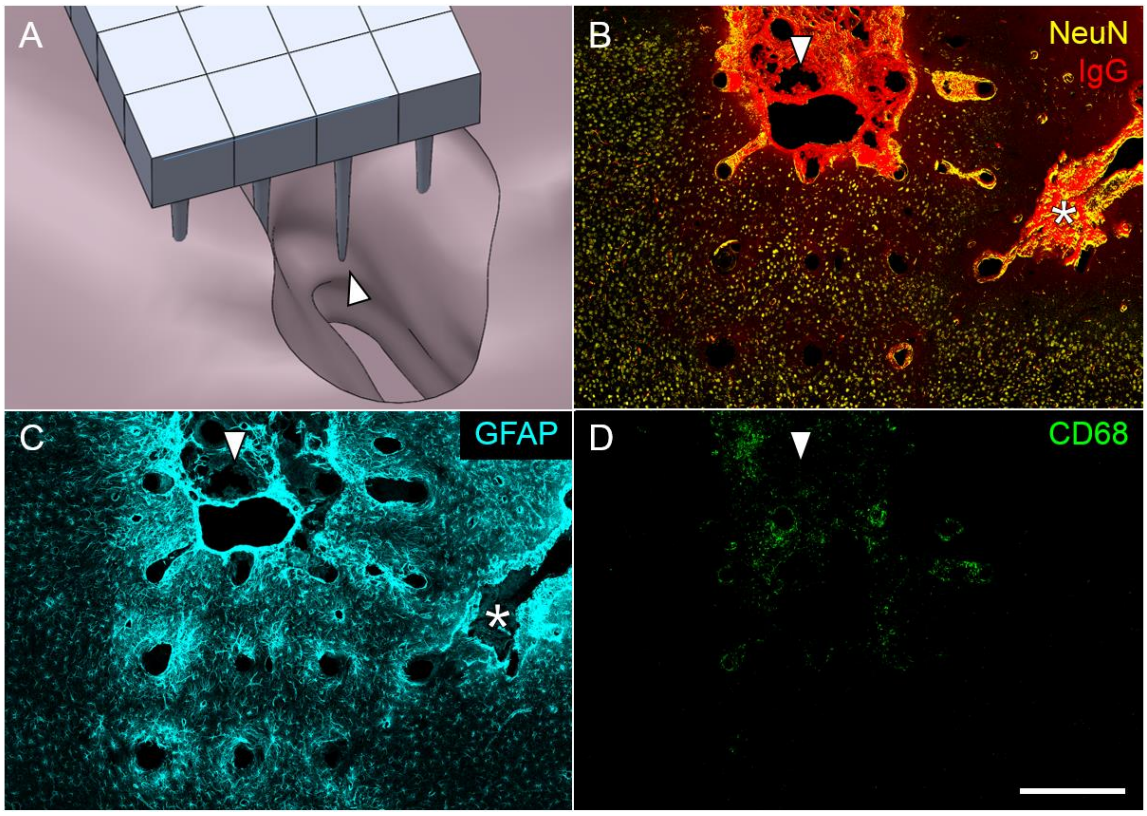

Fig. 3.6. Description of the FBR. (A) SolidWorks rendering of a deep but narrow lesion cavity in relation to one of the microelectrode tips (arrowhead). (B) Horizontal section from the same animal showing BBB leakage (IgG) and neuronal nuclei (NeuN) at a depth near the tips of the 4x4 array of microelectrodes. The microelectrode inside the lesion cavity in (a) is indicated with an arrowhead in (b-d). Another, more narrow cavity extending off the edge of the array is indicated with an asterisk. IgG was highly concentrated in lesion cavities and was minimally present in intact parenchyma. Neural cell body loss was evident at the margins of lesion cavities. (C) Hypertrophic astrocytes (GFAP) were visible around each microelectrode track and surrounding the lesion cavities. (D) Activated macrophages/microglia were present in the larger cavity and around some of the microelectrodes. Scale bar = 500 µm.

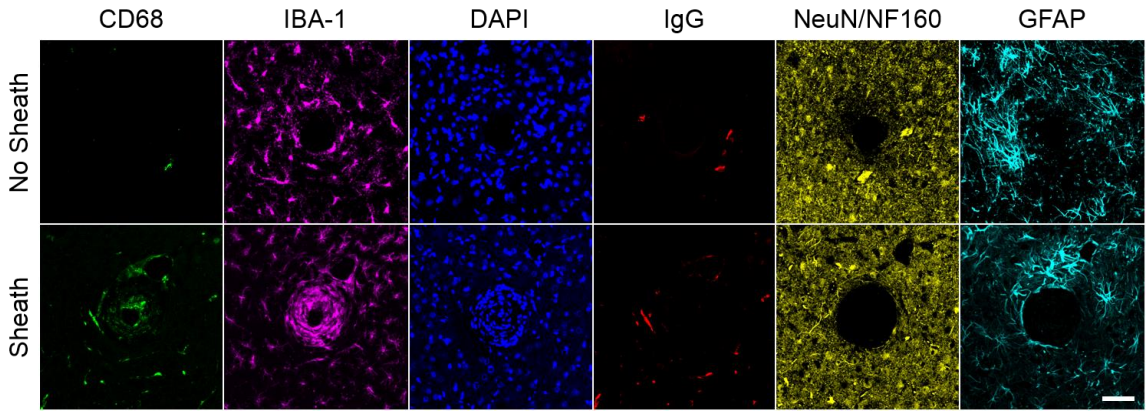

Fig. 3.7. High-magnification view of two principal types of microelectrode tracks in horizontal sections taken at a depth near the tip. The top row shows a representative microelectrode track that did not have a CD68+ sheath. In this case, activated macrophages/microglia (CD68) were absent and the track hole was devoid of macrophages/microglia (IBA-1) and cell nuclei (DAPI). Surrounding the track, BBB leakage (IgG) was minimal, neurons (NeuN/NF160) were absent inside the track, and astrocyte cytoskeletal intermediate filaments (GFAP) were slightly increased. The bottom row shows a representative microelectrode tip section with a CD68+ sheath. A compact, CD68+, IBA-1+, hypercellular sheath surrounded a small track hole. IgG, NeuN/NF160 and GFAP appeared similar. Scale bar = 100 µm.

Stab-wounded animals (N = 5) sacrificed four weeks after implantation also had lesion cavities on the surface of their brains, with an average volume of 2.5 ± 1.3 mm^3. The general histological characteristics and gross appearance of such lesions in stab-wounded animals four weeks after stab wound injury were similar to lesion cavities in the implanted animals sacrificed at 12 weeks with the exception of the size difference. No microelectrode tracks were visible in stab-wounded animal tissue sections.

3.4.6 Analysis of Recording Performance and Histology

In the final week of recording, all surviving animals had arrays that were able to record at least one single unit. The arrays with the smallest lesion cavity volumes recorded the largest number of single units (Table 3.1). The two arrays with the largest lesions and with

Table 3.1. Summary of recording performance and gross characteristics of 12-week animals.

Animal	**Electrodes with units at week 12**	**Cavity volume (mm^3)**	**Tissue on explanted array**
1952	8	0.86	Base only
1954	5	0.85	Base only
1950	2	2.22	Entire array
1955	1	7.35	Entire array
1953	1	1.21	Base only

the largest amount of encapsulation tissue on the explanted arrays had only 1-2 microelectrodes that were recording single units.

Quantification of FBR-associated biomarkers in the brain tissue surrounding the recording tip revealed that reactivity for GFAP was significantly higher around microelectrodes that did not record units ($p = 0.047$) (Fig. 3.8). Levels of CD68 and IgG were similar between microelectrodes that recorded at least one unit and those that did not.

3.5 Discussion

In this study, we implanted 18-month-old rats with 4x4 UEAs and examined recording performance over a 12-week indwelling period. Based on a 25-month median lifespan for male Sprague Dawley breeder rats [173] and an 80-year median lifespan for American males [174], the equivalent human age for these rats was 53 years at implantation and 62 years after the 12-week implant duration [175].

We found that chronic recording performance was more robust in aged rats than in a

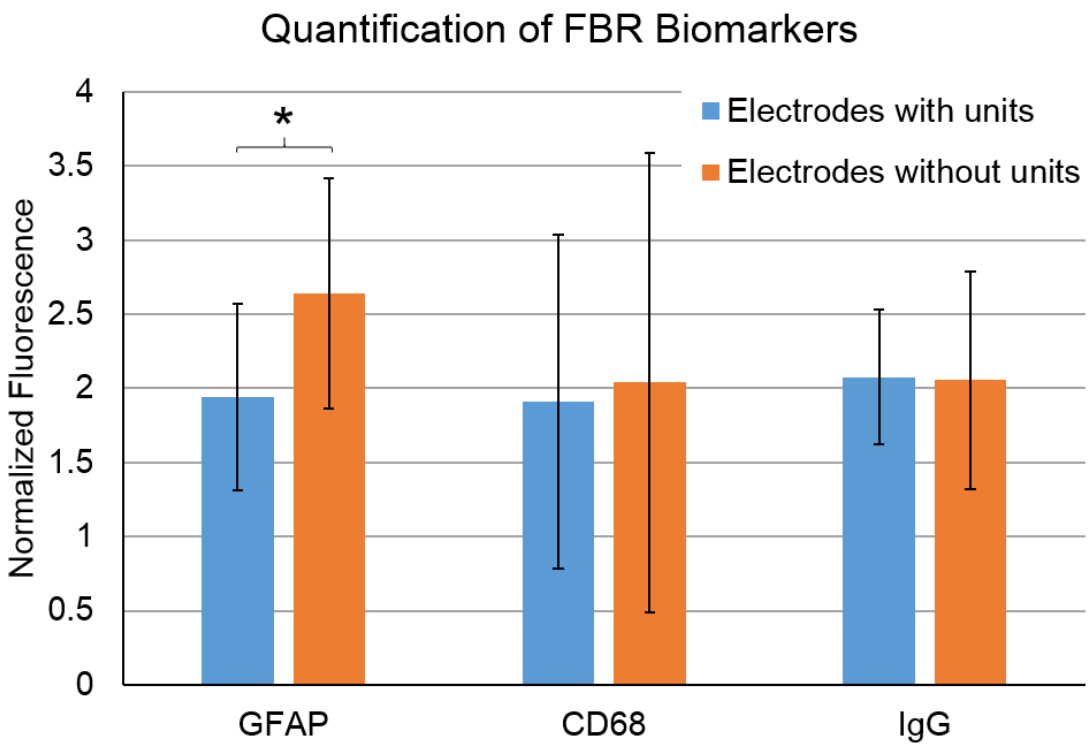

Fig. 3.8. Quantification of FBR biomarkers in brain tissue within a 100 µm radius of the tip of individual microelectrodes. Microelectrodes that recorded at least one unit in the final week of recording had significantly lower levels of astrocyte cytoskeleton (GFAP) ($p = 0.047$). Levels of activated macrophages/microglia (CD68) and IgG were not statistically different.

previous study performed with younger adult rats using similar methods [171].

High recording performance in this study was surprising considering the relatively low performance in a previous study [171] and a body of literature that suggests that the biological effects of aging might decrease performance. Peak performance was higher in aged rats, where the best recording session for each rat had 12.7 ± 5.9 units compared to 8.1 ± 4.6 units in a younger cohort ($p = 0.13$) [171]. SNR was also similar, and in both studies gradually decreased. The main difference was that, in this study, we were able to record single units on multiple sessions in 6 out of 8 aged rats, compared to 10 out of 28 younger adult rats in the previous study ($p = 0.049$) [171]. Recording longevity was greatly

improved, with 5 out of 8 aged rats recording units after 12 weeks, compared to 2 out of 28 young rats ($p < 0.001$). Thus, it can be said that recording performance was more consistent across animals and over time in aged rats than in the previous study in young rats.

The aged rat brain's increased sensitivity to injury and inflammation, outlined in the introduction section, was expected to have a negative impact on recording performance. Although it is possible that features of the aged brain and immune system had a positive impact on single unit recording performance, we believe that other factors may be responsible for the differences observed.

Aged rats have thicker skulls, and in this study, had lower physical activity and grooming behavior than one observes in younger adult rats. The rat skull's thickness increases rapidly during childhood and adolescence [176], and continues at a slower rate during adulthood. Low physical activity levels are typical of aged, *ad libitum*-fed rats without exercise regimens [177]. The rigid acrylic headstages were well anchored at the end of the three-month indwelling period. The data suggest that a combination of these factors reduced headstage-related failures and likely reduced movement translated to the indwelling microelectrode array. Such motion has been proposed as an explanation for the increased FBR observed when a device implanted into the rat brain is fixed to the skull [54, 145, 178], has high mass density [152], or has high stiffness [153].

We generally observed less immunoreactivity for IgG and CD68 in the aged rats in this study compared to an earlier published young adult rat study [171]. This is likely at least partly related to the longer implant durations in the aged rats. IgG has been reported to decrease with time for single-shank planar silicon electrodes in rats [59] and mice [77].

Literature on CD68 immunoreactivity describes reduced [36, 59, 72, 77] or not significantly different [35, 55, 56] levels of CD68 at 12 or more weeks compared to two or four weeks. CD68 is indicative of phagocytosis by activated macrophages, so as cellular debris clearance reaches conclusion, less phagocytic activity is likely observed.

The final notable difference between the aged rats in this study and the younger adult rats in a previous study was the increased amount of encapsulation tissue on explanted arrays in the aged rats. In this study, encapsulation tissue was present on UEAs from all rats, whether they were sacrificed at 4, 5, 7, or 12 weeks. The amount of tissue was variable and did not clearly correlate with time, however it did correlate with the volume of the lesion cavity in the brain. It is likely that brain tissue lost due to implantation injury fills in with non-neural tissue, which may anchor or otherwise minimize movement of the microelectrode array. Increased tissue adhering to individual microelectrode shafts explains the lack of a CD68+ sheath surrounding some microelectrode tracks in horizontal sections. In the previous study in younger adult rats, a large amount of encapsulation tissue was present on the two UEAs retrieved from rats 12 weeks after implantation [171]. In most of the other rats, however, the UEAs were cleanly removed from cortex, and an empty cavity with a small amount of lacy CD68+ tissue was found in tissue sections. The most probable explanation is that non-neural encapsulation/fibrotic tissue accumulates at a variable rate beginning 2-5 weeks after implantation, after macrophages clear the lesion cavity.

Recording performance was found to negatively correlate with lesion cavity size. In this study and a previous study [171], lesion cavities occurred in both implanted and stab-wounded rats, suggesting that neural tissue loss primarily results from the initial injury of

device implantation. The lesion cavities were smaller in the implanted rats sacrificed at 12 weeks than in the stab-wounded rats sacrificed at four weeks, possibly due to astroglial wound contracture. Outside of our work, lesion cavities have only been reported in rats in a subset of studies that used high-density, multishank microelectrodes [80, 155, 166], and not in those using planar microelectrode arrays with one or a few shanks. Williams et al. found significantly altered impedance spectra for microwires associated with lesions but did not attempt to record single units [166]. Saxena et al. and Ward et al. each show lesion cavities in their figures, but their N was too small for them to draw statistically-based conclusions [80, 155]. Two studies by Prasad et al. did not report any neural tissue loss, but did report that increased injury during implantation, as evidenced by bleeding, was associated with reduced recording performance [35, 36].

Reduced recording performance also correlated with increased levels of astrogliosis. We found that individual microelectrodes that did not record any units in the final week of recordings had significantly higher levels of GFAP immunoreactivity within a 100 μm radius of microelectrode tips in sections near the recording zone. These findings agree with previous findings, in which higher levels of GFAP corresponded with reduced SNR for individual microelectrodes within the same array [171]. This relationship may be causal if hypertrophic astrocytes interfere with normal neuronal function in the vicinity of the microelectrodes, or it may be that GFAP immunoreactivity is a good indicator of subtle neuroinflammatory processes that reduce recording performance.

A previous study found a relationship between BBB leakage (indicated by IgG) and recording performance [171], but that relationship was not statistically significant in this study. It is likely that the overall lower levels of IgG in this study reduced its usefulness

as an indicator. Another possibility is that the IgG present in the CD68+ sheath immediately adjacent to (and often removed with) the microelectrode would have been predictive of microelectrode performance, but could not be included in our quantification in this study. Saxena et al. found that IgG was associated with reduced performance, but only when comparing two different types of devices, or when comparing just one high-performing and one low-performing microwire array [80]. It is unclear how such a conclusion was drawn given the low N. Two studies by Prasad et al. did not look at IgG, but rather ferritin, an iron storage protein found in macrophages after BBB disruption when iron sequestration is needed. The researchers reported that higher levels of ferritin were associated with reduced performance, although this relationship was not supported by statistical methods [35, 36].

To summarize, we found that skull thickness, animal activity level, and use of well-anchored headstages were likely responsible for improving single unit recording performance in aged rats relative to the younger adult rats in a previous study. At the same time, we observed reduced markers of activated macrophages and BBB leakage as well as increased levels of encapsulation tissue, which may have been the result of reduced motion of the implant or an increased indwelling period. Finally, we found additional evidence that increased astrogliosis and tissue loss correlated with decreased single unit recording performance.

These findings have implications for studies in larger animals and humans. They continue to support the idea that reducing the FBR and the impact of implantation injury are likely to improve chronic single unit recording performance. This could be accomplished by reducing device surface area [57, 67], increasing device permeability

[58], reducing device size [156], reducing device stiffness [153], increasing spacing between microelectrodes [72, 147], administering drugs locally [78] or systemically [134, 136], and implanting single-shank devices away from surface vessels [165], to name a few strategies that are supported by peer-reviewed studies.

Furthermore, our results suggest that functional issues related to the headstage and wire bundle may be underappreciated. Fibrotic tissue buildup that results in removal of the device from cortex has been described for UEAs in nonhuman primates [39] and cats [37, 68] and for microwire arrays in cats [170]. Barrese et al., in a retrospective analysis of numerous experiments with UEAs in macaques, determined that 53% of all chronic (slowly-progressing) failures were due to fibrotic tissue buildup that either pushed or pulled the array out of cortical tissue [39], a similar rate of occurrence to a previous study [171]. Solving this issue by fixing the microelectrode to the skull is not advisable in larger animals, since the brain has significantly more freedom to move within the cranium, but efforts to reduce the FBR and implantation injury may have the additional benefit of reducing the occurrence of this failure mode by reducing the amount of fibrotic tissue produced downstream of the initial vasculature damage. Reducing tethering forces with extremely flexible wire bundles or wireless transmitters may also help.

3.6 Conclusions

Looking forward, the results of this study are encouraging for the future of BMIs. If there are differences in recording performance and the FBR between young and aged animals, they do not appear dramatic enough to necessitate age-specific measures at this time. This study provides support for the notion that BMIs, which have already achieved

exciting results in experimental trials in humans and nonhuman primates, will be able to perform even better if next-generation microelectrodes are designed to reduce implantation injury, minimize the FBR, and reduce tethering force-related inflammatory sequelae.

CHAPTER 4

FINITE ELEMENT MODELING OF CYTOKINE DIFFUSION TO PREDICT THE FOREIGN BODY RESPONSE TO THE UTAH ELECTRODE ARRAY

4.1 Abstract

Microelectrodes have the potential to provide persons with disabilities volitional control over prosthetic devices. However, a major issue with these devices is unreliable long-term recording of neural signals from brain tissue. It is widely believed that the foreign body response (FBR) mounted against electrodes negatively impacts recording performance. Therefore, strategies to reduce the FBR are expected to improve the reliability of microelectrodes and help bring this technology to the clinic. Toward this end, we have developed a finite element model of cytokine diffusion. This study applies the model for the first time to a large, complex, clinically-relevant device: the Utah Electrode Array (UEA). Model predictions are validated with histological data in rats 4-12 weeks after implantation and cats 240-511 days after implantation. We found that the model was successful in predicting features of the FBR, although it was more successful for the long-duration implants in cats than for the shorter-duration implants in rats. Next, we used the model to rationally design modifications for the UEA and found that reducing surface area and adding a permeable cytokine layer are both promising strategies to reduce the FBR.

Finally, we built a foundation for future improvements in the model by modeling the distribution of a variety of cytokines. With further validation and refinement, the model has the potential to speed design cycles for next-generation intracortical microelectrode arrays.

4.2 Introduction

Intracortical microelectrode arrays can record neural information from neurons in deeper cortical layers and send the signals to a computer in real time. This type of "brain-computer interface" or "brain-machine interface" (BMI) has been a useful research approach and, more recently, has shown promise as a way to restore functions lost to incurable neurological injuries and diseases. Microelectrode arrays implanted in motor cortex can allow individuals with tetraplegia to control computer cursors [27] and multiple degree-of-freedom robotic arms [5] with conscious thought. However, the clinical utility of these devices is limited by their inability to consistently record neural signals at chronic time points.

Studies dating back to the 1950s have consistently reported the development of a foreign body response (FBR) to microelectrode arrays implanted into brain tissue. This FBR involves activated macrophages and microglia, secretion of proinflammatory cytokines, blood-brain barrier (BBB) leakiness, and reductions in neuron cell bodies, dendrites, and myelin near chronically implanted microelectrodes [52-62, 64, 65, 71, 72, 160]. Since microelectrodes can only record from neuronal cell bodies within about 100 μm of the device's recording sites [41], the FBR is believed to be associated with recording inconsistency. Direct experimental evidence is accumulating in support of this claim [35,

36, 134, 171].

To improve recording performance, a number of investigators have attempted to modulate the FBR by modifying device design. Device material composition [60, 71, 118-124], bioactive coatings [125-127], protein-resistant coatings [128-131], thick hydrogel coatings [58, 132, 133], systemically-administered drugs [66, 134-136], locally-administered drugs [78, 139-141], device size [144, 145], interelectrode spacing [72, 147], device surface area [57, 67], and stiffness [153, 154] have all been reported to reduce the FBR in at least some cases. To move the field forward, investigators will now need to select the most promising strategies and test them in larger animals, for long periods of time, in studies that include evaluations of recording performance.

Finite element modeling allows engineers in many fields of engineering to design and test devices and structures *in silico* before full-scale testing. Due to the high cost and time-consuming nature of *in vivo* studies in the field of BMIs – especially studies using animals larger than rodents that include electrophysiological recordings – any tool that allows engineers to test designs *in silico* will greatly speed the process of optimization and testing. To fill this need, our lab has developed a finite element model of the FBR.

Our model focuses on one particular aspect of the FBR: the diffusion of proinflammatory cytokines. The model simulates production, diffusive transport, and degradation of proinflammatory cytokines in brain tissue. High concentrations of proinflammatory cytokines are interpreted as areas of brain tissue likely to develop a more severe FBR.

Proinflammatory cytokines are a crucial component of the FBR. Adsorbed proteins on the surface of a device are recognized by macrophages [44], which secrete

proinflammatory cytokines such as monocyte chemotactic protein 1 (MCP-1), tumor necrosis factor alpha (TNF-α), interleukin 1β (IL-1β), recruiting and activating additional macrophages [42, 45]. The presence of macrophages on intracortical microelectrodes and their production of TNF-α and MCP-1 have been confirmed by culturing explanted microelectrodes [53]. Macrophages also secrete reactive oxygen species (ROS) [48] and vasoactive molecules such as nitric oxide (NO) [46]. In the brain, the combined result of these inflammatory processes includes BBB dysfunction, neuronal death, demyelination, and loss of neural processes.

Thus far, two studies have been performed to validate the model. Skousen et al. in 2011 designed planar silicon microelectrodes with a lattice architecture that reduced the total surface area by about half [57]. The devices were implanted in rats for eight weeks and compared to solid planar silicon microelectrodes with identical penetrating profiles. The authors reported decreased immunoreactivity for activated macrophages, decreased BBB leakage, and increased numbers of neurons near the lattice devices. This effect was successfully predicted by the model, since the lattice devices had less surface area available for macrophage attachment and therefore reduced quantities of proinflammatory cytokines being produced. Skousen et al. in 2014 implanted rats with planar silicon microelectrodes coated with a 400 μm thick layer of alginate for 16 weeks [58]. They reported reduced macrophages, reduced activated macrophages, reduced astrogliosis, reduced BBB leakage, and increased numbers of neuronal cell bodies near the thickly-coated microelectrodes compared to both uncoated and nanoscale-coated devices. This effect was also successfully predicted by our model, since alginate is permeable to proinflammatory cytokines and allows a portion of them to diffuse into the alginate layer and passively

degrade. The fact that the reduced FBR resulting from these two distinctly different strategies was predicted by the model is certainly encouraging, but additional validation is needed.

In this work, we applied the model to a larger and more complex device, the UEA, which is the only intracortical microelectrode currently used in humans. Modeling results were validated with histological data in rats and cats. Then, we explored whether the strategies of reducing surface area and adding a permeable hydrogel layer can be successfully adapted to the UEA. Finally, we expanded our modeling efforts to a variety of proinflammatory cytokines in order to provide insights for future model improvements.

4.3 Materials and Methods

4.3.1 Finite Element Model

Finite element modeling was performed in COMSOL (COMSOL Group, Stockholm, SE) using isotropic Fickian diffusion, a closed boundary at the top surface of the brain and open boundaries elsewhere, a 10 μm thick activated macrophage layer covering all device surfaces producing cytokines at a constant rate, and first-order decay of cytokines. Parameters were based on literature values and are summarized in Table 4.1. Model geometry was based on photographic measurements of a 4x4 UEA. Fig. 4.1 shows the photograph used, a side view of the modeled UEA, and the location of the 10 μm thick activated macrophage layer.

Table 4.1. Parameters for soluble species examined in this study.

	Diffusion coefficient (m^2/s)	**Half-life**	**Decay rate (s^{-1})**	**Length constant (μm)**	**Reference**
Fibrinogen	$8.22x10^{-12}$	48 h	$4.01x10^{-6}$	1431	[179]
H_2O_2	$1.97x10^{-10}$	7 min	$1.65x10^{-3}$	328	[180]
TNF-α	$1.54x10^{-11}$	30 min	$3.85x10^{-4}$	200	[181, 182]
MCP-1	$2.44x10^{-11}$	10 min	$1.16x10^{-3}$	145	[183]
IL-1β	$2.21x10^{-11}$	7.5 min	$1.54x10^{-3}$	120	[184]
NO	$1.20x10^{-10}$	5 s	$1.39x10^{-1}$	36	[185]

4.3.2 Validation Data

Model predictions were validated qualitatively against immunohistochemical studies of 4x4 UEAs in rats and 10x10 UEAs in cats. All procedures involving animals were approved by the University of Utah Animal Care and Use Committee. Rat histological data were obtained from the previously published study by Nolta et al. in 2015 [171]. To briefly recapitulate their methods, 4x4 1 mm long UEAs with 400 μm interelectrode spacing were purchased from Blackrock Microsystems, Salt Lake City, UT. The UEA, connector, and associated wiring were fitted into a custom-fabricated polyurethane headstage and implanted using stainless steel screws into 28 rats weighing 300-350 g for up to 12 weeks. Elizabethan collars (Kent Scientific, Torrington, CT) were used to prevent rats from manipulating their headstages. In order to investigate the effects of implantation injury without the presence of an indwelling device, three additional rats had a UEA was implanted and withdrawn two minutes later.

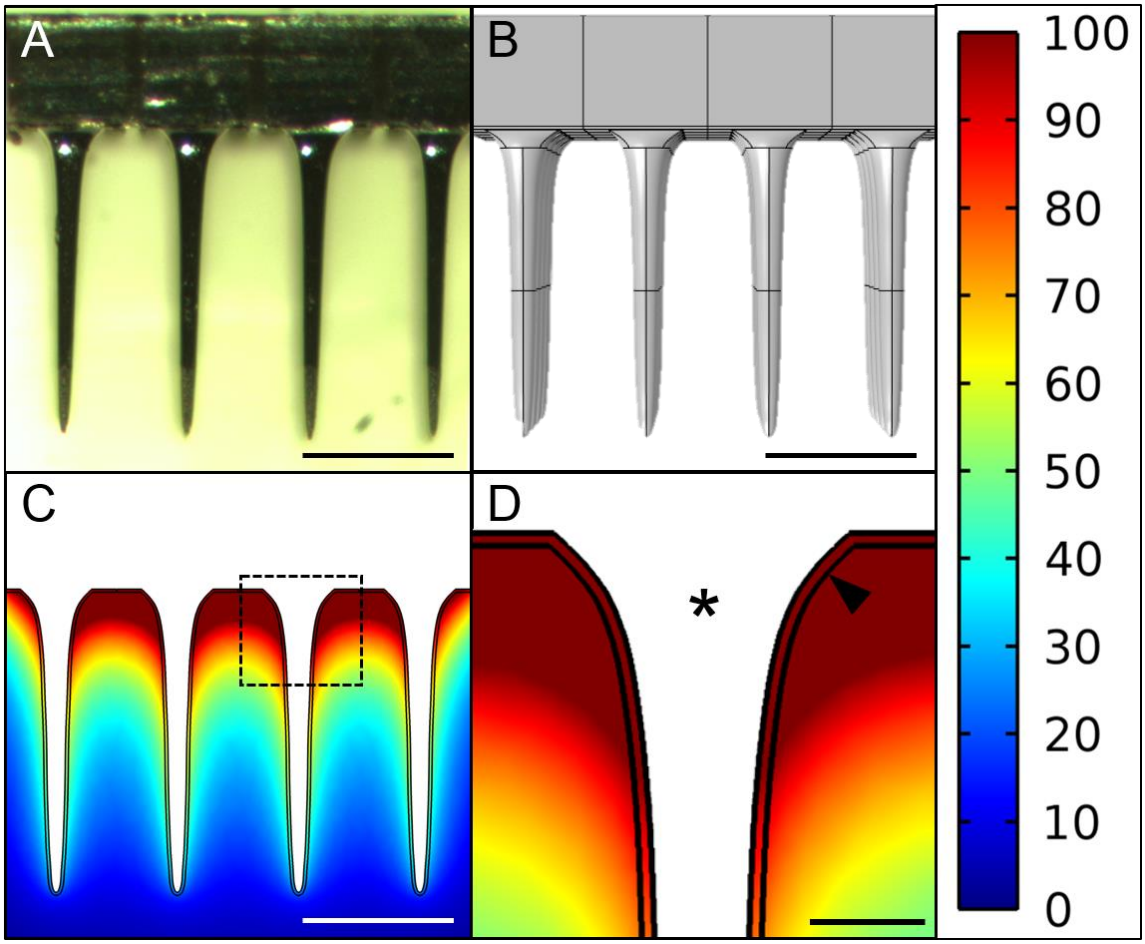

Fig. 4.1. Modeling methods. (A) Photograph of 4x4 UEA used for creation of model geometry. (B) COMSOL model of 4x4 UEA geometry. (C) Model predictions for TNF-α concentrations surrounding a 4x4 UEA. The view is a vertical cross section through four of the microelectrodes. Dotted square represents frame of view in (D). (D) Close-up of the base of a UEA microelectrode shaft (asterisk) covered with 10 µm thick macrophage layer (arrowhead). Color scale indicates percent relative to the peak predicted cytokine concentration of a 300 µm wide planar silicon microelectrode. Scale bars = 500 µm in A-C, 100 µm in D.

Cats implanted with UEAs were received from the Neural Engineering Laboratory at the University of Utah (now at Arizona State University). Three cats received 10x10 UEAs for 240 to 511 days. The percutaneous connector was built into a pedestal fixed to the skull using screws.

At sacrifice, rats and cats were anesthetized and perfused transcardially with phosphate buffered saline (PBS) followed by 4% paraformaldehyde in PBS. Their brains were removed from the skull and the arrays dissected free. Brains were postfixed for 24 h in 4% paraformaldehyde and equilibrated in a 30% sucrose solution before 30 µm horizontal brain sections were obtained using a cryostat. Free-floating brain sections were blocked overnight in PBS with 4% v/v goat serum (Invitrogen, Carlsbad, CA), 0.5% v/v Triton-X 100, and 0.1% sodium azide then incubated overnight with the following primary antibodies in blocking solution: IgG (biotinylated goat anti-rat IgG, Southern Biotec, .5 µg/ml) to assess BBB leakage, NF200 (Sigma, St. Louis, MO, 8 µg/ml) to examine the spatial distribution of axons, NeuN (EMD Millipore, Billerica, MA, 1 µg/ml) to identify neuronal nuclei, GFAP (DAKO North America Inc., Carpinteria, CA, 2.9 µg/ml) to examine astrocyte cytoskeleton location and hypertrophy, and lectin to identify activated immune cells. Sections were then rinsed three times with PBS for 1 h each before being incubated overnight in fluorescently labeled secondary antibodies plus 10 µM DAPI to label cell nuclei, then finally rinsed again three times with PBS for 1 h each. All incubations were performed at room temperature on a rocker. Sections were mounted on slides and coverslipped in Fluoromount-G (Southern Biotec) then imaged with a confocal microscope.

4.4 Results

4.4.1 Model Predictions

Predicted cytokine concentrations for the 4x4 and 10x10 UEAs are shown in diagonal cutaway in Fig. 4.2. For both devices, cytokine concentrations were highest near the base of the array (i.e., superficial cortex) and gradually decreased along the lengths of the microelectrode shafts. The peak cytokine concentration, corresponding to the base of the array, was 71% higher than the peak concentration predicted for a 300 µm wide planar silicon electrode, while the UEA microelectrode tips were much lower [57, 58]. Predicted concentrations were also slightly lower around microelectrodes on the outer edges of the arrays, an effect that was most pronounced near the base. Non-edge microelectrodes had very similar cytokine concentrations to one another.

The two different UEA designs had similar spatial distributions of cytokines. The only observable difference was that the 10x10 UEA, with its longer microelectrode shafts, had a longer region of moderate cytokine concentration in between the base and the tips.

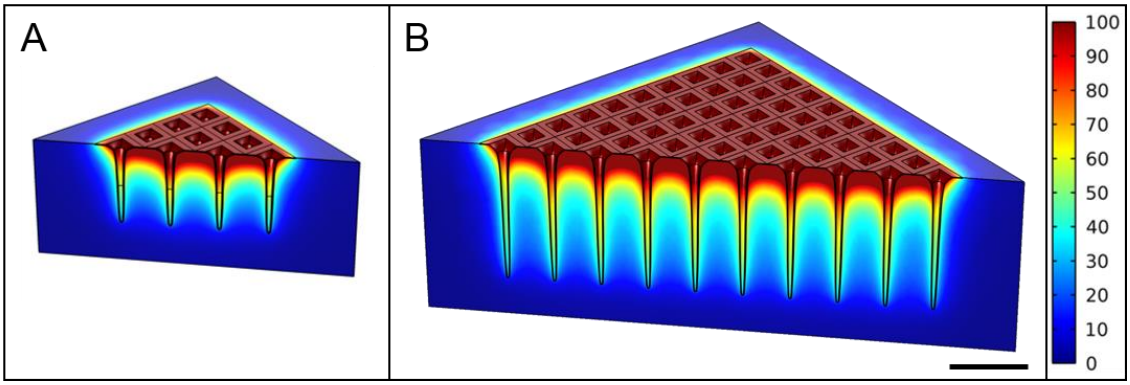

Fig. 4.2. Model predictions. (A) Model predictions for TNF-α concentrations surrounding a 4x4 UEA. The view is a diagonal cutaway. (B) Model predictions for 10x10 UEA shown at same scale. Color scale indicates percent relative to the peak predicted cytokine concentration of a 300 µm wide planar silicon microelectrode. Scale bar = 1 mm.

4.4.2 Validation with Rats at 4-12 Weeks

As previously reported by Nolta et al. in 2015 [171], gross inspection of rat cortex implanted with 4x4 UEAs revealed cavities of tissue loss in superficial cortex. These cavities had a jagged, pyramidal shape with the pyramid's base at the brain surface and the tip pointing down into cortex. In horizontal sections, the cavities appeared as acellular gaps in the tissue, partially filled with lacy, hypercellular tissue positive for activated macrophages (CD68) and blood constitutents (IgG) and negative for axons (NF-200). The border of the cavity had increased levels of astrocyte cytoskeleton (GFAP). Away from the cavities, individual electrode tracks were visible. Each track was surrounded by a layer of densely packed CD68+ cells. This layer, in turn, was surrounded by a somewhat diffuse zone of increased IgG and GFAP. Stab-wounded rats sacrificed at 4 weeks showed similarly sized and shaped cavities, albeit with reduced macrophages and blood constituents, and showed no signs of electrode tracks.

Predicted cytokine concentrations in horizontal planes corresponding to histological images are shown in Fig. 4.3. The model predicts decreasing concentrations with depth into brain tissue. BBB leakage (indicated by IgG) and loss of cortical tissue (indicated by areas lacking NF-200) associated with lesion cavities also decreased with depth. However, markers of the FBR were relatively constant with depth surrounding individual microelectrode tracks that were not near lesion cavities.

4.4.3 Validation with Cats at 240-511 Days

Gross inspection of cat cortex implanted with 10x10 UEAs for 240-511 days showed that the UEA had settled down into brain cortex, leaving a square-shaped depression when

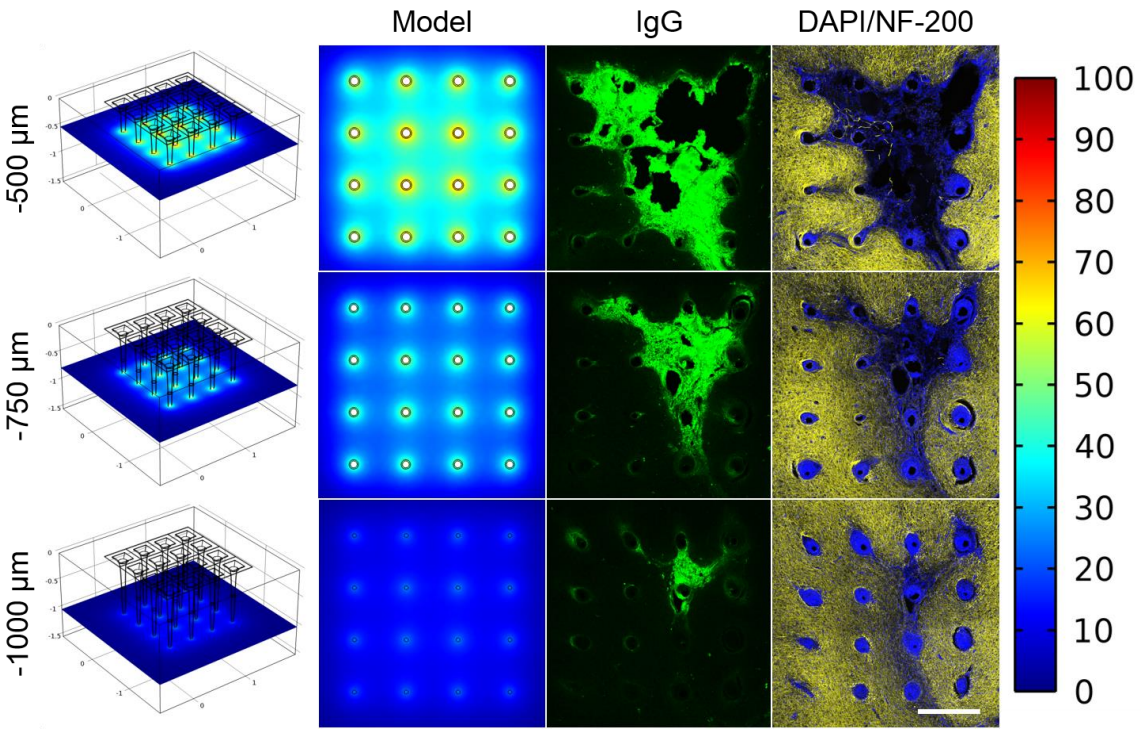

Fig. 4.3. Validation with rats. Predicted TNF-α concentrations surrounding a 4x4 UEA shown in horizontal cross section at three different depths. Also shown are representative 30 µm horizontal sections at corresponding depths from a rat implanted with a 4x4 UEA for 4 weeks, labeled for blood constituents (IgG, green), cell nuclei (DAPI, blue), and axons (NF-200, yellow). Color scale indicates percent relative to the peak predicted cytokine concentration of a 300 µm wide planar silicon microelectrode. Scale bar = 500 µm.

removed (Fig. 4.4). The tissue immediately under the array was darkly colored, likely due to blood constitutents. The square-shaped depression was mostly flat, but had some shallow irregularities in the surface.

Modeling results (not shown) displayed the same spatial pattern described in Fig. 4.3 of decreasing concentrations with depth. In horizontal histological sections, small cavities of tissue loss were visible as well as lacy, hypercellular, non-neuronal tissue in superficial cortex towards the center of the array (Fig. 4.4). The cavities were generally shallower

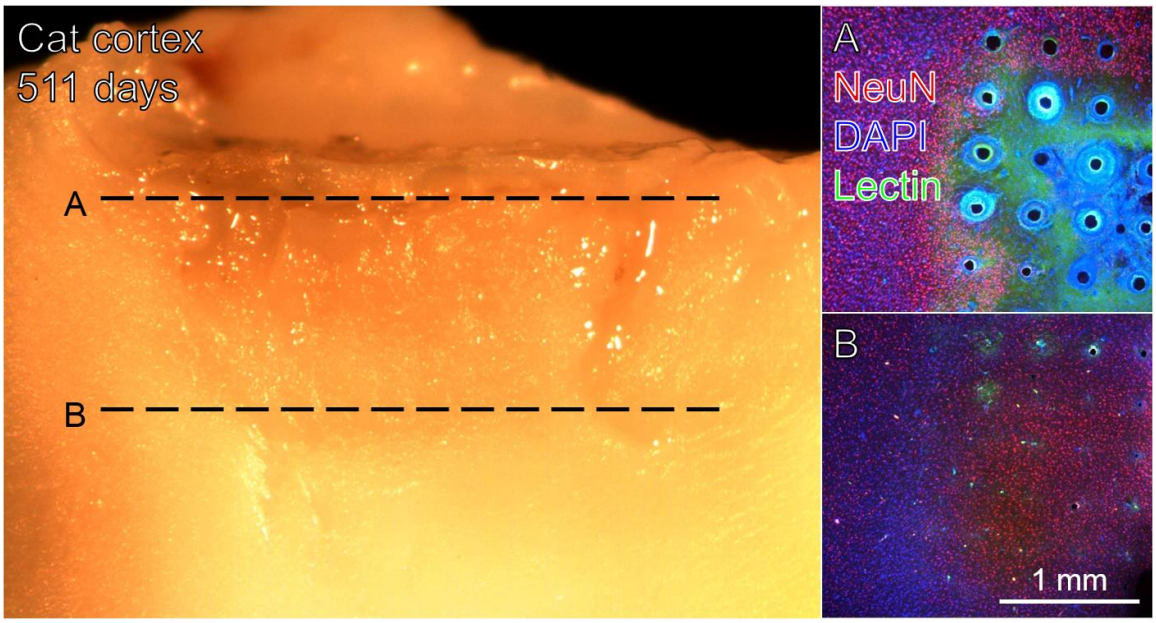

Fig. 4.4. Validation with cats. Gross image of implantation site of a 10x10 UEA in a cat for 511 days. The implant site was cut vertically and is shown in cross section. Settling of the UEA into tissue was apparent, as well as discoloration of cortical tissue. 30 µm horizontal sections at the depths indicated by the dotted lines labeled A and B are shown at right. In (A), lacy, hypercellular, lectin+ tissue is visible towards the center of the array, while neural tissue is associated with microelectrode tracks at the edges. Microelectrode tracks had hypercellular, lectin+ layers of cells surrounding them that were highly variable in thickness but tended to decrease with depth. In (B), just below the microelectrode tips, little evidence of the FBR is apparent.

than in the rats, but the lacy hypercellular tissue was equally extensive, suggesting that the cavities may become filled in with hypercellular tissue. Tissue near the edge microelectrodes appeared relatively healthy. Individual microelectrode tracks were surrounded by a layer of activated immune cells positive for lectin. This layer was highly variable between electrode tracks, with no overarching spatial pattern. However, unlike in rats, the thickness of this layer tended to decrease steadily with depth into brain cortex. Just below the electrode tips, there were small areas with increased lectin immunoreactivity.

4.4.4 Rational Design of Modified UEAs

Three strategies to reduce the FBR were analyzed using the model and their predicted cytokine distributions are shown in Fig. 4.5. Increasing the interelectrode spacing led to a 13% reduction in the peak cytokine level compared to a standard 4x4 UEA. The reduction was mostly localized to the spaces in between microelectrodes. Creating 300 μm diameter holes in the base (allowing cytokines to diffuse out through the holes) reduced the peak cytokine level by 42%, and adding a 400 μm thick layer of alginate reduced the peak cytokine level by 50%. Both of these last two strategies greatly reduced cytokine concentrations near the base of the array. Concentrations near the tips were unaffected.

4.4.5 Analysis of Other Solutes

To develop a conceptual framework for characterizing the diffusion and degradation of other proinflammatory cytokines, we first obtained a closed-form solution to a simplified problem geometry. In a system with an infinite plane wall producing a fixed flux of cytokines, isotropic Fickian diffusion, and 1st-order cytokine decay at equilibrium, the differential equations can be solved explicitly. The solution was found to be an exponential function:

$$c = \frac{F}{\sqrt{Dk}} e^{-x/\sqrt{D/k}}$$

where c is the concentration of cytokines, F is the flux of cytokines at the wall, D is the diffusion coefficient, k is the decay rate constant, and x is the distance from the wall. In this simplified system, the concentration of cytokines decrease e-fold over a length constant of $\lambda = \sqrt{D/k}$, and the concentration of cytokines at the wall is $A = F/\sqrt{Dk}$. Diffusion

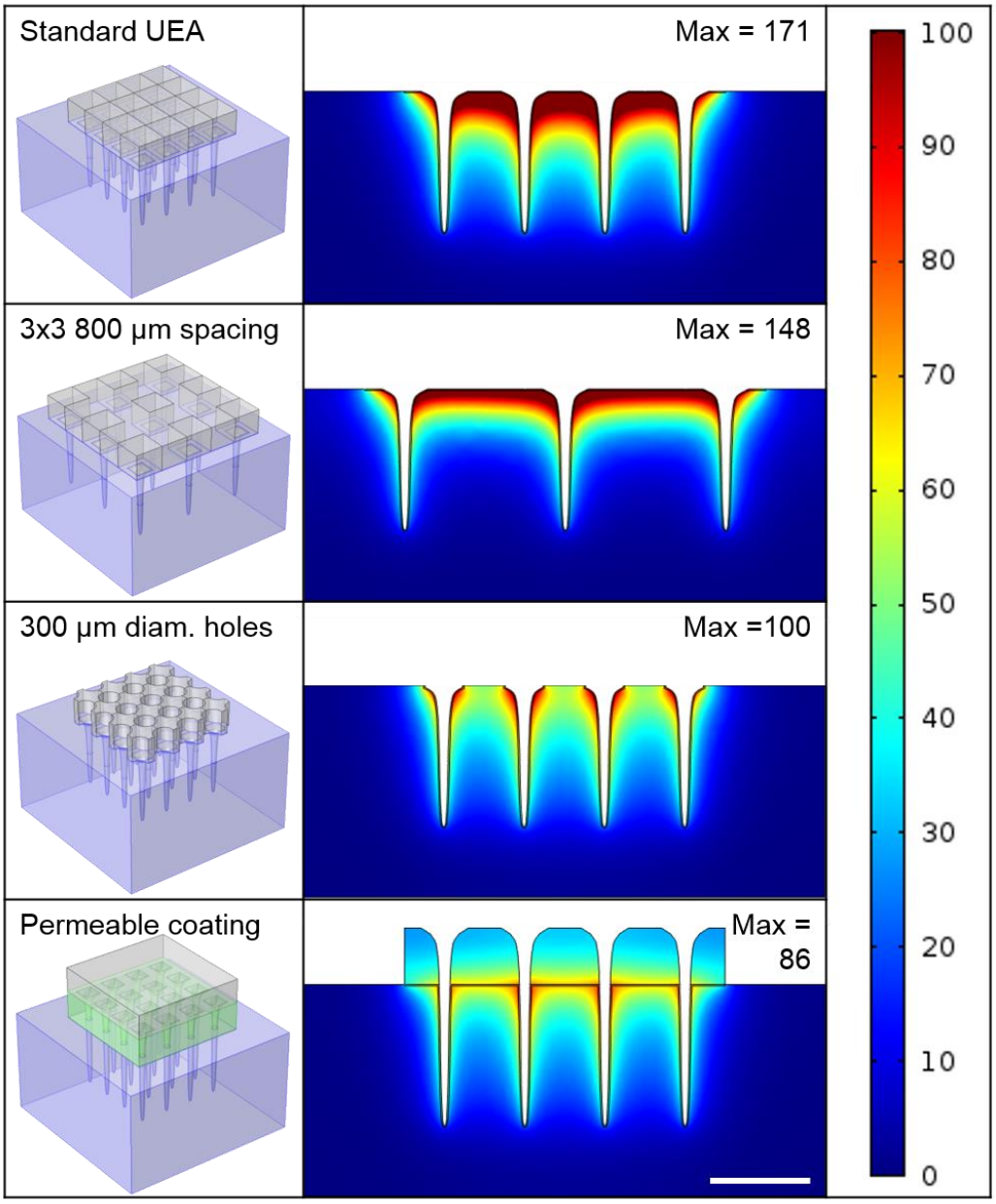

Fig. 4.5. Model geometry and predicted TNF-α concentrations associated with a standard 4x4 UEA and three modified UEAs. Peak cytokine concentrations for each modification are also listed. Color scale indicates percent relative to the peak predicted cytokine concentration of a 300 µm wide planar silicon microelectrode. Scale bar = 500 µm.

coefficients, half-lives, decay rates, and length constants for fibrinogen, hydrogen peroxide (H_2O_2), TNF-α, MCP-1, IL-1β, and NO were calculated based on literature values are shown in Table 4.1.

The analysis presented in Figs. 4.1-4.3 used diffusion and decay rate values for TNF-α and used the same color scale as in the studies by Skousen et al. [57, 58] in order to facilitate comparison with modeling results for planar silicon devices. Next, we examined the predicted cytokine concentrations for other species and looked at their normalized concentration – in other words, the maximum for the color scale was set to the peak concentration in each simulation's results. Fibrinogen, with the longest length constant of 1431 μm, diffused the farthest distance from the UEA (Fig. 4.6). NO, with the shortest length constant of 36 μm, had a spatial distribution that conformed very closely to the device surface. The other species had length constants and spatial distributions that were between these two extremes.

4.5 Discussion

In this study, we extended the validation of a finite element model of cytokine diffusion that was previously successful for single-shank devices [57, 58] to the larger and more complex UEA, and found that the model was most successful at predicting the FBR to the UEA in cats at 240-511 days after implantation. We also used the model to rationally design modifications to the UEA and compared their predicted cytokine concentrations. Finally, we extended the model to additional proinflammatory cytokines besides TNF-α to provide insights for future improvements in the model.

Validation with rats 4-12 weeks after implantation was only moderately successful.

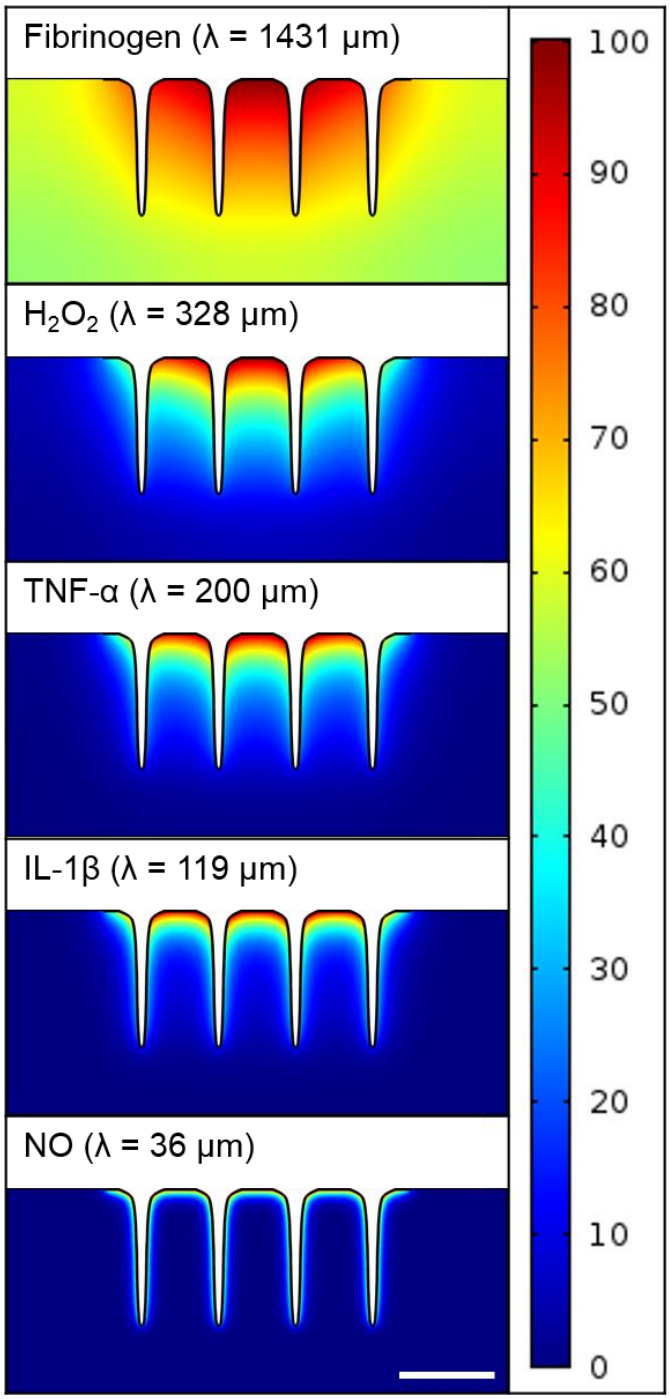

Fig. 4.6. Predicted relative concentrations for five different soluble species. Each species' results are normalized so that the highest concentration is represented by dark red. Fibrinogen, with the longest length constant, diffused farthest from the UEA, while NO, with the shortest length constant, remained very close to the contours of the device.

Although the FBR decreased in intensity with depth, much of this response could be attributed to lesions from the injury of implantation, since it was visible four weeks after stab wound injury experiments that left no indwelling device. The vascular damage from the implantation of a large, complex device such as the UEA [70, 171, 186] is significantly greater than it is for single-shank planar silicon devices [53, 59, 165]. The response associated with individual microelectrode tracks away from lesion cavities was relatively constant with depth, unlike modeling predictions. It remains an open question whether the FBR would have been more similar to modeling predictions if the injury of implantation could be greatly reduced.

Validation in cats 240-511 days after implantation was more successful. Lesion cavities were smaller, and the lacy hypercellular tissue surrounding them tended to be more inflamed near the base and towards the center of the UEA. The response to a stab wound injury from a 10x10 UEA in cat cortex is unknown, but the lesion cavities appeared to account for less of the response than in the rats. This could be related to the longer implant duration, as damaged tissue and blood proteins are cleared away, and tissue remodeling, wound closure, and fibrosis have had time to fully develop. There may also be differences in animal physiology. Meanwhile, the intensity of the FBR associated with individual microelectrode tracks tended to decrease gradually with depth, as in the model. The variability in the FBR to individual microelectrodes could be due to the proximity of blood vessels near particular microelectrodes.

The model was also successful in predicting the high intensity (compared to the FBR around 300 μm wide planar silicon devices [57, 58]) of the FBR at the base of the UEA and the low intensity of the FBR at the tips of the UEA, especially in cats.

Modeling modified UEAs showed that the strategies of reducing surface area [57] and increasing permeability [58] can be successfully applied to the UEA to reduce predicted TNF-α levels. We focused our efforts on the base of the UEA since the majority of proinflammatory cytokines accumulated in that region. Even though the recording sites are at the tips, reducing the FBR to the base is still a worthwhile design goal for the following reasons. First, the FBR to the base may be responsible for the settling of UEAs into – or fibrotic extrusion out of – cortical tissue observed in cats [37, 38, 68, 169, 170] and nonhuman primates [39], which causes the recording sites to move into suboptimal layers of cortex for recordings. Second, destruction of superficial cortical layers may interfere with proper operation of cortical circuits. Finally, inflammation anywhere in the brain can impact neurogenesis [187] and may contribute to side effects such as cognitive decline seen in patients receiving deep brain stimulators and hydrocephalic shunts [188]. Modifying the UEA by adding a permeable layer of alginate achieved the greatest reduction out of the modifications proposed, followed closely by the base with reduced surface area, suggesting that these two strategies are likely to be successful for the UEA.

Our model in its current state is an extremely simple representation of the FBR *in vivo*. In order to lay the groundwork for model improvements, we explored additional cytokines and soluble factors besides TNF-α. We found that the distribution of a particular soluble species near a device can be conveniently characterized by a length constant equal to the square root of its diffusion coefficient over its decay rate. Different soluble species were found to have cytokine distributions that extended various distances into tissue corresponding to their length constants. Future improvements to the model may incorporate contributions from multiple soluble species and sum their contributions in

order to more accurately match validation data.

4.6 Conclusions

In this work, a finite element model of cytokine diffusion was applied to the UEA and validated with rats implanted for 4-12 weeks and cats implanted for 240-511 days. The model successfully predicted the intense FBR to the base of the UEA and relatively minor FBR at the microelectrode tips. The distribution of FBR biomarkers was most similar to model predictions in cats, where the effect of the initial implantation injury had partly subsided. Examination of modified UEA designs showed that reducing surface area and adding a permeable cytokine layer are both likely to be effective strategies to reduce the FBR to the UEA. Finally, the distribution of various other cytokines was predicted. With additional validation and refinement, this model may grow into a powerful tool for developing next-generation intracortical microelectrode arrays with reduced FBRs.

CHAPTER 5

SUMMARY, CONCLUSIONS, AND FUTURE WORK

5.1 Summary and Conclusions

Paralysis and limb loss often result in devastating and permanent disabilities for the persons affected. Brain machine interfaces offer the hope of restoring lost functions by allowing the brain to directly control external devices via volitional thought. The clinical utility of these devices is currently limited by the inconsistent performance of intracortical microelectrodes at chronic time points. Available evidence suggests that the FBR to intracortical electrodes likely contributes to inconsistent performance, but little is known about the exact mechanisms responsible.

In Chapter 2, a large cohort of young adult rats was implanted with 4x4 UEAs for up to 12 weeks. This study provided the first in-depth description of the FBR to the UEA in the rat. This allowed the FBR to the UEA to be compared with the extensive literature on the FBR to simpler devices implanted into rats. It was found that the FBR to the UEA differs from the FBR to simpler devices in that the injury of implantation plays a much greater role in the long-term response, likely due to the increased potential for vascular injury from the multiple penetrating features of the UEA. The effects of implantation injury were manifested as cavities in superficial brain cortex. These cavities were

associated with reduced recording performance. We also found evidence that astrogliosis and BBB leakage correlated with decreased SNR for electrodes towards the center of the UEA. These findings contribute to the field by drawing attention to the importance of minimizing vascular damage for large, complex microelectrode arrays, and by providing evidence that astrogliosis and BBB leakage are components of the FBR that are related to recording performance.

In Chapter 3, a cohort of aged rats was implanted with 4x4 UEAs for up to 12 weeks. Although we expected to find increased inflammation and decreased recording performance due to the animals' aged immune systems, we found overall higher recording performance compared to the young cohort and a comparable level of inflammation. These findings suggest that recording quality may be dependent on animal activity level, skull thickness, and method of fixation to the skull. These findings are also encouraging for the field of BMIs, since aged humans represent a large share of patients likely to receive intracortical microelectrode arrays. Lastly, we found additional evidence that astrogliosis and tissue loss are associated with reduced recording performance.

In Chapter 4, we extended our previous work modeling the production, diffusion, and decay of proinflammatory cytokines near single-shank planar silicon devices to the more complex geometry of the UEA. We found that the model predicted increased concentrations of proinflammatory cytokines towards the center and towards the base of the UEA, suggesting that the FBR would be the most intense in these areas. Validating these predictions against histological data from our studies of the UEA in rats and cats revealed that these predictions corresponded well to the actual distribution of the FBR in cats implanted for 240-511 days but only somewhat well in rats implanted for 4-12 weeks.

We then found that the strategies of reducing device surface area and adding a permeable layer of alginate could be successfully adapted to reduce the FBR to the UEA. Finally, we modeled the distribution of a variety of soluble species and found that different species likely conform more or less closely to the device. The validation of UEA modeling data, and the analysis of multiple soluble species, will be useful to future efforts to refine and expand the finite element model.

5.2 Future Work

One possible direction to proceed in the future would be to extend the work of Chapter 2 and press further towards the goal of understanding the mechanisms of recording inconsistency. This work provided evidence that astrogliosis, tissue loss, and BBB leakage are associated with recording inconsistency. These correlations are statistically significant, but they fall short of providing a complete explanation for recording inconsistency. For each of these markers, a high degree of variability was observed, and there were numerous exceptional cases, e.g., electrodes with high GFAP and high performance. It may be that numerous processes simultaneously contribute to recording inconsistency, so that only the collection of processes can explain recording consistency and no single metric is sufficient. Or, it may be that there is a more reliable marker for recording inconsistency, and the markers we have found to correlate thus far are merely unreliable indicators of a more proximal cause. A future study could use a similar approach to the studies in Chapters 2 and 3, but make significant improvements in methodology based on what was learned from this work, such as: use of a large cohort of middle-aged or aged rats; use of a microelectrode that creates less vascular damage; use of a device that does not need to be explanted prior

to histology; development of histological techniques that can image a cube of tissue containing the device without explanting it; implantation into another area of cortex and using protocols to create evoked potentials in order to obtain action potentials more reliably [32, 37, 68, 69]; and use of immunolabeling techniques that reduce the impact of IgG cross-reactivity and hemosiderin autofluorescence [189]. There are other factors that could be added to the analysis as well, such as electrode impedance, pre- and post-explant analysis of device materials integrity, and measurement of blood pNF-H levels, as in the two studies by Prasad et al. [35, 36]. Refining our approach may provide a clearer picture of the mechanisms of recording inconsistency than could be gained in these first efforts.

A different direction would be to instead use the knowledge gained from this work and previous literature to design a next-generation device. The ultimate goal of bioengineering is to provide patients with better medical technologies, and at this stage there are already multiple strategies that are ripe for further testing. Demonstrating improved single unit recording performance for a modified UEA would be the fastest route towards clinical use, since the UEA is already used in humans. Potential modifications could include those described in Chapter 4 (increased interelectrode spacing, decreased surface area, and addition of a permeable layer), modifications designed to reduce the effects of implantation injury (increased interelectrode spacing or coating the device with hemostatic materials), or pharmacological interventions [66, 134, 135, 139, 146]. If it could be demonstrated that the modified UEAs performed more reliably than the standard UEA, this would be unprecedented in the field, which has so far only examined modifications to planar silicon and microwire devices, and has only rarely performed chronic recording experiments using modified devices. Concurrent immunohistochemical evaluation could provide insight into

mechanisms.

Although modifying the UEA has the potential to provide the greatest clinical benefit to the field in the near term, it is likely that the UEA will eventually be leapfrogged by another technology. As investigators push towards richer, higher-fidelity BMI control, ever greater numbers of neurons will need to be recorded from [17, 40]. Since the UEA has microelectrodes that are regularly spaced and are inserted all at once, as microelectrode density increases, the difficulty of implantation and the potential for vascular damage become prohibitive. An approach that would allow for a greater density of microelectrodes to be implanted into brain tissue would be to image the brain's vasculature, then individually implant microwire electrodes in locations that avoid the larger blood vessels, an approach which has been accomplished for planar silicon devices [165]. Robotic surgery would be advisable if a very large number of microwires are to be implanted. Using extremely small microwires would have the added benefit of reducing the FBR [144, 145, 156]. The main challenge with this approach is in connecting the microwires to recording equipment, as individually-wired connections may become unmanageable for large numbers of microwires. It may be possible to communicate with the microwires wirelessly via light, ultrasound [190], or radiofrequency signals, especially if the microwires are only designed to communicate threshold events, rather than high-fidelity, highly temporally-resolved waveforms. If so, this would further reduce the FBR by reducing tethering forces [54, 145]. A vast improvement in density accompanied by a decrease in the FBR could greatly improve performance and be transformative in the field of BMI and for brain research in general.

With regards to the finite element model, a promising future direction would be to

perform quantitative validation. In fields such as electrical engineering, physics, mechanical engineering, and materials science, quantitative data can be closely matched against model predictions. Even in bioengineering, biomechanical models are subjected to quantitative validation [191]. In our model of the foreign body response, however, there is a leap from quantitative cytokine concentration predictions to the complex, qualitative description of histological biomarkers used as validation data. To provide a more convincing case for the model's validity, future experiments could be designed to validate predicted cytokine concentrations against actual measured cytokine concentrations. This could be accomplished by using a device capable of sensing concentrations of cytokines or other soluble species, e.g., using cyclic voltammetry [192-195]. Soluble species could be measured over time, on differently-designed devices, and on different parts of the device in order to provide a rich dataset for model validation. While measuring soluble species concentrations would be ideal, quantitative validation could also be carried out with histological markers. Our lab is well acquainted with histological quantification techniques ([53-58] and this work), so the primary challenge would be adapting the model so that it predicts GFAP, IgG, neurofilament, or CD68 immunoreactivity, or NeuN cell counts. Direct, quantitative validation would be significantly more convincing than the qualitative validation of the downstream effects of cytokines performed so far.

As a side note, due to the influence of implantation injury, it would be wise to use small, single-shank microelectrodes for further development of the model. Or, implantation injury could be modeled and validated using stab wound injuries. As seen in this work, implantation injury is significant for large, complex microelectrode arrays. Therefore, a finite element model for implantation injury may be nearly as useful to

engineers as a model for the FBR. Eventually, the FBR and implantation injury models could be combined.

In addition to quantitative validation, it would also be convincing to explore situations in which the model makes unexpected predictions, and then test whether those predictions are correct. This has already been observed in a few reports. Increased inflammation on the inside corners of microelectrodes has been reported [67], which aligns with our model predictions, but not with predictions based on mechanical motion. Decreased or equivalent FBR at the tips of microelectrodes [37, 55, 56, 171], successfully predicted by our model, also runs contrary to mechanical modeling which reports the highest tissue strains at the microelectrode tips [196]. The decreased FBR surrounding thick hydrogels [58] and hollow-fiber membranes [181] is also surprising, considering the increased size of these devices. Ideas for future studies along this line of inquiry include: studying the FBR to parallel plates (the model would predict a severe FBR between plates that are placed close together), studying the FBR to hollow fiber membranes or hydrogel cylinders of varying diameter (the model would predict a more severe FBR for devices in a particular size range where macrophage attachment area is high but device permeability is not yet a significant factor), and comparing a device with a permeable grating and hollow interior vs. a device with an identical grating but a filled-in interior (the devices would be nearly identical in all respects except permeability). If cases where model predictions outperform traditional predictions based on size and mechanical motion continue to accumulate, the model will likely gain increased attention in the literature.

REFERENCES

1. *One Degree of Separation: Paralysis and Spinal Cord Injury in the United States*. 2009, Christopher & Dana Reeve Foundation.

2. *2014 Annual Statistical Report - Complete Public Version*. 2014, University of Alabama at Birmingham: Birmingham, Alabama.

3. Ziegler-Graham, K., et al., *Estimating the prevalence of limb loss in the United States: 2005 to 2050.* Arch Phys Med Rehabil, 2008. **89**(3): p. 422-9.

4. Hochberg, L.R., et al., *Reach and grasp by people with tetraplegia using a neurally controlled robotic arm.* Nature, 2012. **485**(7398): p. 372-5.

5. Collinger, J.L., et al., *High-performance neuroprosthetic control by an individual with tetraplegia.* The Lancet, 2013. **381**(9866): p. 557-564.

6. Mugler, E.M., et al., *Direct classification of all American English phonemes using signals from functional speech motor cortex.* J Neural Eng, 2014. **11**(3): p. 035015.

7. Ledbetter, N.M., et al., *Intrafascicular stimulation of monkey arm nerves evokes coordinated grasp and sensory responses.* J Neurophysiol, 2013. **109**(2): p. 580-90.

8. Lewis, P.M., et al., *Restoration of vision in blind individuals using bionic devices: A review with a focus on cortical visual prostheses.* Brain Res, 2015. **1595C**: p. 51-73.

9. Bensmaia, S.J. and L.E. Miller, *Restoring sensorimotor function through intracortical interfaces: progress and looming challenges.* Nat Rev Neurosci, 2014. **15**(5): p. 313-25.

10. Berger, T.W., et al., *A hippocampal cognitive prosthesis: multi-input, multi-output nonlinear modeling and VLSI implementation.* IEEE Trans Neural Syst Rehabil Eng, 2012. **20**(2): p. 198-211.

11. Yawn, R., et al., *Cochlear implantation: a biomechanical prosthesis for hearing loss.* F1000Prime Rep, 2015. **7**: p. 45.

12. Lin, T.C., et al., *Retinal prostheses in degenerative retinal diseases.* J Chin Med Assoc, 2015.

13. Navarro, X., et al., *A critical review of interfaces with the peripheral nervous system for the control of neuroprostheses and hybrid bionic systems.* J Peripher Nerv Syst, 2005. **10**(3): p. 229-58.

14. Clark, G.A., et al., *Using multiple high-count electrode arrays in human median and ulnar nerves to restore sensorimotor function after previous transradial amputation of the hand.* Conf Proc IEEE Eng Med Biol Soc, 2014. **2014**: p. 1977-80.

15. Wark, H.A., et al., *Restoration From Acute Urinary Dysfunction Using Utah Electrode Arrays Implanted Into the Feline Pudendal Nerve.* Neuromodulation, 2014.

16. Moghimi, S., et al., *A review of EEG-based brain-computer interfaces as access pathways for individuals with severe disabilities.* Assist Technol, 2013. **25**(2): p. 99-110.

17. Lebedev, M.A., et al., *Future developments in brain-machine interface research.* Clinics (Sao Paulo), 2011. **66 Suppl 1**: p. 25-32.

18. Moran, D., *Evolution of brain-computer interface: action potentials, local field potentials and electrocorticograms.* Curr Opin Neurobiol, 2010. **20**(6): p. 741-5.

19. Strumwasser, F., *Long-term recording' from single neurons in brain of unrestrained mammals.* Science, 1958. **127**(3296): p. 469-70.

20. Hubel, D.H., *Tungsten Microelectrode for Recording from Single Units.* Science, 1957. **125**(3247): p. 549-50.

21. Lehew, G. and M.A.L. Nicolelis, *State-of-the-Art Microwire Array Design for Chronic Neural Recordings in Behaving Animals*, in *Methods for Neural Ensemble Recordings*, M.A.L. Nicolelis, Editor. 2008: Boca Raton (FL).

22. Williams, J.C., R.L. Rennaker, and D.R. Kipke, *Long-term neural recording characteristics of wire microelectrode arrays implanted in cerebral cortex.* Brain Res Brain Res Protoc, 1999. **4**(3): p. 303-13.

23. Liu, X., et al., *Evaluation of the stability of intracortical microelectrode arrays.* IEEE Trans Neural Syst Rehabil Eng, 2006. **14**(1): p. 91-100.

24. Wise, K.D., J.B. Angell, and A. Starr, *An integrated-circuit approach to extracellular microelectrodes.* IEEE Trans Biomed Eng, 1970. **17**(3): p. 238-47.

25. Kipke, D.R., et al., *Silicon-substrate intracortical microelectrode arrays for long-*

term recording of neuronal spike activity in cerebral cortex. IEEE Trans Neural Syst Rehabil Eng, 2003. **11**(2): p. 151-5.

26. Campbell, P.K., et al., *A silicon-based, three-dimensional neural interface: manufacturing processes for an intracortical electrode array.* IEEE Trans Biomed Eng, 1991. **38**(8): p. 758-68.

27. Hochberg, L.R., et al., *Neuronal ensemble control of prosthetic devices by a human with tetraplegia.* Nature, 2006. **442**(7099): p. 164-71.

28. Kruger, J., et al., *Seven years of recording from monkey cortex with a chronically implanted multiple microelectrode.* Front Neuroeng, 2010. **3**: p. 6.

29. Chestek, C.A., et al., *Long-term stability of neural prosthetic control signals from silicon cortical arrays in rhesus macaque motor cortex.* J Neural Eng, 2011. **8**(4): p. 045005.

30. Ifft, P.J., et al., *A brain-machine interface enables bimanual arm movements in monkeys.* Sci Transl Med, 2013. **5**(210): p. 210ra154.

31. Simeral, J.D., et al., *Neural control of cursor trajectory and click by a human with tetraplegia 1000 days after implant of an intracortical microelectrode array.* J Neural Eng, 2011. **8**(2): p. 025027.

32. Kozai, T.D., et al., *Comprehensive chronic laminar single-unit, multi-unit, and local field potential recording performance with planar single shank electrode arrays.* J Neurosci Methods, 2015. **242**: p. 15-40.

33. Vetter, R.J., et al., *Chronic neural recording using silicon-substrate microelectrode arrays implanted in cerebral cortex.* IEEE Trans Biomed Eng, 2004. **51**(6): p. 896-904.

34. Freire, M.A., et al., *Comprehensive analysis of tissue preservation and recording quality from chronic multielectrode implants.* PLoS One, 2011. **6**(11): p. e27554.

35. Prasad, A., et al., *Comprehensive characterization and failure modes of tungsten microwire arrays in chronic neural implants.* J Neural Eng, 2012. **9**(5): p. 056015.

36. Prasad, A., et al., *Abiotic-biotic characterization of Pt/Ir microelectrode arrays in chronic implants.* Front Neuroeng, 2014. **7**: p. 2.

37. Rousche, P.J. and R.A. Normann, *Chronic recording capability of the Utah Intracortical Electrode Array in cat sensory cortex.* J Neurosci Methods, 1998. **82**(1): p. 1-15.

38. Liu, X., et al., *Stability of the interface between neural tissue and chronically implanted intracortical microelectrodes.* IEEE Trans Rehabil Eng, 1999. **7**(3): p. 315-26.

39. Barrese, J.C., et al., *Failure mode analysis of silicon-based intracortical microelectrode arrays in non-human primates.* J Neural Eng, 2013. **10**(6): p. 066014.

40. Schwarz, D.A., et al., *Chronic, wireless recordings of large-scale brain activity in freely moving rhesus monkeys.* Nat Methods, 2014. **11**(6): p. 670-6.

41. Henze, D.A., et al., *Intracellular features predicted by extracellular recordings in the hippocampus in vivo.* J Neurophysiol, 2000. **84**(1): p. 390-400.

42. Anderson, J.M., A. Rodriguez, and D.T. Chang, *Foreign body reaction to biomaterials.* Semin Immunol, 2008. **20**(2): p. 86-100.

43. Tang, L., *Mechanisms of fibrinogen domains: biomaterial interactions.* J Biomater Sci Polym Ed, 1998. **9**(12): p. 1257-66.

44. Nilsson, B., et al., *The role of complement in biomaterial-induced inflammation.* Mol Immunol, 2007. **44**(1-3): p. 82-94.

45. Feghali, C.A. and T.M. Wright, *Cytokines in acute and chronic inflammation.* Front Biosci, 1997. **2**: p. d12-26.

46. Ryan, G.B. and G. Majno, *Acute inflammation. A review.* Am J Pathol, 1977. **86**(1): p. 183-276.

47. Tang, L. and J.W. Eaton, *Natural responses to unnatural materials: A molecular mechanism for foreign body reactions.* Mol Med, 1999. **5**(6): p. 351-8.

48. Robinson, J.M., *Reactive oxygen species in phagocytic leukocytes.* Histochem Cell Biol, 2008. **130**(2): p. 281-97.

49. Abramowitch, S.D., et al., *List of Contributors*, in *Host Response to Biomaterials*, S.F. Badylak, Editor. 2015, Academic Press: Oxford. p. xi-xii.

50. Teller, P. and T.K. White, *The physiology of wound healing: injury through maturation.* Surg Clin North Am, 2009. **89**(3): p. 599-610.

51. Anderson, J.M., *Multinucleated giant cells.* Curr Opin Hematol, 2000. **7**(1): p. 40-7.

52. Collias, J.C. and E.E. Manuelidis, *Histopathological changes produced by implanted electrodes in cat brains; comparison with histopathological changes in human and experimental puncture wounds.* J Neurosurg, 1957. **14**(3): p. 302-28.

53. Biran, R., D.C. Martin, and P.A. Tresco, *Neuronal cell loss accompanies the brain tissue response to chronically implanted silicon microelectrode arrays.* Exp Neurol, 2005. **195**(1): p. 115-26.

54. Biran, R., D.C. Martin, and P.A. Tresco, *The brain tissue response to implanted silicon microelectrode arrays is increased when the device is tethered to the skull.* J Biomed Mater Res A, 2007. **82**(1): p. 169-78.

55. Winslow, B.D., et al., *A comparison of the tissue response to chronically implanted Parylene-C-coated and uncoated planar silicon microelectrode arrays in rat cortex.* Biomaterials, 2010. **31**(35): p. 9163-72.

56. Winslow, B.D. and P.A. Tresco, *Quantitative analysis of the tissue response to chronically implanted microwire electrodes in rat cortex.* Biomaterials, 2010. **31**(7): p. 1558-67.

57. Skousen, J.L., et al., *Reducing surface area while maintaining implant penetrating profile lowers the brain foreign body response to chronically implanted planar silicon microelectrode arrays.* Prog Brain Res, 2011. **194**: p. 167-80.

58. Skousen, J.L., M.J. Bridge, and P.A. Tresco, *A strategy to passively reduce neuroinflammation surrounding devices implanted chronically in brain tissue by manipulating device surface permeability.* Biomaterials, 2014.

59. Potter, K.A., et al., *Stab injury and device implantation within the brain results in inversely multiphasic neuroinflammatory and neurodegenerative responses.* J Neural Eng, 2012. **9**(4): p. 046020.

60. Stensaas, S.S. and L.J. Stensaas, *Histopathological evaluation of materials implanted in the cerebral cortex.* Acta Neuropathol, 1978. **41**(2): p. 145-55.

61. Schultz, R.L. and T.J. Willey, *The ultrastructure of the sheath around chronically implanted electrodes in brain.* J Neurocytol, 1976. **5**(6): p. 621-42.

62. Edell, D.J., et al., *Factors influencing the biocompatibility of insertable silicon microshafts in cerebral cortex.* IEEE Trans Biomed Eng, 1992. **39**(6): p. 635-43.

63. Schmidt, S., K. Horch, and R. Normann, *Biocompatibility of silicon-based electrode arrays implanted in feline cortical tissue.* J Biomed Mater Res, 1993. **27**(11): p. 1393-9.

64. Turner, J.N., et al., *Cerebral astrocyte response to micromachined silicon implants.* Exp Neurol, 1999. **156**(1): p. 33-49.

65. Szarowski, D.H., et al., *Brain responses to micro-machined silicon devices.* Brain Research, 2003. **983**(1-2): p. 23-35.

66. Spataro, L., et al., *Dexamethasone treatment reduces astroglia responses to inserted neuroprosthetic devices in rat neocortex.* Exp Neurol, 2005. **194**(2): p. 289-300.

67. Seymour, J.P. and D.R. Kipke, *Neural probe design for reduced tissue*

encapsulation in CNS. Biomaterials, 2007. **28**(25): p. 3594-607.

68. Maynard, E.M., E. Fernandez, and R.A. Normann, *A technique to prevent dural adhesions to chronically implanted microelectrode arrays.* J Neurosci Methods, 2000. **97**(2): p. 93-101.

69. Nordhausen, C.T., E.M. Maynard, and R.A. Normann, *Single unit recording capabilities of a 100 microelectrode array.* Brain Res, 1996. **726**(1-2): p. 129-40.

70. House, P.A., et al., *Acute microelectrode array implantation into human neocortex: preliminary technique and histological considerations.* Neurosurg Focus, 2006. **20**(5): p. E4.

71. Dymond, A.M., et al., *Brain tissue reaction to some chronically implanted metals.* J Neurosurg, 1970. **33**(5): p. 574-80.

72. McConnell, G.C., et al., *Implanted neural electrodes cause chronic, local inflammation that is correlated with local neurodegeneration.* J Neural Eng, 2009. **6**(5): p. 056003.

73. Huang, Y.H., et al., *Astrocyte glutamate transporters regulate metabotropic glutamate receptor-mediated excitation of hippocampal interneurons.* J Neurosci, 2004. **24**(19): p. 4551-9.

74. Abbott, N.J., *Astrocyte-endothelial interactions and blood-brain barrier permeability.* J Anat, 2002. **200**(6): p. 629-38.

75. Allen, N.J., *Astrocyte regulation of synaptic behavior.* Annu Rev Cell Dev Biol, 2014. **30**: p. 439-63.

76. Fawcett, J.W. and R.A. Asher, *The glial scar and central nervous system repair.* Brain Res Bull, 1999. **49**(6): p. 377-91.

77. Ravikumar, M., et al., *The roles of blood-derived macrophages and resident microglia in the neuroinflammatory response to implanted Intracortical microelectrodes.* Biomaterials, 2014. **35**(28): p. 8049-64.

78. Zhong, Y. and R.V. Bellamkonda, *Dexamethasone-coated neural probes elicit attenuated inflammatory response and neuronal loss compared to uncoated neural probes.* Brain Res, 2007. **1148**: p. 15-27.

79. Lok, J., et al., *Intracranial hemorrhage: mechanisms of secondary brain injury.* Acta Neurochir Suppl, 2011. **111**: p. 63-9.

80. Saxena, T., et al., *The impact of chronic blood-brain barrier breach on intracortical electrode function.* Biomaterials, 2013. **34**(20): p. 4703-13.

81. *Spinal Cord Injury (SCI) Facts and Figures at a Glance*. 2015, University of

Alabama at Birmingham: Birmingham, AL.

82. Rao, A.N., M.N. Avula, and D.W. Grainger, *Chapter 11 - Aging and the Host Response to Implanted Biomaterials*, in *Host Response to Biomaterials*, S.F. Badylak, Editor. 2015, Academic Press: Oxford. p. 269-313.

83. Ponnappan, S. and U. Ponnappan, *Aging and immune function: molecular mechanisms to interventions.* Antioxid Redox Signal, 2011. **14**(8): p. 1551-85.

84. Weiskopf, D., B. Weinberger, and B. Grubeck-Loebenstein, *The aging of the immune system.* Transpl Int, 2009. **22**(11): p. 1041-50.

85. Fagiolo, U., et al., *Increased cytokine production in mononuclear cells of healthy elderly people.* Eur J Immunol, 1993. **23**(9): p. 2375-8.

86. Baggio, G., et al., *Lipoprotein(a) and lipoprotein profile in healthy centenarians: a reappraisal of vascular risk factors.* FASEB J, 1998. **12**(6): p. 433-7.

87. Cohen, H.J., et al., *The association of plasma IL-6 levels with functional disability in community-dwelling elderly.* J Gerontol A Biol Sci Med Sci, 1997. **52**(4): p. M201-8.

88. Dobbs, R.J., et al., *Association of circulating TNF-alpha and IL-6 with ageing and parkinsonism.* Acta Neurol Scand, 1999. **100**(1): p. 34-41.

89. Kania, D.M., et al., *Elevated plasma levels of interleukin-6 in postmenopausal women do not correlate with bone density.* J Am Geriatr Soc, 1995. **43**(3): p. 236-9.

90. Paolisso, G., et al., *Advancing age and insulin resistance: role of plasma tumor necrosis factor-alpha.* Am J Physiol, 1998. **275**(2 Pt 1): p. E294-9.

91. Bruunsgaard, H., et al., *Elevated levels of tumor necrosis factor alpha and mortality in centenarians.* Am J Med, 2003. **115**(4): p. 278-83.

92. Bruunsgaard, H., et al., *A high plasma concentration of TNF-alpha is associated with dementia in centenarians.* J Gerontol A Biol Sci Med Sci, 1999. **54**(7): p. M357-64.

93. Bruunsgaard, H., et al., *Ageing, tumour necrosis factor-alpha (TNF-alpha) and atherosclerosis.* Clin Exp Immunol, 2000. **121**(2): p. 255-60.

94. Ross, R., *Atherosclerosis--an inflammatory disease.* N Engl J Med, 1999. **340**(2): p. 115-26.

95. Eikelenboom, P. and R. Veerhuis, *The importance of inflammatory mechanisms for the development of Alzheimer's disease.* Exp Gerontol, 1999. **34**(3): p. 453-61.

96. Pacifici, R., *Aging and cytokine production.* Calcif Tissue Int, 1999. **65**(5): p. 345-51.

97. Gosain, A. and L.A. DiPietro, *Aging and wound healing.* World J Surg, 2004. **28**(3): p. 321-6.

98. Franceschi, C., et al., *Inflamm-aging. An evolutionary perspective on immunosenescence.* Ann N Y Acad Sci, 2000. **908**: p. 244-54.

99. von Bernhardi, R., J.E. Tichauer, and J. Eugenin, *Aging-dependent changes of microglial cells and their relevance for neurodegenerative disorders.* J Neurochem, 2010. **112**(5): p. 1099-114.

100. Sierra, A., et al., *Microglia derived from aging mice exhibit an altered inflammatory profile.* Glia, 2007. **55**(4): p. 412-24.

101. Hart, A.D., et al., *Age related changes in microglial phenotype vary between CNS regions: grey versus white matter differences.* Brain Behav Immun, 2012. **26**(5): p. 754-65.

102. Perry, V.H., M.K. Matyszak, and S. Fearn, *Altered antigen expression of microglia in the aged rodent CNS.* Glia, 1993. **7**(1): p. 60-7.

103. Ritzel, R.M., et al., *Age- and location-related changes in microglial function.* Neurobiol Aging, 2015. **36**(6): p. 2153-63.

104. Ye, S.M. and R.W. Johnson, *Increased interleukin-6 expression by microglia from brain of aged mice.* J Neuroimmunol, 1999. **93**(1-2): p. 139-48.

105. Amenta, F., et al., *Astrocyte changes in aging cerebral cortex and hippocampus: a quantitative immunohistochemical study.* Microsc Res Tech, 1998. **43**(1): p. 29-33.

106. Juraska, J.M. and N.C. Lowry, *Neuroanatomical changes associated with cognitive aging.* Curr Top Behav Neurosci, 2012. **10**: p. 137-62.

107. Lindsay, J., et al., *Risk factors for Alzheimer's disease: a prospective analysis from the Canadian Study of Health and Aging.* Am J Epidemiol, 2002. **156**(5): p. 445-53.

108. Van Den Eeden, S.K., et al., *Incidence of Parkinson's disease: variation by age, gender, and race/ethnicity.* Am J Epidemiol, 2003. **157**(11): p. 1015-22.

109. Macciocchi, S.N., et al., *Ischemic stroke: relation of age, lesion location, and initial neurologic deficit to functional outcome.* Arch Phys Med Rehabil, 1998. **79**(10): p. 1255-7.

110. Hukkelhoven, C.W., et al., *Patient age and outcome following severe traumatic brain injury: an analysis of 5600 patients.* J Neurosurg, 2003. **99**(4): p. 666-73.

111. Lanzino, G., et al., *Age and outcome after aneurysmal subarachnoid hemorrhage: why do older patients fare worse?* J Neurosurg, 1996. **85**(3): p. 410-8.

112. Kumar, A., et al., *Traumatic brain injury in aged animals increases lesion size and chronically alters microglial/macrophage classical and alternative activation states.* Neurobiol Aging, 2013. **34**(5): p. 1397-411.

113. Rosen, C.L., et al., *Influence of age on stroke outcome following transient focal ischemia.* J Neurosurg, 2005. **103**(4): p. 687-94.

114. Voges, J., et al., *Thirty days complication rate following surgery performed for deep-brain-stimulation.* Mov Disord, 2007. **22**(10): p. 1486-9.

115. Charles, P.D., et al., *Predictors of effective bilateral subthalamic nucleus stimulation for PD.* Neurology, 2002. **59**(6): p. 932-4.

116. Welter, M.L., et al., *Clinical predictive factors of subthalamic stimulation in Parkinson's disease.* Brain, 2002. **125**(Pt 3): p. 575-83.

117. Saint-Cyr, J.A., et al., *Neuropsychological consequences of chronic bilateral stimulation of the subthalamic nucleus in Parkinson's disease.* Brain, 2000. **123 (Pt 10)**: p. 2091-108.

118. Robinson, F.R. and M.T. Johnson, *Histopathological studies of tissue reactions to various metals implanted in cat brains.* ASD Tech Rep, 1961. **61**(397): p. 13.

119. Bickford, R.G., G. Fischer, and G.P. Sayre, *Histologic changes in the cat's brain after introduction of metallic and plastic coated wire used in electro-encephalography.* Proc Staff Meet Mayo Clin, 1957. **32**(1): p. 14-21.

120. Cooper, R. and H.J. Crow, *Toxic effects of intra-cerebral electrodes.* Med Biol Eng, 1966. **4**(6): p. 575-81.

121. Levine, S. and R. Sowinski, *Lymphocytic inflammation produced by intracerebral implantation of zinc and other metals.* J Neuropathol Exp Neurol, 1978. **37**(5): p. 471-8.

122. Fontani, G., *A technique for long term recording from single neurons in unrestrained behaving animals.* Physiol Behav, 1981. **26**(2): p. 331-3.

123. Ismailova, E., et al., *Plastic neuronal probes for implantation in cortical and subcortical areas of the rat brain.* International Journal of Nanotechnology, 2012. **9**: p. 517.

124. Yuen, T.G. and W.F. Agnew, *Histological evaluation of polyesterimide-insulated gold wires in brain.* Biomaterials, 1995. **16**(12): p. 951-6.

125. He, W., G.C. McConnell, and R.V. Bellamkonda, *Nanoscale laminin coating*

modulates cortical scarring response around implanted silicon microelectrode arrays. J Neural Eng, 2006. **3**(4): p. 316-26.

126. He, W., et al., *A Novel Anti-inflammatory Surface for Neural Electrodes.* Advanced Materials, 2007. **19**(21): p. 3529-3533.

127. Azemi, E., C.F. Lagenaur, and X.T. Cui, *The surface immobilization of the neural adhesion molecule L1 on neural probes and its effect on neuronal density and gliosis at the probe/tissue interface.* Biomaterials, 2011. **32**(3): p. 681-92.

128. Lu, Y., et al., *Poly(vinyl alcohol)/poly(acrylic acid) hydrogel coatings for improving electrode-neural tissue interface.* Biomaterials, 2009. **30**(25): p. 4143-51.

129. Rao, L., et al., *Polyethylene glycol-containing polyurethane hydrogel coatings for improving the biocompatibility of neural electrodes.* Acta Biomater, 2012. **8**(6): p. 2233-42.

130. Gutowski, S.M., et al., *Host response to microgel coatings on neural electrodes implanted in the brain.* J Biomed Mater Res A, 2014. **102**(5): p. 1486-99.

131. Lee, J.Y., et al., *Surface modification of neural electrodes with a pyrrole-hyaluronic acid conjugate to attenuate reactive astrogliosis in vivo.* RSC Advances, 2015. **5**(49): p. 39228-39231.

132. Lind, G., et al., *Gelatine-embedded electrodes--a novel biocompatible vehicle allowing implantation of highly flexible microelectrodes.* J Neural Eng, 2010. **7**(4): p. 046005.

133. Shen, W., et al., *Extracellular matrix-based intracortical microelectrodes: Toward a microfabricated neural interface based on natural materials.* Microsystems & Nanoengineering, 2015. **1**: p. 15010.

134. Rennaker, R.L., et al., *Minocycline increases quality and longevity of chronic neural recordings.* J Neural Eng, 2007. **4**(2): p. L1-5.

135. Potter, K.A., et al., *The effect of resveratrol on neurodegeneration and blood brain barrier stability surrounding intracortical microelectrodes.* Biomaterials, 2013. **34**(29): p. 7001-15.

136. Potter-Baker, K.A., et al., *Implications of chronic daily anti-oxidant administration on the inflammatory response to intracortical microelectrodes.* J Neural Eng, 2015. **12**(4): p. 046002.

137. Sawyer, A.J., et al., *The effect of inflammatory cell-derived MCP-1 loss on neuronal survival during chronic neuroinflammation.* Biomaterials, 2014. **35**(25): p. 6698-706.

138. Kozai, T.D., et al., *Effects of caspase-1 knockout on chronic neural recording quality and longevity: insight into cellular and molecular mechanisms of the reactive tissue response.* Biomaterials, 2014. **35**(36): p. 9620-34.

139. Purcell, E.K., et al., *Flavopiridol reduces the impedance of neural prostheses in vivo without affecting recording quality.* J Neurosci Methods, 2009. **183**(2): p. 149-57.

140. Misra, A., et al., *Preventing neuronal damage and inflammation in vivo during cortical microelectrode implantation through the use of poloxamer P-188.* J Neural Eng, 2013. **10**(1): p. 016011.

141. Hayn, L. and M. Koch, *Suppression of excitotoxicity and foreign body response by memantine in chronic cannula implantation into the rat brain.* Brain Res Bull, 2015. **117**: p. 54-68.

142. Huang, W.C., et al., *Multifunctional 3D Patternable Drug-Embedded Nanocarrier-Based Interfaces to Enhance Signal Recording and Reduce Neuron Degeneration in Neural Implantation.* Adv Mater, 2015. **27**(28): p. 4186-93.

143. Purcell, E.K., et al., *In vivo evaluation of a neural stem cell-seeded prosthesis.* J Neural Eng, 2009. **6**(2): p. 026005.

144. Stice, P., et al., *Thin microelectrodes reduce GFAP expression in the implant site in rodent somatosensory cortex.* J Neural Eng, 2007. **4**(2): p. 42-53.

145. Thelin, J., et al., *Implant size and fixation mode strongly influence tissue reactions in the CNS.* PLoS One, 2011. **6**(1): p. e16267.

146. Shih, A.Y., et al., *The smallest stroke: occlusion of one penetrating vessel leads to infarction and a cognitive deficit.* Nat Neurosci, 2013. **16**(1): p. 55-63.

147. McConnell, G.C., et al., *Extraction force and cortical tissue reaction of silicon microelectrode arrays implanted in the rat brain.* IEEE Trans Biomed Eng, 2007. **54**(6 Pt 1): p. 1097-107.

148. Lind, G., et al., *Multiple implants do not aggravate the tissue reaction in rat brain.* PLoS One, 2012. **7**(10): p. e47509.

149. Wood, N.K., E.J. Kaminski, and R.J. Oglesby, *The significance of implant shape in experimental testing of biological materials: disc vs. rod.* J Biomed Mater Res, 1970. **4**(1): p. 1-12.

150. Chen, T., et al., *Motion artifact correction of multi-photon imaging of awake mice models using speed embedded HMM.* Med Image Comput Comput Assist Interv, 2010. **13**(Pt 3): p. 473-80.

151. Harrison, R.R., et al., *Wireless neural recording with single low-power integrated*

circuit. IEEE Trans Neural Syst Rehabil Eng, 2009. **17**(4): p. 322-9.

152. Lind, G., C.E. Linsmeier, and J. Schouenborg, *The density difference between tissue and neural probes is a key factor for glial scarring.* Sci Rep, 2013. **3**: p. 2942.

153. Harris, J.P., et al., *Mechanically adaptive intracortical implants improve the proximity of neuronal cell bodies.* J Neural Eng, 2011. **8**(6): p. 066011.

154. Nguyen, J.K., et al., *Mechanically-compliant intracortical implants reduce the neuroinflammatory response.* J Neural Eng, 2014. **11**(5): p. 056014.

155. Ward, M.P., et al., *Toward a comparison of microelectrodes for acute and chronic recordings.* Brain Res, 2009. **1282**: p. 183-200.

156. Kozai, T.D., et al., *Ultrasmall implantable composite microelectrodes with bioactive surfaces for chronic neural interfaces.* Nat Mater, 2012. **11**(12): p. 1065-73.

157. Karumbaiah, L., et al., *Relationship between intracortical electrode design and chronic recording function.* Biomaterials, 2013. **34**(33): p. 8061-74.

158. Vitale, F., et al., *Neural stimulation and recording with bidirectional, soft carbon nanotube fiber microelectrodes.* ACS Nano, 2015. **9**(4): p. 4465-74.

159. Perge, J.A., et al., *Reliability of directional information in unsorted spikes and local field potentials recorded in human motor cortex.* J Neural Eng, 2014. **11**(4): p. 046007.

160. Groothuis, J., et al., *Physiological challenges for intracortical electrodes.* Brain Stimul, 2014. **7**(1): p. 1-6.

161. Bjornsson, C.S., et al., *Effects of insertion conditions on tissue strain and vascular damage during neuroprosthetic device insertion.* J Neural Eng, 2006. **3**(3): p. 196-207.

162. Xue, M., M.R. Del Bigio, and J.P. Muizelaar, *Intracortical Hemorrhage Injury in Rats : Relationship Between Blood Fractions and Brain Cell Death Editorial Comment: Relationship Between Blood Fractions and Brain Cell Death.* Stroke, 2000. **31**(7): p. 1721-1727.

163. Santhanam, G., et al., *A high-performance brain-computer interface.* Nature, 2006. **442**(7099): p. 195-8.

164. Ohsawa, K., et al., *Involvement of Iba1 in membrane ruffling and phagocytosis of macrophages/microglia.* J Cell Sci, 2000. **113 (Pt 17)**: p. 3073-84.

165. Kozai, T.D., et al., *Reduction of neurovascular damage resulting from microelectrode insertion into the cerebral cortex using in vivo two-photon*

mapping. J Neural Eng, 2010. **7**(4): p. 046011.

166. Williams, J.C., et al., *Complex impedance spectroscopy for monitoring tissue responses to inserted neural implants.* J Neural Eng, 2007. **4**(4): p. 410-23.

167. Venkatachalam, S., M.S. Fee, and D. Kleinfeld, *Ultra-miniature headstage with 6-channel drive and vacuum-assisted micro-wire implantation for chronic recording from the neocortex.* J Neurosci Methods, 1999. **90**(1): p. 37-46.

168. Nelson, T.S., et al., *Seizure severity and duration in the cortical stimulation model of experimental epilepsy in rats: a longitudinal study.* Epilepsy Res, 2010. **89**(2-3): p. 261-70.

169. Agnew, W.F., et al., *Histopathologic evaluation of prolonged intracortical electrical stimulation.* Exp Neurol, 1986. **92**(1): p. 162-85.

170. McCreery, D., V. Pikov, and P.R. Troyk, *Neuronal loss due to prolonged controlled-current stimulation with chronically implanted microelectrodes in the cat cerebral cortex.* J Neural Eng, 2010. **7**(3): p. 036005.

171. Nolta, N.F., et al., *BBB leakage, astrogliosis, and tissue loss correlate with silicon microelectrode array recording performance.* Biomaterials, 2015. **53**: p. 753-62.

172. Tresco, P.A. and B.D. Winslow, *The challenge of integrating devices into the central nervous system.* Crit Rev Biomed Eng, 2011. **39**(1): p. 29-44.

173. Cameron, T.P., et al., *Longevity and reproductive comparisons for male ACI and Sprague-Dawley rat aging colonies.* Lab Anim Sci, 1982. **32**(5): p. 495-9.

174. Arias, E., *United States Life Tables, 2010,* in *National Vital Statistics Reports*. 2014, Centers for Disease Control and Prevention.

175. Sengupta, P., *The Laboratory Rat: Relating Its Age With Human's.* Int J Prev Med, 2013. **4**(6): p. 624-30.

176. Gefen, A., et al., *Age-dependent changes in material properties of the brain and braincase of the rat.* J Neurotrauma, 2003. **20**(11): p. 1163-77.

177. Kim, J.D., R.J. McCarter, and B.P. Yu, *Influence of age, exercise, and dietary restriction on oxidative stress in rats.* Aging (Milano), 1996. **8**(2): p. 123-9.

178. Kim, Y.-T., et al., *Chronic response of adult rat brain tissue to implants anchored to the skull.* Biomaterials, 2004. **25**(12): p. 2229-2237.

179. Stein, T.P., M.J. Leskiw, and H.W. Wallace, *Measurement of half-life human plasma fibrinogen.* Am J Physiol, 1978. **234**(5): p. D504-10.

180. Gulden, M., et al., *Cytotoxic potency of H2O2 in cell cultures: impact of cell*

concentration and exposure time. Free Radic Biol Med, 2010. **49**(8): p. 1298-305.

181. Kim, Y.T., M.J. Bridge, and P.A. Tresco, *The influence of the foreign body response evoked by fibroblast transplantation on soluble factor diffusion in surrounding brain tissue.* J Control Release, 2007. **118**(3): p. 340-7.

182. Cheong, R., et al., *Transient IkappaB kinase activity mediates temporal NF-kappaB dynamics in response to a wide range of tumor necrosis factor-alpha doses.* J Biol Chem, 2006. **281**(5): p. 2945-50.

183. Smith, M.J., K.L.J. White, and G.L. Bowlin, *Feasibility of Electrospun Polydioxanone – Monocyte Chemotactic Protein-1 (MCP-1) Hybrid Scaffolds as Potential Cellular Homing Devices* Journal of Engineered Fibers and Fabrics, 2010. **5**(4).

184. Eastgate, J.A., J.A. Symons, and G.W. Duff, *Identification of an interleukin-1 beta binding protein in human plasma.* FEBS Lett, 1990. **260**(2): p. 213-6.

185. Tjalkens, R.B., D.L. Carbone, and G. Wu, *Detection of nitric oxide formation in primary neural cells and tissues.* Methods Mol Biol, 2011. **758**: p. 267-77.

186. Fernandez, E., et al., *Acute human brain responses to intracortical microelectrode arrays: challenges and future prospects.* Front Neuroeng, 2014. **7**: p. 24.

187. Ekdahl, C.T., et al., *Inflammation is detrimental for neurogenesis in adult brain.* Proc Natl Acad Sci U S A, 2003. **100**(23): p. 13632-7.

188. Hirshler, Y.K., U. Polat, and A. Biegon, *Intracranial electrode implantation produces regional neuroinflammation and memory deficits in rats.* Exp Neurol, 2010. **222**(1): p. 42-50.

189. Potter, K.A., et al., *Reduction of autofluorescence at the microelectrode-cortical tissue interface improves antibody detection.* J Neurosci Methods, 2012. **203**(1): p. 96-105.

190. Seo, D., et al., *Model validation of untethered, ultrasonic neural dust motes for cortical recording.* J Neurosci Methods, 2015. **244**: p. 114-22.

191. Moore, S.M., et al., *The glenohumeral capsule should be evaluated as a sheet of fibrous tissue: a validated finite element model.* Ann Biomed Eng, 2010. **38**(1): p. 66-76.

192. Kawagoe, K.T., J.B. Zimmerman, and R.M. Wightman, *Principles of voltammetry and microelectrode surface states.* J Neurosci Methods, 1993. **48**(3): p. 225-40.

193. Brovkovych, V., et al., *Direct electrochemical measurement of nitric oxide in vascular endothelium.* J Pharm Biomed Anal, 1999. **19**(1-2): p. 135-43.

194. Zhang, M., et al., *Carbon nanotube-modified carbon fiber microelectrodes for in vivo voltammetric measurement of ascorbic acid in rat brain.* Anal Chem, 2007. **79**(17): p. 6559-65.

195. Wilson, G.S. and R. Gifford, *Biosensors for real-time in vivo measurements.* Biosens Bioelectron, 2005. **20**(12): p. 2388-403.

196. Subbaroyan, J., D.C. Martin, and D.R. Kipke, *A finite-element model of the mechanical effects of implantable microelectrodes in the cerebral cortex.* J Neural Eng, 2005. **2**(4): p. 103-13.